EXPERIMENTAL AND ANALYTICAL INVESTIGATION OF AN ARRAY OF SESSILE DROPLETS BEHAVIOUR ON HEATED AND UNHEATED SUBSTRATES

AHMED AZZAM

A DISSERTATION SUBMITTED TO
THE FACULTY OF GRADUATE STUDIES
IN PARTIAL FULFILLMENT OF THE REQUIREMENTS
FOR THE DEGREE OF
DOCTOR OF PHILOSOPHY

GRADUATE PROGRAM IN MECHANICAL ENGINEERING
YORK UNIVERSITY
TORONTO, ONTARIO

April 2025

Abstract

The evaporation and interaction dynamics of sessile droplets play an important role in various engineering and scientific applications, including thermal management, microfluidics, and surface wetting. This thesis presents a comprehensive investigation into the evaporation dynamics and vapor-induced interactions of sessile droplets, combining analytical modeling and experimental validation. A novel, computationally efficient Point Source Model (PSM) was developed to predict the evaporation behavior of multiple droplets on both isothermal and heated substrates. The model simplifies complex mass transfer processes by representing droplets as point sources, enabling accurate predictions with minimal computational cost.

The PSM was first used to model the purely diffusive, quasi-steady evaporation of a pair of sessile droplets. It accurately captured the effects of separation distance and evaporation mode—Constant Contact Angle (CCA) and Constant Contact Radius (CCR)—with excellent agreement between model predictions and experimental results (deviations < 9%). A critical separation ratio ($L/d \geq 10$) was identified, beyond which droplets behave independently.

To account for heated surfaces, the model was extended to include the effects of natural convection. A novel empirical correlation was developed to predict evaporation rates under combined diffusion and convection, validated through experiments over a wide range of substrate temperatures (40–80°C). It was found that for $Ra \cdot L/d < 400$, diffusion dominates, while for $Ra \cdot L/d > 2400$, the contributions of convection and diffusion stabilize.

Further investigation focused on the vapor-mediated interaction between a water droplet and a propylene glycol (PG)-water mixture droplet on a heated substrate (24–135°C). Results showed a 20-fold increase in droplet velocity at temperatures above the boiling point of water. At 20%

PG concentration, intense surface tension gradients caused chaotic motion and droplet fragmentation, demonstrating the strong coupling of composition and temperature in controlling droplet dynamics.

The PSM was finally generalized to a three-droplet array. Interaction effects were quantified using an extended correction factor (η), showing that the threshold for isolated droplet behavior shifts to $L/d > 20$ due to increased vapor shielding. Variations in droplet arrangement and angular orientation were shown to significantly influence evaporation rates, providing new insight for the design of droplet-based cooling and microfluidic systems.

Acknowledgments

As I stepped off the plane on December 17, 2020, and looked out through the window, I saw a land blanketed in white. A wave of uncertainty and fear washed over me—fear of failure, of the unknown, of the challenges that awaited me in a new country with unfamiliar people, a different culture, and a daunting academic journey ahead. The transition was overwhelming, and I questioned whether I had made the right choice. However, as time passed, the unwavering support and continuous encouragement from my supervisors, colleagues, and friends helped me navigate this journey with confidence and resilience.

First and foremost, I extend my deepest gratitude to my supervisors, **Professor Alidad Amirfazli** and **Dr. Roger Kempers**. Their invaluable guidance, constructive feedback, and steadfast support made this work possible. I am profoundly grateful for the freedom they granted me to explore my research interests and the encouragement they provided throughout this journey. Their belief in my capabilities gave me the confidence to overcome challenges and persist in my academic endeavors.

I would also like to express my sincere appreciation to my supervisory committee members, **Dr. Thomas Cooper** and **Dr. Magdalena Krol**, for their invaluable support, insightful discussions, and constructive feedback throughout this challenging yet rewarding journey. Their guidance has been instrumental in shaping my research and broadening my understanding.

Beyond academia, I have been fortunate to cross paths with many wonderful individuals who made this journey less daunting. Arriving in Canada alone, I was welcomed with warmth and kindness by friends who became my family away from home. **Milad Shakeri Bonab, Ahmed Elkholy, Khaled Youssef, and Mahmoud Rouby**—your companionship and unwavering

support made the transition easier, and I am grateful for the moments we shared. To my current lab mates, **Ismail Alkomy, Pierre Lesbats, and Yatin Hu**, I sincerely appreciate your camaraderie and insightful discussions that enriched my research experience. A special thank you to **Yvonne Yim**, our graduate program coordinator, for always being available with timely responses, genuine care, and unwavering support whenever needed.

No words can adequately express my heartfelt gratitude to my mother, **Safaa Mohamed**, whose unconditional love and endless prayers have been my greatest source of strength. Her unwavering belief in me has been my guiding light through the toughest times, and I owe so much of this achievement to her sacrifices and encouragement.

Finally, my deepest appreciation goes to my small yet invaluable family. To my incredible wife, **Mariam Abdelbary**, thank you for standing by my side, lifting me when I felt defeated, and constantly pushing me to strive for better. Your patience, love, and unwavering support have been my anchor. A special thank you to my little angels, **Moaz**—my best friend and biggest cheerleader—and **Roqaya**, my sweet princess, who brought endless joy and laughter into my life even during the most challenging moments.

This journey has been one of resilience, learning, and growth, made possible by the unwavering support of those around me. To all who have been a part of this experience—thank you from the depths of my heart.

Ahmed Azzam
April 2025

Table of Contents

List of Tables

List of Figures

Chapter 1 Introduction and Motivation

1.1 Theoretical Background

1.1.1 Importance of Sessile Droplets Evaporation Process

Evaporation is a vital natural process, responsible for about 90% of the water vapour in the Earth's atmosphere [1] and plays a key role in many industrial applications. Sessile droplet evaporation is widespread in nature, from sweat droplets evaporating on skin and respiratory droplets released during coughing or sneezing, to the drying of spilled coffee and rain droplets on leaves. Its prevalence has made it a topic of significant interest, with research into this phenomenon expanding rapidly over the past five decades [2].

Sessile droplet evaporation occurs naturally and is also intentionally utilized in various industries, including healthcare, food and beverage, and automotive sectors [3]. In combustion systems such as boilers, rockets, gas turbines, and diesel engines, fuel droplet evaporation can be optimized by understanding how sessile droplets evaporate [4]. By effectively controlling fuel droplet evaporation, combustion characteristics, operating temperature, and emissions can be significantly improved. Similarly, this process is essential in heat transfer applications, improving efficiency in spray cooling systems and the thermal management of microprocessors through evaporative cooling [5, 6].

Furthermore, controlling droplet evaporation can enhance the deposition of particles on surfaces, making it relevant to a wide range of applications from microscopic to large-scale processes. In healthcare, sessile droplet evaporation plays a critical role in the drying of blood around wounds [7] and the development of bacterial biofilms [8]. It also supports important

applications like disease diagnosis, the creation of DNA microarrays [9], DNA mapping [10], and forensic bloodstain analysis [11].

1.1.2 Definition of Sessile Droplets

When a liquid droplet is placed on a solid surface, it naturally seeks to minimize its surface area to achieve a stable state. This behavior is driven by thermodynamic favourability, as reducing surface area lowers the system's overall energy. The droplet spreads and wets the surface, wetting process, until it reaches an equilibrium contact angle (θ) between the droplet and the solid surface. Such a liquid droplet in this system is referred to as a sessile droplet. In the literature, a sessile droplet is typically characterized by three key parameters: the contact angle (θ), the contact radius (a), and the droplet height (h), as shown in **Figure 1-1**. Additionally, **Figure 1-1** highlights the Triple Contact Line (TCL), which is the line where the liquid, vapor, and solid interfaces meet.

Wetting behavior is governed by the balance between adhesive and cohesive intermolecular forces. When the adhesive forces between the liquid and the solid surface exceed the cohesive forces within the liquid, the droplet spreads more extensively, resulting in a smaller contact angle. Conversely, if the cohesive forces within the liquid are stronger than the adhesive interactions with the solid, the droplet reduces its contact with the surface, forming a larger contact angle. Based on this behavior, systems can be broadly classified as *hydrophilic* or *hydrophobic*. A system is considered hydrophilic when the contact angle is less than 90°, whereas a contact angle greater than 90° indicates a hydrophobic system. At the extremes of wettability, further distinctions can be made; contact angles approaching less than 10° signify *super-hydrophilic* behavior, while contact angles $150° < \theta < 180°$ correspond to *super-hydrophobic* behavior.

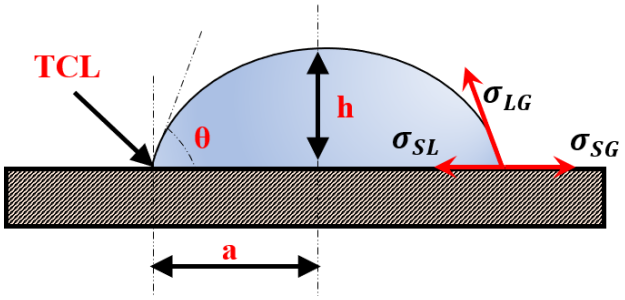

Figure 1-1 Schematic of a sessile liquid droplet, illustrating its key physical properties: contact radius (a), height (h), and contact angle (θ). The force balance at the Triple Contact Line (TCL) under mechanical equilibrium is also shown, where σ_{SL}, σ_{LG} and σ_{SG} represent the surface tensions at the solid/liquid, liquid/gas, and solid/gas interfaces, respectively.

In **Figure 1-1**, three distinct phases coexist: the solid substrate, the liquid droplet surface, and the ambient gas. As a result, a partially wetted system features three interfaces: solid/liquid, liquid/gas, and solid/gas, each associated with a specific surface tension. Surface tension represents the interfacial tension between two phases and arises from the balance between adhesive and cohesive forces. Stronger cohesive forces within the liquid enhance its resistance to external forces, leading to higher surface tension. At mechanical equilibrium, the relationship between surface tensions and the contact angle is described by a force balance known as Young's Equation: $\sigma_{SG} = \sigma_{SL} + \sigma_{LG}\, cos\theta$. Young's equation holds true only for idealized systems, where the droplet is composed of a single pure liquid and the solid surface is entirely flat, smooth, rigid, and chemically uniform.

Contact angle hysteresis (CAH) refers to the difference between the advancing contact angle, θ_a, and a receding contact angle, θ_r, mathematically expressed as $CAH = \theta_a - \theta_r$. The definitions of these angles depend on how the sessile droplet system is analyzed. In static systems, where the triple contact line (TCL) remains stationary, the advancing contact angle represents the maximum contact angle that the system can thermodynamically achieve, while the

receding contact angle corresponds to the minimum thermodynamically achievable value. In dynamic systems, where the TCL is in motion, the advancing contact angle is observed as the droplet spreads and the liquid-solid contact area increases, whereas the receding contact angle occurs when the droplet retracts, and the contact area decreases.

1.1.3 Fundamentals of Evaporation Process of Sessile Droplets

When a sessile droplet sits on a solid surface, evaporation, or mass transfer, takes place from the droplet's surface to the surrounding air as long as water vapor concentration gradient exists. This concentration gradient refers to the difference in liquid vapor concentration between the droplet's surface, where the vapor is saturated, and the surrounding ambient air, which typically has a lower vapor concentration. This difference drives the diffusion of vapor away from the droplet. Although the process appears simple and is common in nature, the evaporation of sessile droplets is highly complex. It involves a dynamic liquid-vapor interface and the interplay of heat and mass transfer mechanisms. Mass transfer of liquid vapor, or evaporation process, from the droplet to the surroundings happens through both diffusion and convection.

Mass transfer during droplet evaporation occurs in two stages: phase change at the liquid-vapor interface and the transport of saturated vapor of the liquid from the interface into the surrounding gas. For small droplets (with volumes of μL range), the rate of phase change at the interface is significantly slower than the rate at which vapor is transported into the environment. As a result, liquid vapor transport becomes the limiting factor in the process [12, 13].

This transport occurs through both diffusion and convection, with their relative contributions determined by the Péclet number (Pe), which represents the ratio of convective to diffusive transfer. When the Péclet number is low, diffusion dominates, and convection plays a negligible

role. According to Langmuir's findings [14], a Péclet number <<1 suggests that the gas phase can be considered stationary—a valid assumption for many evaporating sessile droplets of non-volatile liquids sitting on unheated substrates. Consequently, the assumption that evaporation is primarily diffusion-driven, with minimal convection, is widely adopted in existing literature.

The primary factor driving diffusive evaporation is the vapor concentration gradient (difference in liquid vapor concentration between the droplet's surface and the surrounding). This relationship is described by Fick's First Law of Diffusion, expressed in Eq. (1-1), which models the diffusion of saturated vapor (i.e. RH=100%) from the droplet's surface into the surrounding gas. In Eq. (1-1), *J* represents the evaporation flux across the droplet's surface, *D* is the diffusion coefficient of the vapor in air, and ∇C denotes the concentration gradient at the droplet's surface.

$$J = -D\,\nabla C \qquad (1\text{-}1)$$

The evaporation of a sessile droplet is a dynamic process that inherently operates far from equilibrium. During evaporation, the balance of forces and free energy at the contact line, as shown in **Figure 1-1**, evolves continuously. Studies in the literature [15–21] have established that, under the influence of (CAH), sessile droplet evaporation typically follows three distinct modes: the Constant Contact Angle (CCA) mode, the Constant Contact Radius (CCR) mode, and the Mixed mode. In the CCA mode, the contact radius decreases while the contact angle remains nearly constant. Conversely, the CCR mode is characterized by a fixed contact line with a progressively decreasing contact angle. The Mixed mode, often referred to as the "stick-slip" (SS) mode, combines elements of both CCA and CCR behaviors. In this mode, both the contact angle and the contact radius decrease over time in a manner resembling a stick-and-slide process, which explains the alternate name. **Figure 1-2** illustrates the contact line dynamics associated

with the pure CCA and CCR modes, while the SS mode exhibits feature of both, with simultaneous changes in contact angle and contact radius.

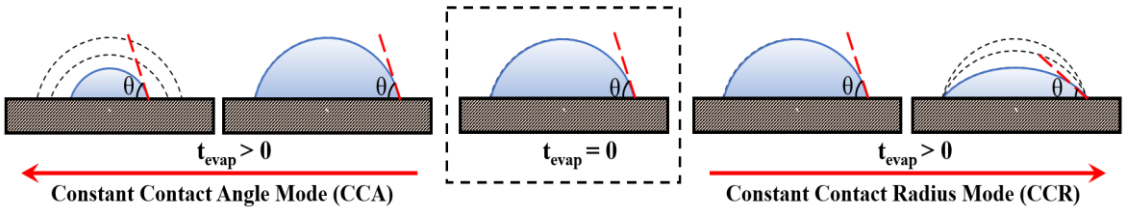

Figure 1-2 Illustration of Constant Contact Angle (CCA), and Constant Contact Radius (CCR) evaporation modes.

In many applications, the evaporation of sessile droplets differs fundamentally from that of suspended, contact-free droplets. For suspended droplets, the evaporation flux across the surface of the droplet is generally uniform. However, this uniformity does not apply to sessile droplets, as the solid substrate significantly influences the evaporation process. The evaporative flux from the surface of a sessile droplet is influenced by the solid substrate and is strongly dependent on the contact angle between the droplet and the substrate. Recent findings reveal that the flux across the droplet's surface is not uniform when the contact angle deviates from 90°. As shown in **Figure 1-3**, in hydrophilic systems, the evaporative flux is highest near the droplet's base and decreases toward the apex [22, 23]. Conversely, in hydrophobic systems, the flux is greater at the apex than at the base [24, 25]. Accurately modeling sessile droplet evaporation requires accounting for this spatial variation in evaporative flux. The non-uniform distribution of flux over the droplet's surface introduces additional complexity to understanding and describing the evaporation process.

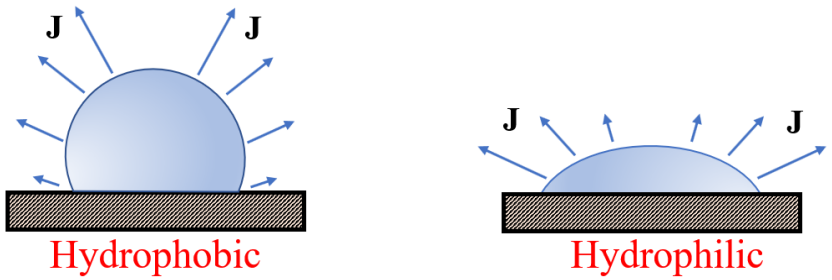

Figure 1-3 Evaporation flux distribution over the free surface of the droplets for hydrophilic system (Right) and hydrophobic system (Left).

1.1.4 Evaporation of an Array of Sessile Droplets on an Unheated Substrate

As discussed in the **Section1.1.3**, despite its apparent simplicity, the evaporation of sessile droplets is a highly complex process. For this reason, early research focused on single, isolated droplets to gain a deeper understanding of the various mechanisms involved in the transfer of mass, momentum, and energy [12, 15, 22, 26–30]. Nonetheless, in most real-world and practical situations, droplet evaporation typically occurs in arrays of droplets rather than as a single isolated droplet [31–33]. Although studies on single isolated droplets are valuable, the rates of energy, mass, and momentum transfer in droplet arrays differ significantly due to the interactions between neighboring droplets. [34].

The evaporation of an array of sessile droplets differs significantly from that of single isolated droplets due to the formation of wedge regions between adjacent droplets [35]. In these regions, vapor accumulates, leading to a reduction in the evaporation rate and an increase in the evaporation time compared to an isolated droplet [36]. The evaporation of an array of N-droplets can be simplified by representing it as smaller units, each containing three droplets. To better understand the behavior of such an array, the evaporation process can first be analysed for two adjacent droplets [24, 25, 31, 37], followed by examining the influence of a third droplet.

Modeling the evaporation process of a pair of sessile droplets on an unheated substrate, while accounting for the non-uniform evaporation flux and the dynamic surface movement caused by mass loss, demands significant computational resources. The semi-analytical models proposed by Shaikeea et al.[24, 25] are limited to a specific contact angle, 115 °, and a certain fluid type, water, with unclear evaporation mode. Similarly, the factors in the model proposed by Hatte et al. [38] are dependent on certain experimental conditions. The asymptotic analytical model proposed by Wilson et al. [39] by adopting the integral method proposed by [40], was complex and it was restricted to thin droplets condition. Finally, Tonini and Cossali [41] developed both analytical and numerical models to study the evaporation of linear arrays of sessile droplets. Their analytical approach involved solving Laplace's equation to calculate concentration at specific points, incorporating complex mathematical elements like the Legendre function of the first kind with a complex index.

1.1.5 Effect of Substrate Temperature on The Evaporation Behaviour of Sessile Droplets

When a droplet of a non-volatile liquid is placed on an unheated substrate, the evaporation process is slow enough to be governed solely by diffusive mass transfer. However, when the same droplet is placed on a heated substrate, the evaporation rate increases significantly. This raises the question: is the assumption of purely diffusive mass transfer still valid in this case.?

Numerous researchers developed models to describe the evaporation dynamics of sessile droplets on unheated surfaces [12, 15, 22, 23, 43–45]. These traditional models typically assume that evaporation occurs under steady-state conditions, driven solely by diffusion, and with the system maintained at ambient temperature. Recent investigations, however, reveal that while diffusive models are suitable for unheated substrates, they fail to accurately predict evaporation rates when the substrate temperature exceeds the ambient. In such cases, convection plays a

significant role, leading to an underestimation of the evaporation rate [10, 44, 46–51]. As substrate temperature rises, natural convection of the liquid vapor at the surface of the droplet intensifies, enhancing mass transfer in the vapor phase through flow around the droplet [52].

To address the problem associated with heated substrate condition, Kelly-Zion et al. [51] and Carle *et al.* [46] developed empirical correlations to predict the evaporation rate of single droplets on heated substrates, incorporating both diffusive and convective mass transfer mechanisms. However, their studies, along with others [12, 15, 22, 23, 43–45], focus exclusively on the evaporation behavior of single, isolated droplets on heated surfaces. Furthermore, the models proposed by [24, 25], [38], [39], and [41] primarily focus on studying the behavior of an array of sessile droplets. However, as discussed in **Section 1.1.4**, these models have certain limitations. Notably, none of these studies have investigated the impact of substrate temperature on the evaporation behavior of an array of sessile droplets. Additionally, their models are based solely on the assumption of diffusive mass transfer and fail to account for the combined effects of convection, which play a significant role on heated substrates.

1.1.6 Vapour-Mediated Droplets Interactions

The ability to control the movement of droplets across surfaces plays a vital role in many fields such as microfluidics [53], biology [54], heat transfer [55], self-cleaning [56], and chemical analysis [57]. To enable precise droplet motion on surfaces, several techniques have been explored, including creating surface energy gradients [58], modifying surface properties [59, 60], and applying external fields such as thermal or acoustic fields [61–74]. Despite their effectiveness, these strategies often demand a substantial surface tension gradient to counteract contact line pinning, which arises due to surface imperfections, both chemical and physical [69, 75].

Recent studies have revealed that the vapor field interactions between neighboring droplets can generate sufficient force to drive droplet motion on high-energy surfaces without triggering contact line pinning. When two propylene glycol (PG)-water droplets of varying compositions are positioned within a distance of three diameters, their interaction occurs in two distinct phases. The first phase, referred to as the long-range interaction, involves either attraction or repulsion between the droplets. In the second phase, known as the short-range interaction, the droplets either merge or engage in a chasing behavior [76–80].

Numerous experimental and theoretical studies have been conducted to investigate the interactions between binary liquid droplets(e.g. [77–79, 81–83]). Although these studies provide important understanding of the mechanisms driving the movement of sessile droplets on inert surfaces, numerous aspects remain unexplored. In practical applications like 3D printing and heat exchangers, the temperature of the substrate plays a critical role in determining liquid wetting behavior and influencing droplet dynamics. However, prior research, both experimental and theoretical, has predominantly concentrated on inert substrates at ambient temperature, leaving the effects of substrate heating on droplet motion largely unexamined.

The impact of varying droplet compositions on their velocity remains an open question. For instance, the experiments conducted by Cira et al. [83] were limited to droplets containing 10% PG. Similarly, studies in [79] and [78] investigated droplet velocities using concentrations of 20% PG and 10% PG, respectively. Since droplet composition directly affects the strength of the surface tension gradient, it can significantly influence the velocity of the droplets.

1.1.7 Impact of Adding Third Droplet to a Droplet Pair

As highlighted in **Section 1.1.4**, although previous studies have extensively explored the evaporation behaviour of single isolated droplets, the evaporation dynamics of an array of sessile droplets exhibit distinct and more complex characteristics. To simplify the analysis of an array of N-droplets, it can be broken down into smaller units, each consisting of three droplets. A logical approach to this simplification is to first investigate the evaporation behavior of a pair of sessile droplets, followed by examining the effect of introducing a third droplet.

1.2 Scientific Gaps and Research Objectives

As a result, extensive knowledge about the evaporation process of single droplets has been gained through previous studies. These investigations are useful for comprehending the evaporative behaviour of isolated sessile droplets. However, in practical applications, evaporation often occurs in arrays of droplets, where interactions between neighboring droplets significantly alter transfer rates due to vapor accumulation in wedge regions, reducing evaporation rates and increasing evaporation times. Simplifying the evaporation dynamics of droplet arrays can be achieved by studying smaller units, such as two or three adjacent droplets. Existing models in the literature are limited by specific conditions, complexities, or computational demands. Therefore, the first objective of this study is to develop a simple method to model the evaporation process of two sessile droplets. This method should be flexible to accommodate the different evaporation modes, CCA and CCR. Also, it should simplify complexities associated with coupled mass and heat transfer dynamics at the moving interface. It is found that the most applicable choice for these requirements is to use adapt the point source modelling (PSM) approach [42]. The key benefit of this approach lies in its ability to capture the essential characteristics of the process while minimizing computational demands. This method

simplifies the analysis by representing droplets as point sources, eliminating the complexities involved in coupled heat and mass transfer at the moving interface. The droplet is considered a point source positioned at its center. The goal is to model the evaporation process of a pair of sessile droplets and to validate this model experimentally. This objective is discussed in detail in *Chapter 2*.

Additionally, the evaporation of non-volatile liquid droplets on unheated substrates is predominantly governed by diffusive mass transfer, but this assumption becomes questionable when droplets are placed on heated surfaces, where evaporation rates increase significantly due to enhanced natural convection. While traditional models describe evaporation on unheated surfaces under steady-state, diffusive conditions, they fail to account for the combined effects of diffusion and convection at elevated substrate temperatures, leading to an underestimation of evaporation rates. Existing studies, primarily focus on single isolated droplets and do not explore the evaporation dynamics of droplet arrays under heated conditions. So, the second objective of this thesis is to adapt the previously developed and validated PSM model to model the evaporation of a pair of sessile droplets on a heated substrate. The proposed model assumes a purely diffusive, isothermal, and quasi-steady-state evaporation process. Building on this, this objective focuses on extending the model to investigate how substrate temperature influences the evaporation behavior of a pair of sessile droplets. The primary question is whether the proposed diffusive PSM model remains applicable under heated substrate conditions. Additionally, we aim to establish the limitations of the diffusive model by comparing its predictions with experimental results. This objective is discussed in detail in *Chapter 3*.

Furthermore, controlling droplet motion on surfaces is critical in fields like microfluidics, biology, heat transfer, self-cleaning, and chemical analysis. Techniques such as creating surface energy gradients, modifying surface properties, and applying external fields have been employed to achieve precise motion, but these often require significant surface tension gradients to overcome contact line pinning caused by surface imperfections. Recent studies show that vapor field interactions between neighboring droplets can drive motion on high-energy surfaces without inducing pinning, with interactions occurring in two phases: long-range (attraction or repulsion) and short-range (coalescence or chasing). While prior research has explored droplet interactions and movement on inert substrates at ambient temperature, the effects of substrate heating remain largely unexamined. Additionally, the influence of droplet composition on velocity is not fully understood, as previous studies focused on limited compositions. Therefore, the third objective of this research is to investigate the effects of substrate temperature and droplet composition on droplet velocities during short-range interactions. This analysis involves a water droplet and a propylene glycol (PG)-water mixture droplet with varying compositions, both placed on a heated glass substrate maintained at different temperatures. This objective is discussed in detail in *Chapter 4*.

Finally, previous studies on single isolated droplets have shown that the evaporation behavior of an array of sessile droplets is notably different. To simplify the analysis of an N-droplet array, it can be represented as smaller units of three droplets. This study addresses the evaporation behavior of a pair of sessile droplets under three different conditions: (1) on an unheated substrate, (2) on a heated substrate, and (3) with varying droplet compositions. These correspond to the first, second, and third objectives of this study, respectively. The final objective is to analyse how the addition of a third droplet influences the evaporation rates of each droplet within

the system. This will be accomplished by extending the model developed for the first objective by utilizing the PSM approach to account for the impact of the third droplet. The details of this objective are thoroughly discussed in *Chapter 5*.

1.3 Thesis Goals, and Outlines

The main goal of this study is to model the evaporation process (evaporation rate and evaporation time) of a pair of sessile droplets placing on an unheated substrate using the PSM approach. This is an important step toward understanding the behavior of an array of sessile droplets. Additionally, the substrate temperature influences the evaporation process of a pair of sessile droplets, transitioning it from a purely diffusive mass transfer mechanism to a combined diffusive-convective process. Lastly, the substrate temperature impacts the movement of a pair of sessile droplets with different concentrations. In summary, the key research questions to be addressed are:

- How can the (PSM) be applied to determine the evaporation rate of a pair of sessile droplets on an unheated substrate?
- How can the evaporation time be calculated for a pair of sessile droplets evaporating under the CCR and CCA modes?
- How can the model be experimentally validated, and what are its limitations beyond which the model is no longer applicable?
- What is the impact of substrate temperature on the evaporation behavior of a pair of sessile water droplets?
- Is the assumption of diffusive mass transfer still valid for heated substrates, and what are the limitations of the proposed diffusive model?

- How does substrate temperature influence the motion of a pair of sessile droplets with different compositions (water and PG)?
- In what ways does the concentration of PG affect the motion behavior of the droplets?
- How can the PSM be extended to determine the evaporation rate of a system of three sessile droplets on an unheated substrate?

Based on the outlined research questions, the objectives of this study are as follows:

1. Develop a model for evaporation of a pair of sessile droplets on unheated substrates:
    - Create a model using the PSM approach to determine the evaporation rate of a pair of sessile droplets on an unheated substrate.
    - Determine the evaporation time of a pair of sessile droplets under the Constant Contact Radius (CCR) and Constant Contact Angle (CCA) modes.
2. Validate and assess model limitations:
    - Experimentally validate the proposed PSM model for evaporation.
    - Identify the limitations of the model and establish conditions where the model becomes invalid.
3. Investigate substrate temperature effects on evaporation a pair of sessile droplets:
    - Examine how substrate temperature influences the evaporation behavior of sessile droplets.
    - Determine if the assumption of purely diffusive mass transfer holds for heated substrates and identify the limits of the diffusive model.
4. Investigate the effect of substrate temperature and the role of droplet composition on the motion of droplets of different PG concentrations:
    - Investigate how substrate temperature impacts the motion of a pair of sessile droplets with different compositions (water and PG).

- Explore the effect of PG concentration on the motion behavior and velocity of sessile droplets during short-range interactions.

5. Characterize the evaporation rate of an array of three droplets on an unheated substrate:
    - Analyse how introducing a third droplet impacts the evaporation rates of each droplet in a two-droplet system by extending the model developed for a droplet pair.

This thesis is structured in a "sandwich thesis" format, comprising 5 chapters. Each chapter begins with a detailed introduction and a thorough review of relevant literature. *Chapter 1* serves as an overview, offering a concise introduction and background, along with the research motivation, objectives, and a brief literature survey. *Chapter 2* addresses the first two research objectives, objective 1 and 2, and is extracted from a published technical journal paper. *Chapters 3, 4* and *5* focus on the third, fourth, and fifth objectives, respectively. Finally, *Chapter 6* concludes the thesis by summarizing the key findings and proposing recommendations for future research. Additional information is provided in the appendices following the main chapters.

1.4 References

1. Quante M, Matthias V (2006) Water in the Earth ' s atmosphere. J Phys IV 139:37–61
2. Sefiane K (2014) Patterns from drying drops. Adv Colloid Interface Sci 206:372–381. https://doi.org/10.1016/j.cis.2013.05.002
3. Liu Huimin A, Altan MC R (2000) Science and Engineering of Droplets Fundamentals and Applications. Appl Mech Rev 55:. https://doi.org/10.1115/1.1445335
4. Annamalai K, Ryan W, Chandra S (1993) Evaporation of multicomponent drop arrays. J Heat Transfer 115:707–716
5. Chakraborty S, Rosen MA, MacDonald BD (2017) Analysis and feasibility of an evaporative cooling system with diffusion-based sessile droplet evaporation for cooling microprocessors. Appl Therm Eng 125:104–110. https://doi.org/10.1016/j.applthermaleng.2017.07.006
6. Tissot J, Boulet P, Labergue A, et al (2012) Experimental study on air cooling by spray in the upstream flow of a heat exchanger. Int J Therm Sci 60:23–31. https://doi.org/10.1016/j.ijthermalsci.2012.06.005
7. Lanotte L, Laux D, Charlot B, Abkarian M (2017) Role of red cells and plasma composition

on blood sessile droplet evaporation. Phys Rev E 96:53114. https://doi.org/10.1103/PhysRevE.96.053114

8. Wilking JN, Zaburdaev V, De Volder M, et al (2013) Liquid transport facilitated by channels in Bacillus subtilis biofilms. Proc Natl Acad Sci U S A 110:848–852. https://doi.org/10.1073/pnas.1216376110
9. Dugas V, Broutin J, Souteyrand E (2005) Droplet Evaporation Study Applied to DNA Chip Manufacturing. Langmuir 21:9130–9136. https://doi.org/10.1021/la050764y
10. Wang W, Lin J, Schwartz DC (1998) Scanning force microscopy of DNA molecules elongated by convective fluid flow in an evaporating droplet. Biophys J 75:513–520. https://doi.org/10.1016/S0006-3495(98)77540-X
11. Attinger D, Moore C, Donaldson A, et al (2013) Fluid dynamics topics in bloodstain pattern analysis: Comparative review and research opportunities. Forensic Sci Int 231:375–396. https://doi.org/https://doi.org/10.1016/j.forsciint.2013.04.018
12. Popov YO (2005) Evaporative deposition patterns: Spatial dimensions of the deposit. Phys Rev E - Stat Nonlinear, Soft Matter Phys 71:1–17. https://doi.org/10.1103/PhysRevE.71.036313
13. Chini SF, Amirfazli A (2013) Understanding the evaporation of spherical drops in quiescent environment. Colloids and Surfaces 432:82–88. https://doi.org/10.1016/j.colsurfa.2013.05.013
14. Langmuir I (1918) The evaporation of small spheres. Phys Rev 12:368–370. https://doi.org/10.1103/PhysRev.12.368
15. Picknett RG, Bexon R (1977) The evaporation of sessile or pendant drops in still air. J Colloid Interface Sci 61:336–350. https://doi.org/10.1016/0021-9797(77)90396-4
16. Nguyen TAH, Nguyen A V (2012) On the Lifetime of Evaporating Sessile Droplets. Langmuir 28:1924–1930. https://doi.org/10.1021/la2036955
17. Sáenz PJ, Sefiane K, Kim J, et al (2015) Evaporation of sessile drops: A three-dimensional approach. J Fluid Mech 772:705–739. https://doi.org/10.1017/jfm.2015.224
18. Yu DI, Kwak HJ, Doh SW, et al (2015) Dynamics of contact line depinning during droplet evaporation based on thermodynamics. Langmuir 31:1950–1957. https://doi.org/10.1021/la504971y
19. Birdi KS, Vu DT (1993) Wettability and the evaporation rates of fluids from solid surfaces. J Adhes Sci Technol 7:485–493. https://doi.org/10.1163/156856193X00808
20. Bourgès-Monnier C, Shanahan MER (1995) Influence of Evaporation on Contact Angle. Langmuir 11:2820–2829
21. Manger R, Baer E (1962) The evaporation of water drops from a Teflon surface. Chem Eng Sci 17:705–706. https://doi.org/10.1016/0009-2509(62)85029-5
22. Hu H, Larson RG (2002) Evaporation of a sessile droplet on a substrate. J Phys Chem B 106:1334–1344. https://doi.org/10.1021/jp0118322
23. Semenov S, Starov VM, Rubio RG, Velarde MG (2010) Instantaneous distribution of fluxes in the course of evaporation of sessile liquid droplets: Computer simulations. Colloids

Surfaces A Physicochem Eng Asp 372:127–134. https://doi.org/10.1016/j.colsurfa.2010.10.004
24. Shaikeea AJD, Basu S (2016) Evaporating sessile droplet pair: Insights into contact line motion, flow transitions and emergence of universal vaporisation pattern. Appl Phys Lett 108:. https://doi.org/10.1063/1.4953836
25. Shaikeea AJD, Basu S (2016) Insight into the Evaporation Dynamics of a Pair of Sessile Droplets on a Hydrophobic Substrate. Langmuir 32:1309–1318. https://doi.org/10.1021/acs.langmuir.5b04570
26. Birdi KS, Vu DT, Winter A (1989) A study of the evaporation rates of small water drops placed on a solid surface. J Phys Chem 93:3702–3703. https://doi.org/10.1021/j100346a065
27. Erbil HY, McHale G, Newton MI (2002) Drop evaporation on solid surfaces: Constant contact angle mode. Langmuir 18:2636–2641. https://doi.org/10.1021/la011470p
28. McHale G, Rowan SM, Newton MI, Banerjee MK (1998) Evaporation and the wetting of a low-energy solid surface. J Phys Chem B 102:1964–1967. https://doi.org/10.1021/jp972552i
29. Chen X, Ma R, Li J, et al (2012) Evaporation of droplets on superhydrophobic surfaces: Surface roughness and small droplet size effects. Phys Rev Lett 109:116101. https://doi.org/10.1103/PhysRevLett.109.116101
30. Nguyen TAH, Nguyen A V., Hampton, Marc A. Xu, Zhi Ping Huang, Longbin Rudolph V (2012) Theoretical and experimental analysis of droplet evaporation on solid surfaces. Chem Eng Sci 69:522–529. https://doi.org/10.1016/j.ces.2011.11.009
31. Shaikeea A, Basu S, Hatte S, Bansal L (2016) Insights into vapor-mediated interactions in a nanocolloidal droplet system: Evaporation dynamics and affects on self-assembly topologies on macro- to microscales. Langmuir 32:10334–10343. https://doi.org/10.1021/acs.langmuir.6b03024
32. Moon JP and J (2006) Control of Colloidal Particle Deposit Patterns within Picoliter Droplets Ejected by Ink-Jet Printing. Langmuir 22:3506–3513. https://doi.org/10.1021/LA053450J
33. Style RW, Che Y, Park SJ, et al (2013) Patterning droplets with durotaxis. Proc Natl Acad Sci 110:12541–12544. https://doi.org/10.1073/PNAS.1307122110
34. Labowsky M (1976) The effects of nearest neighbor interactions on the evaporation rate of cloud particles. Chem Eng Sci 31:803–813. https://doi.org/10.1016/0009-2509(76)80054-1
35. Chen L, Evans JRG (2009) Arched structures created by colloidal droplets as they dry. Langmuir 25:11299–11301. https://doi.org/10.1021/la902918m
36. Hatte S, Pandey, Keshav Pandey, Khushboo Chakraborty, Suman Basu S (2019) Universal evaporation dynamics of ordered arrays of sessile droplets. J Fluid Mech 866:61–81. https://doi.org/10.1017/jfm.2019.105
37. Pradhan TK, Panigrahi PK (2015) Deposition pattern of interacting droplets. Colloids Surfaces A Physicochem Eng Asp 482:562–567. https://doi.org/10.1016/j.colsurfa.2015.07.013

38. Hatte S, Pandey K, Pandey K, et al (2019) Universal evaporation dynamics of ordered arrays of sessile droplets. J Fluid Mech 866:61–81. https://doi.org/10.1017/jfm.2019.105
39. Wray AW, Duffy BR, Wilson SK (2019) Competitive evaporation of multiple sessile droplets. J Fluid Mech 884:. https://doi.org/10.1017/jfm.2019.919
40. Fabrikant VI (1985) On the potential flow through membranes. ZAMP Zeitschrift für Angew Math und Phys 36:616–623. https://doi.org/10.1007/BF00945301
41. Tonini S, Cossali GE (2022) Analytical modeling of the evaporation of sessile drop linear arrays. Phys Rev E 105:1–13. https://doi.org/10.1103/PhysRevE.105.054803
42. Malcolm S, Azzam A, Amirfazli A (2024) Point source modelling approach for sessile droplet evaporation. Phys Fluids 36:. https://doi.org/10.1063/5.0180908
43. Deegan RD, Bakajin O, Dupont TF, et al (1997) Capillary flow as the cause of ring stains from dried liquid drops. Nature 389:827–829. https://doi.org/10.1038/39827
44. Gelderblom H, Marín ÁG, Nair H, et al (2011) How water droplets evaporate on a superhydrophobic substrate. Phys Rev E - Stat Nonlinear, Soft Matter Phys 83:1–6. https://doi.org/10.1103/PhysRevE.83.026306
45. Sobac B, Brutin D (2011) Triple-line behavior and wettability controlled by nanocoated substrates: Influence on sessile drop evaporation. Langmuir 27:14999–15007. https://doi.org/10.1021/la203681j
46. Carle F, Semenov S, Medale M, Brutin D (2016) Contribution of convective transport to evaporation of sessile droplets: Empirical model. Int J Therm Sci 101:35–47. https://doi.org/10.1016/j.ijthermalsci.2015.10.012
47. Gurrala P, Katre P, Balusamy S, et al (2019) Evaporation of ethanol-water sessile droplet of different compositions at an elevated substrate temperature. Int J Heat Mass Transf 145:. https://doi.org/10.1016/j.ijheatmasstransfer.2019.118770
48. Dash S, Garimella S V. (2014) Droplet evaporation on heated hydrophobic and superhydrophobic surfaces. Phys Rev E - Stat Nonlinear, Soft Matter Phys 89:1–8. https://doi.org/10.1103/PhysRevE.89.042402
49. Gatapova EY, Semenov AA, Zaitsev D V., Kabov OA (2014) Evaporation of a sessile water drop on a heated surface with controlled wettability. Colloids Surfaces A Physicochem Eng Asp 441:776–785. https://doi.org/10.1016/j.colsurfa.2013.05.046
50. Sobac B, Brutin D (2012) Thermal effects of the substrate on water droplet evaporation. Phys Rev E - Stat Nonlinear, Soft Matter Phys 86:1–10. https://doi.org/10.1103/PhysRevE.86.021602
51. Kelly-Zion PL, Pursell CJ, Vaidya S, Batra J (2011) Evaporation of sessile drops under combined diffusion and natural convection. Colloids Surfaces A Physicochem Eng Asp 381:31–36. https://doi.org/10.1016/j.colsurfa.2011.03.020
52. Carle F, Sobac B, Brutin D (2013) Experimental evidence of the atmospheric convective transport contribution to sessile droplet evaporation. Appl Phys Lett 102:. https://doi.org/10.1063/1.4792058
53. Chou WL, Lee PY, Yang CL, et al (2015) Recent advances in applications of droplet

microfluidics. Micromachines 6:1249–1271. https://doi.org/10.3390/mi6091249
54. Schneider T, Kreutz J, Chiu DT (2013) The potential impact of droplet microfluidics in biology. Anal Chem 85:3476–3482. https://doi.org/10.1021/ac400257c
55. Daniel S, Chaudhury MK, Chen JC (2001) Fast drop movements resulting from the phase change on a gradient surface. Science (80-) 291:633–636. https://doi.org/10.1126/science.291.5504.633
56. Lu Y, Sathasivam S, Song J, et al (2015) Robust self-cleaning surfaces that function when exposed to either air or oil. Science (80-) 347:1132–1135. https://doi.org/10.1126/science.aaa0946
57. Theberge AB, Courtois F, Schaerli Y, et al (2010) Microdroplets in microfluidics: An evolving platform for discoveries in chemistry and biology. Angew Chemie - Int Ed 49:5846–5868. https://doi.org/10.1002/anie.200906653
58. Chowdhury IU, Sinha Mahapatra P, Sen AK (2019) Self-driven droplet transport: Effect of wettability gradient and confinement. Phys Fluids 31:. https://doi.org/10.1063/1.5088562
59. Zhang P, Peng B, Wang J, Jiang L (2019) Bioinspired Self-Propulsion of Water Droplets at the Convergence of Janus-Textured Heated Substrates. Adv Funct Mater 29:1–8. https://doi.org/10.1002/adfm.201904535
60. Li P, Cao M, Bai H, et al (2019) Unidirectional Liquid Manipulation Via an Integrated Mesh with Orthogonal Anisotropic Slippery Tracks. Adv Funct Mater 29:1–7. https://doi.org/10.1002/adfm.201904446
61. Irajizad P, Ray S, Farokhnia N, et al (2017) Remote Droplet Manipulation on Self-Healing Thermally Activated Magnetic Slippery Surfaces. Adv Mater Interfaces 4:1–7. https://doi.org/10.1002/admi.201700009
62. Wixforth A, Strobl C, Gauer C, et al (2004) Acoustic manipulation of small droplets. Anal Bioanal Chem 379:982–991. https://doi.org/10.1007/s00216-004-2693-z
63. Abdelgawad M, Wheeler AR (2009) The digital revolution: A new paradigm for microfluidics. Adv Mater 21:920–925. https://doi.org/10.1002/adma.200802244
64. Tang X, Zhu P, Tian Y, et al (2017) Mechano-regulated surface for manipulating liquid droplets. Nat Commun 8:1–10. https://doi.org/10.1038/ncomms14831
65. Gallardo BS, Gupta VK, Eagerton FD, et al (1999) Electrochemical principles of active control of liquids on submillimeter scales. Science (80-) 283:57–60. https://doi.org/10.1126/science.283.5398.57
66. Mertaniemi H, Jokinen V, Sainiemi L, et al (2011) Superhydrophobic tracks for low-friction, guided transport of water droplets. Adv Mater 23:2911–2914. https://doi.org/10.1002/adma.201100461
67. Berná J, Leigh DA, Lubomska M, et al (2005) Macroscopic transport by synthetic molecular machines. Nat Mater 4:704–710. https://doi.org/10.1038/nmat1455
68. Kavokine N, Anyfantakis M, Morel M, et al (2016) Light-Driven Transport of a Liquid Marble with and against Surface Flows. Angew Chemie - Int Ed 55:11183–11187. https://doi.org/10.1002/anie.201603639

69. Ichimura K, Oh SK, Nakagawa M (2000) Light-driven motion of liquids on a photoresponsive surface. Science (80-) 288:1624–1626. https://doi.org/10.1126/science.288.5471.1624
70. Khalil KS, Mahmoudi SR, Abu-Dheir N, Varanasi KK (2014) Active surfaces: Ferrofluid-impregnated surfaces for active manipulation of droplets. Appl Phys Lett 105:. https://doi.org/10.1063/1.4891439
71. Zhao Y, Fang J, Wang H, et al (2010) Magnetic liquid marbles: Manipulation of liquid droplets using highly hydrophobic Fe3O4 nanoparticles. Adv Mater 22:707–710. https://doi.org/10.1002/adma.200902512
72. Brunet P, Eggers J, Deegan RD (2007) Vibration-induced climbing of drops. Phys Rev Lett 99:3–6. https://doi.org/10.1103/PhysRevLett.99.144501
73. Chaudhury MK, Whitesides GW, Lee SW, et al (1992) On-chip manipulation of free droplets Tiny free-floating drops can be driven across a liquid medium by an electric field. Curr Opin Coll Interface Sci 256:2240–2243
74. Gascoyne PRC, Vykoukal J V., Schwartz JA, et al (2004) Dielectrophoresis-based programmable fluidic processors. Lab Chip 4:299–309. https://doi.org/10.1039/b404130e
75. Chaudhury MK, Whitesides GM (1992) How to Make Water Run Uphill. Science (80-) 256:1539–1541. https://doi.org/10.1126/science.256.5063.1539
76. Wang Z, Orejon D, Takata Y, Sefiane K (2022) Wetting and evaporation of multicomponent droplets. Phys Rep 960:1–37. https://doi.org/10.1016/j.physrep.2022.02.005
77. Sadafi H, Dehaeck S, Rednikov A, Colinet P (2019) Vapor-Mediated versus Substrate-Mediated Interactions between Volatile Droplets. Langmuir 35:7060–7065. https://doi.org/10.1021/acs.langmuir.9b00522
78. Benusiglio A, Cira N, Lai AW, Prakash M (2017) Two-component self-contracted droplets: long-range attraction and confinement effects. 2:1–8
79. You A, Be MAY, In I (2020) Evaporation-induced transport of a pure aqueous droplet by an aqueous mixture droplet Evaporation-induced transport of a pure aqueous droplet by an aqueous mixture droplet. 032003: https://doi.org/10.1063/1.5139002
80. Shi S, Man X, Russell TP (2019) Soft Matter. 15:. https://doi.org/10.1039/c8sm02584c
81. Wen Y, Kim PY, Shi S, et al (2019) Vapor-induced motion of two pure liquid droplets. Soft Matter 15:2135–2139. https://doi.org/10.1039/C8SM02584C
82. Man X, Doi M (2017) Vapor-Induced Motion of Liquid Droplets on an Inert Substrate. Phys Rev Lett 119:44502. https://doi.org/10.1103/PhysRevLett.119.044502
83. Cira NJ, Benusiglio A, Prakash M (2015) Vapour-mediated sensing and motility in two-component droplets. Nature 519:446–450. https://doi.org/10.1038/nature14272

Chapter 2 Modeling of the Evaporation Process of a Pair of Sessile Droplets Using a Point Source Model (PSM) [1]

2.1 Introduction

The evaporation of sessile droplets has applications which range from combustors to everyday phenomena such as coffee ring stain formation [1]. Evaporation can be used to control the temperature and humidity of the upstream airflow of heat exchangers and enhance its efficiency [2] and control the temperature of microprocessors through evaporative cooling [2]. Other applications are DNA mapping by studying the fluid flow of DNA solution inside an evaporating droplet [3], inkjet printing for documents and proteins [4], [5], the paint industry [6], and protein crystallography [7].

The droplet evaporation process is dynamic because the shape of the droplet changes as it evaporates. Picknett and Bexon [8] were among the first to observe three modes of evaporation by using droplets of methyl acetoacetate on a polytetrafluoroethylene (PTFE) substrate: these were constant contact angle (CCA) evaporation mode, constant contact radius (CCR) mode, and mixed mode alternating between CCA and CCR through the stick-slip phenomenon.

CCA mode is characterized by decreasing the contact radius while the contact angle is constant [9], [10], while for the CCR mode, the contact angle decreases with a pinned contact line [11], [12]. There is also a simultaneous decrease in contact angle and pinned contact line for the mixed evaporation mode [8], [13]. It is well known from previous experimental work that the evaporation mode of a water droplet placed on a hydrophilic surface is dominated by the CCR

[1] *This chapter has been published as a peer-reviewed journal article under the same title in the International Communications in Heat and Mass Transfer journal.*

(i.e., the initial contact angle > 90°) [14]. It has been suggested that the difference between the advancing contact angle (θ_{Adv}) and receding contact angle (θ_{Recd}), also known as contact angle hysteresis (CAH), can help determine the mode of evaporation [13], [15]. If the θ_{Recd} of a droplet on a surface is very small (i.e., ≈ 0), evaporation would be purely in CCR mode. On the other hand, if the $\theta_{Recd} < \theta_0 < \theta_{Adv}$, the droplet initially evaporates in CCR mode until the contact angle decreases from initial contact angle, θ_0, to be equal to the receding contact angle (θ_{Recd}). At this angle, θ_{Recd}, the droplet starts evaporating in CCA mode until the end of evaporation process [16], [17].

Most naturally occurring and practical droplet evaporation scenarios involve the evaporation of arrays of droplets rather than a single isolated droplet [18]–[20]. The behavior of an array of droplets can be to a certain degree be understood by the study of single sessile droplets and, as such, many research efforts have been carried out to gain insight into the evaporation process of single droplets [6], [8], [10], [11], [14], [16], [21], [22]. While these studies are helpful, the transfer rate (energy, mass, or momentum) from an array of droplets differs due to the interaction between the droplets [23]. A further step toward understanding the behavior of an array of droplets is to study the evaporation process of two adjacent droplets [18], [24]–[26].

In most applications, the sessile droplet evaporation process is not like the evaporation process of contact-free (i.e., suspended) droplets. While the evaporation flux over the surface of a free suspended droplet can be assumed to be constant, this is not the case for a sessile droplet due to the presence of the substrate. The evaporation flux over the surface of a sessile droplet depends on the droplet's contact angle (i.e., surface wettability). The magnitude of the evaporation flux for a droplet on a hydrophilic surface is higher at the contact line than at the droplet apex [21],

[25], [27]. However, a droplet on a hydrophobic surface has a greater evaporation flux at the droplet apex than at the base [25].

When two droplets are placed on a substrate surface sufficiently close to each other, a "wedge" region is formed between them (see **Figure 2-1**). In the wedge region, vapor accumulation decreases the evaporation rate; this was first reported in [28]. Due to the increased vapor concentration in the wedge region, the lifetime of the droplet increases [29]. Furthermore, increasing the hydrophobicity of the substrate for a single isolated droplet leads to increased vapor accumulation in the region close to the substrate, creating a vapor-trapped area near the contact line. This increase in vapor concentration reduces the evaporation flux in this area. However, the presence of another droplet leads to a further decrease in the evaporation flux [24], [25]. The spatiotemporal variation of the evaporation flux must be considered to model the evaporation process of two droplets precisely.

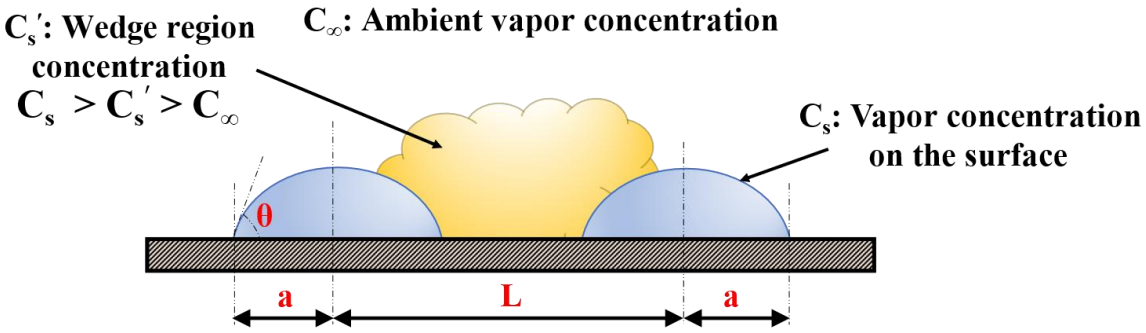

Figure 2-1 Schematics of a central (midplane) sectional plan of a pair of sessile droplets considered as spherical cap drying on a substrate surface. Where: L is the separation distance between the droplets, a is the droplet's contact radius, and θ is the droplet contact angle.

The evaporation process of sessile droplets on an unheated substrate in quiescent ambient air is involved in many practical applications (e.g., DNA mapping). However, modeling the evaporation process of two sessile droplets from an unheated substrate, considering the non-

uniformity of the evaporation flux and the moving surface due to mass loss, requires immense computational power. Therefore, the objective of this study is to model the evaporation process of two sessile droplets by using our previously defined PSM approach [30]. The main advantage of this modeling approach is that it captures the main features of the process with minimum computational requirements. In this method, the droplets are modeled as point sources to remove the complexities associated with coupled mass and heat transfer at the moving interface. The droplet is treated as a point source located at the center of the droplet. Also, the surface area of the droplets may be determined by treating them as spherical caps and applying the principles of mass conservation and geometric constraints. The PSM was developed by analytical analogy to the work of Castillo et al. [31] in which they modeled the condensation process of a droplet by using the point sink model; the droplets in [31] were modeled as point sinks to determine the condensation rate of individual droplets in an array of droplets.

The PSM was employed to systematically examine the impact of the separation distance between the droplets on the rate of evaporation. As such, a critical distance beyond which the two droplets behave like single isolated droplets can be identified. Two relationships to determine the evaporation time of the droplets corresponding to the evaporation mode (i.e., CCA and CCR) were derived. The CCR mode relation is examined experimentally to test the validity of the proposed model. Also, variations in evaporation rate, the contact angle for CCR evaporation mode, and the contact radius for CCA evaporation mode with evaporation time were examined. Finally, the present model was examined to establish its limitations by investigating the impacts of droplet volume, relative humidity, surface wettability, and liquid volatility.

2.2 Model Formulation

The evaporation process of sessile droplets has many complexities; therefore, it is common to simplify the modelling process by neglecting the variation of droplet surface temperature [32]. This is justified because the evaporation of sessile drops in a quiescent environment is a slow process and, thus, the temperature gradients due to the latent heat of vaporization are very small compared with those of rapidly evaporating droplets [33]. We also assume that when the size of the sessile droplet is small (i.e., in the range of μl), it is reasonable to assume that the droplet has a spherical shape [8], [11], [14], [21]. This is justifiable because the droplet shape is governed by the Bond number (ratio of the gravitational force to the surface tension on the droplet's surface) and the capillary number (ratio of the viscous force to capillary force). Therefore, the shape can be considered a spherical cap for a droplet of small Bond and capillary numbers ($<< 1$).

The relatively slow evaporation rate allows us to assume that the mass transport from a sessile droplet is purely diffusive with negligible convection. As such, the evaporation rate depends on either the transfer rate of molecules across the liquid/vapor interface (phase change) or the transport rate of the saturated vapor molecules from the droplet surface to the surrounding air [6], [34]. The transfer rate is characterized by a time scale of an order of 10^{-10} s, while the transport rate due to diffusion has a characteristic time of a^2/D, (where D is the diffusion coefficient for the vapor in the air and a is the radius of the droplet); for water under normal evaporation conditions, the characteristic time is in the order of seconds [6], [35]. The transport rate of vapor molecules from the droplet surface to the surrounding air is governed by diffusion, convection, or both [36]. It has been found experimentally that the evaporation of non-volatile drops at room temperature is dominated by diffusion and not convection [9], [11], [14], [37], [38].

The time required for the concentration field to adjust to the change in the droplet size is of order of (a^2/D) for non-volatile liquids, e.g., water. The ratio between this time a^2/D and the evaporation time of the droplet (t_e) is of the order of $a^2/D.t_e \approx 10^{-5}$ [21]. Considering all of the above, it is acceptable to assume that the evaporation process is steady-state and purely diffusive. Also, assumptions such as the Maxwell assumptions [39] have been applied to successfully determine the evaporation rate of sessile drops in isolation [8]–[12], [14], [34], [36].

2.2.1 Evaporation Rate of a Droplet Within a System of Two Droplets ($\dot{m}_{sys}$)

Using Maxwellian models [39] for sessile droplets and neglecting the effect of the substrate, we start by assuming the evaporation flux on the free surface of a sessile droplet is equal to that of a suspended droplet of the same radius of curvature [36]. The substrate effect will be addressed later. By approximating the surface area of the droplet as a spherical cap $\frac{2\pi\, a^2}{1+cos\theta}$, the total evaporation rate from the surface of a single isolated sessile droplet, $\dot{m}_{iso}$, is given by [12]:

$$\dot{m}_{iso} = \frac{dm}{dt} = J.S = -2\pi aD\, \frac{sin\theta}{1+cos\theta}\, (C_s - C_\infty) \qquad (2\text{-}1)$$

where J is the evaporation flux, S is the droplet surface area, (θ) is the contact angle of the droplet, and (C_s) and (C_∞) are the vapor concentration at the droplet surface and far field, respectively.

Because of the substrate, the evaporation rate ($\dot{m}_{iso}$) should be modified from the Maxwellian model. This is done by applying a multiplier $f(\theta)$ which is a geometrical factor that describes the effect of the contact angle of the droplet and the impermeable substrate [10]. Picknett and Bexon [8] derived an exact solution for $f(\theta)$ by comparing the diffusive flux to the electrostatic potential. They achieved this by calculating the capacitance of a conducting substance with the same shape and size as the droplet, considering contact angles ranging from 10° to 180°. Rowan et al. [12]

found a different method to determine $f(\theta)$ by assuming that the vapor concentration gradient is radially outward only. Another approximated method was developed by Bourges-Monnier and Shanahan [9]; they also assumed that the vapor concentration gradient is purely radial. However, they considered a shell around the droplet, where vapor diffused. It should be noted that in [8], [9], [12], there is no proof that the authors considered the variation of the evaporation flux over the surface of the droplet [36] (i.e., the evaporation flux was assumed to be uniform over the droplet's surface, which is similar to that of a suspended spherical droplet). Chini and Amirfazli [36] provided a closed-form equation, Eq. (2-2), for $f(\theta)$, incorporating the non-uniformity of evaporation flux. This equation is more straightforward and can be used with an error of less than 5% within the range of $8° \leq \theta \leq 131°$.

$$f(\theta)_{[36]} = 56.561\theta^{-0.892} \tag{2-2}$$

Combining Eq. (2-1) and Eq.(2-2), we arrive at Eq. (2-3) which describes the evaporation rate for a sessile drop with both flux variation and the effect of θ captured.

$$\dot{m}_{iso} = \frac{dm}{dt}.f(\theta) = J.S.f(\theta) = -2\pi\, a\, D\, \frac{sin\theta}{1+cos\theta}\,(C_s - C_\infty)\, f(\theta) \tag{2-3}$$

The presence of a second droplet adds further complexity to determination of the evaporation rate of a single droplet in the compilation of two droplets. So, it is beneficial to simplify the solution of the evaporation rate of each droplet in the system by considering a correction factor, η. The correction factor, η, is given by the ratio of the evaporation rate associated with a pair of droplets ($\dot{m}_{sys}$) to that for single isolated droplet ($\dot{m}_{iso}$). In such an approach, the size and the ambient conditions for the droplet system are considered to be the same [1], [23], [25], [40].

$$\eta = \frac{\dot{m}_{sys}}{\dot{m}_{iso}} \tag{2-4}$$

The value of η for two identical sessile droplets sitting on a substrate and separated by distance L can be obtained by an analogy to that developed by Castillo et al. [31] and Annamalai et al. [1].

$$\eta = \frac{1 - \frac{a}{L}}{1 - \frac{a^2}{L^2}} \tag{2-5}$$

Using Eqs. (2-3) to (2-5), the evaporation rate of a droplet in a system of two droplets can be determined by

$$\dot{m}_{sys} = \eta . \dot{m}_{iso} = \frac{1 - \frac{a}{L}}{1 - \frac{a^2}{L^2}} \times \left[-2\pi \, a \, D \, \frac{sin\theta}{1 + cos\theta} \, (C_s - C_\infty) \, 56.561\theta^{-0.892} \right] \tag{2-6}$$

2.2.2 Evaporation Time of Two Droplets (t_e)

Equation (2-6) has three unknowns, *a*, θ, and $\dot{m}_{sys}$. Through $\dot{m}_{sys} = \rho_L . \frac{dV}{dt}$ (see **Figure 2-1**), the unknowns can be reduced to two; the volume of the droplet can be related to *a* and θ. Thus, to determine the evaporation time, it is required to find another equation. The needed equation can be found by knowing the evaporation mode; then, we can determine the evaporation time, as explained below.

2.2.2.1 CCA Mode

The volume of a spherical cap droplet, in terms of *a* and θ, is

$$V = \frac{\pi(1 - cos\theta)(cos\theta + 2) \, a^3}{3 . sin\theta(1 + cos\theta)} \tag{2-7}$$

From Eqs. (2-6) and (2-7), recalling that $\dot{m}_{sys} = \rho_L . \frac{dV}{dt}$, we can find the variation of the contact radius *a* during the evaporation process, as follows:

$$\frac{a^3 - a_0^3}{3} - \frac{a^2 - a_0^2}{2} = \frac{-2LD}{\rho_L}\,(C_S - C_\infty)\,\frac{1 + cos\theta}{2 + cos\theta} f(\theta)\; t_e \qquad (2\text{-}8)$$

where a_0 is the initial contact radius of the droplet. Note a is a function of time, t, i.e., $0 < t < t_e$ (where t_e is the droplet's evaporation time). Eq. (2-8) can be used together with a=0 to find the evaporation time. Also, d_0 and d, are the initial and instantaneous contact diameter of the droplet, respectively.

2.2.2.2 Constant Contact Radius (CCR) Mode

The volume of a spherical cap droplet in terms of a and the height of the droplet, h, is

$$V = \frac{\pi h}{6}(3a^2 + h^2) \qquad (2\text{-}9)$$

From Eqs. (2-6) and (2-9) and recalling that $\dot{m}_{sys} = \rho_L . \frac{dV}{dt}$, one can find the variation of the contact angle during the evaporation process, as follows:

$$\int_{\theta_0}^{\theta_f} \frac{\theta^{0.892}}{56.561\; sin\theta\;\; (1 + cos\theta)}\, d\theta = \frac{-2LD(C_S - C_\infty)}{(a + L)\;\; a^2\, \rho_L}\; t_e \qquad (2\text{-}10)$$

where θ is the instantaneous contact angle of the droplet at any given time $0 < t < t_e$, and θ_0 is the initial contact angle of the droplet, and θ_f is the droplet's final contact angle. Eq. (2-10) can be used to find the evaporation time by setting θ_f =0. We neglected the effect of the droplet contact angle hysteresis at this stage and assumed that the droplet's receding contact angle is zero. The full derivations of Eqs. (2-8) and (2-10) are detailed in the Supplementary Information.

It should be noted that "L/d_0" and "L/d" may vary depending on the evaporation mode. "L/d_0" is equal to "L/d" for droplets undergoing the Constant Contact Radius (CCR) evaporation mode.

However, they are not equal for droplets undergoing the Constant Contact Angle (CCA) mode, reflecting the differences in evaporation behavior under these distinct conditions.

2.2.3 Model Novelty and Significance

In our model, we incorporate $f(\theta)$ to characterize the influence of the substrate. While prior studies have explored various techniques to determine $f(\theta)$ (e.g. (e.g. [8], [14], [41]), none explicitly address the variation of evaporation flux along the surface of sessile droplets. Even Picknett and Bexon [8], the only study providing an exact solution for $f(\theta)$, lacks explicit reference to this variation. In contrast, our model employs a closed-form equation for $f(\theta)$ derived by Chini and Amirfazli [36], explicitly incorporating the non-uniformity of evaporation flux.

Existing semi-analytical models, such as those proposed by Shaikeea et al. [24,25], are limited in scope to specific contact angles (115°), fluid types (water), with unclear evaporation modes. Similar limitations are observed in another semi-analytical model proposed by Hatte et al. [42], where certain factors are contingent on specific experimental conditions. In contrast, our Point Source Model (PSM) accommodates simulations in both Constant Contact Angle (CCA) and Constant Contact Radius (CCR) modes, offering a comprehensive understanding of evaporation dynamics across various scenarios.

Wilson et al. [43] introduced an asymptotic analytical model for the evaporation of multiple sessile droplets, leveraging the integral approach proposed by [44]. However, their model's complexity and restriction to thin droplets pose limitations. In contrast, the PSM that considers droplets with different contact angles, simplifying complexities associated with coupled mass

and heat transfer dynamics at the moving interface, by modeling droplets as point sources located at droplets' centers.

Finally, Tonini and Cossali [45] proposed analytical and numerical models for the evaporation of sessile droplet linear arrays. Their analytical model involves solving Laplace's equation to determine concentration values at specific locations, introducing complexity with terms such as the Legendre function of the first kind with complex index. For their numerical solution, they adopted a 3D numerical approach utilizing COMSOL Multiphysics. Our PSM yields comparable results with deviations of less than 5% in most cases considered by [45] (see **Table 2-1**). So, we can conclude that PSM serves as a versatile predictive tool, streamlining the determination of vapor concentration distributions. By striking a delicate balance between capturing essential process phenomena and minimizing computational complexity, our model addresses the challenges associated with accurately modelling sessile droplet evaporation. These challenges include accounting for the dynamic nature of the droplet interface, evaporation mode, coupled mass and heat transfer dynamics, and the non-uniformity of evaporative flux within a computationally light framework.

Table 2-1 Comparison between the correction factor from the proposed PSM and from the analytical and numerical models proposed by [45]

L/d	θ = 90°		θ = 135°		θ = 45°		η (PSM)	Deviations (%) Min. ➔ Max.
	η_a [45]	η_n [45]	η_a [45]	η_n [45]	η_a [45]	η_n [45]		
2	0.8024	0.8026	0.767	0.7728	0.8859	0.8829	0.8	0.30 ➔ 9 %
5	0.9086	0.9092	0.8853	0.8873	0.9506	0.9497	0.9091	0.06 ➔ 4 %
10	0.9524	0.9524	0.9395	0.9395	0.9766	0.9742	0.9524	0.00 ➔ 2 %

In summary, PSM offers a robust and computationally efficient solution that not only addresses above challenges, but also provides valuable insights into the complex process of sessile droplet evaporation, thereby advancing our understanding of this phenomenon.

2.2.4 Experimental Apparatus

An experimental apparatus was designed and constructed to establish the validity and limitations of the proposed model. The experimental setup is shown in **Figure 2-2**. The droplets were placed on the substrate by using a motorized syringe pump (KDS 100, KD Scientific) with an accuracy of ±0.93%. The distance between the droplets was controlled by using a linear X-stage with an accuracy of ± 0.01 mm. For image processing, two cameras (**Figure 2-2**, Camera I and Camera II) were employed to capture the variation in droplet contact angle and contact radius through evaporation time. Camera I and Camera II (Plugable, 2MP, 250x Magnification) were vertically and horizontally mounted, respectively. The Contact Angle plugin in Image J was used to measure the contact angle of the droplets. All experiments were carried out inside a humidity-controlled chamber with dimensions of L=200 mm, W=167 mm, and H=90 mm. The relative humidity inside the chamber was controlled by a programmable humidity controller (IHC200, Inkbird). The humidity controller can keep the relative humidity in a range of 5%–99 % with an accuracy of ± 3%.

Experiments were conducted to examine the variation in evaporation time and contact angle for a pair of sessile water droplets sitting on a glass substrate. The substrate was a clean microscopic glass slide treated with a Rust-Oleum Never Wet Step 1 base coat to enhance the surface roughness. This was done to immobilize the contact line of the droplet and achieve the CCR mode. The initial contact angle of the water droplet was 81.5°±4.5°. For different separation

distances (3–25 mm), the evaporation time was measured and compared with the corresponding one from the model. For each separation distance, the measurements were repeated five times.

The effect of surface wettability on the evaporation behavior of a pair of sessile droplets was examined using two additional surfaces (pre-treated glass and Teflon). Each surface was, firstly, washed by ethanol; then, it was rinsed with deionized water before it was heated in an oven at 65ºC for two hours. The surfaces were left overnight before they were used in the experiments. The corresponding initial contact angles for the coated glass, pre-treated glass, and pre-treated Teflon surfaces were 81.5° ± 4.5°, 51.4 ° ± 2.8° and 114.5 ° ± 1.1°, respectively. The receding contact angles for the pre-treated glass and pre-treated Teflon surfaces were 14.5° ± 0.8° and 74.2° ± 5.3°, respectively. Finally, the evaporation time for a pair of ethanol sessile droplets on a glass surface at different separating distances was measured and compared with that of the model.

Initially, the evaporation of two droplets of 3.0 ± 0.028 μl at different distances were studied. The relative humidity inside the chamber was kept at 40% ± 3%. The experiments were carried out in a laboratory temperature of 22–23℃. Then, the evaporation for a pair of sessile droplets at different relative humidity (RH) values (i.e., 13 %, 20 %, 30 %, and 40 %) was studied.

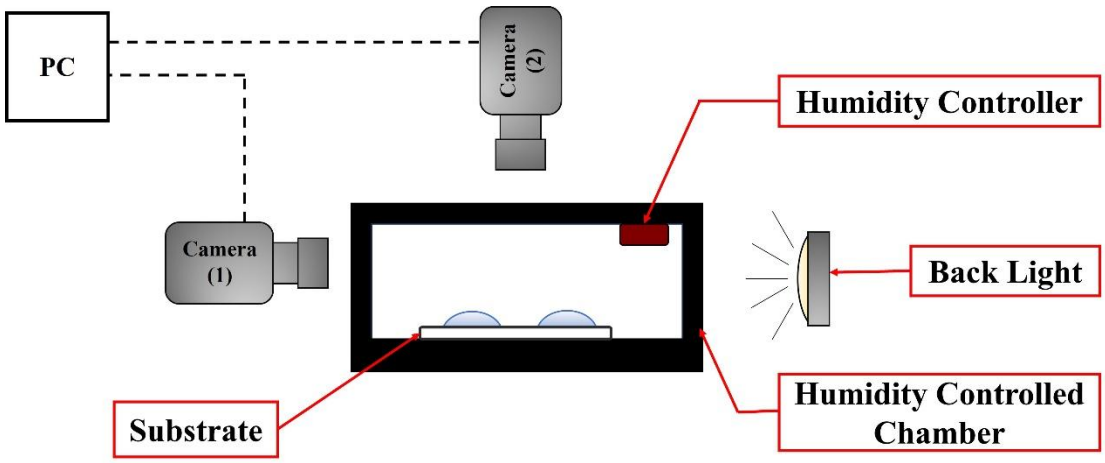

Figure 2-2 Schematic of the experimental apparatus.

2.3 Assumptions and Range of Applicability

For the proposed model we assume the following:

1. The mass transfer process (i.e., evaporation) is assumed to be quasi-steady. This assumption is justified because the time required for the concentration field to adapt to changes in droplet size is on the order of (a^2/D). For non-volatile liquids such as water, the ratio $(a^2/D)/t_e \approx 10^{-5}$, indicating that the adjustment of the concentration field occurs much faster than the overall evaporation process.
2. Convection effects are neglected, assuming diffusion-dominated evaporation. This assumption is valid for both volatile and non-volatile liquids when the Peclet number (Pe), defined as the ratio of convective to diffusive mass transfer, is less than 1.
3. The system is assumed to be isothermal, neglecting variations in droplet surface temperature. This assumption is justified for non-heated substrates where evaporation proceeds slowly enough that temperature gradients induced by latent heat of vaporization are minimal.

2.4 Results and Discussion

2.4.1 Model Validation

The validity of the model predictions were first evaluated by comparing the predicted evaporation times with the measured evaporation time for droplets evaporating under CCR mode, which is the common evaporation mode of water droplets on a glass substrate. Also, the variations of the contact angle were compared with the experimental measurements.

Figure 2-3.a shows the inverse proportional relationship between the evaporation time and the separating distance between the droplets. It is expected that increasing the distance between the droplets decreases the effect of the wedge area and, hence, increases the evaporation rate. Also, **Figure 2-3.a** shows that the experimental results are in excellent agreement with the model predictions with a variation of less than 5%. A similar conclusion is obtained **Figure 2-3.b** for variations in the droplet's contact angles with the normalized instantaneous evaporation time (t/t_e).

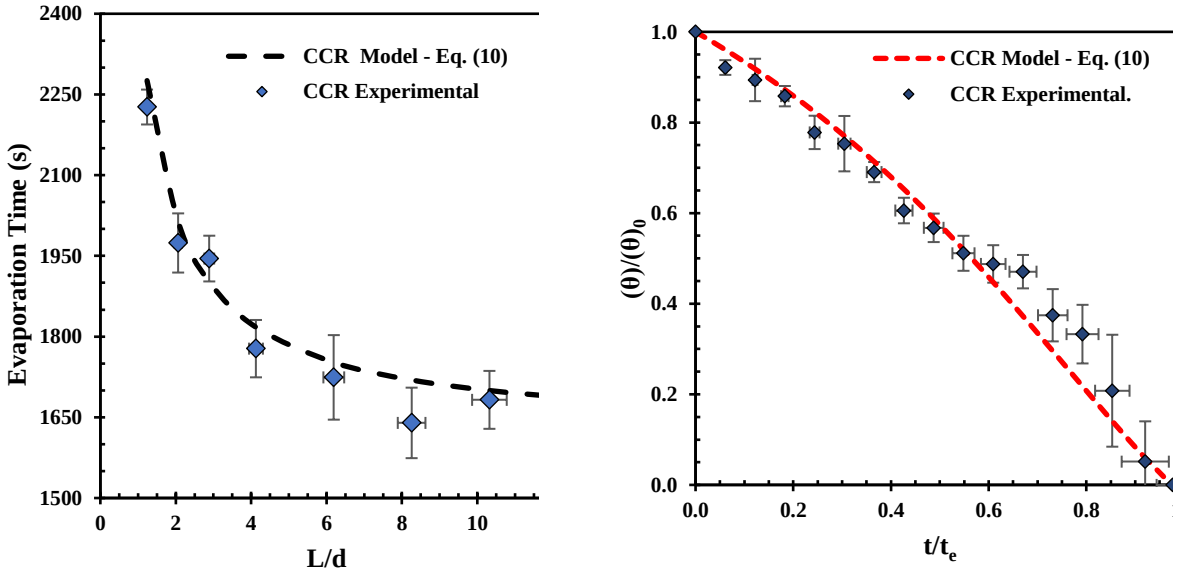

Figure 2-3 (a) Variation of evaporation time for a pair of water sessile droplets (V= 3.0 µL) on a coated glass substrate at different distances (L/d). (b) Variation of the normalized contact angle with normalized instantaneous evaporation time. The relative humidity was 40%.

Figure 2-4 shows the variation in the evaporation time of a pair of water sessile droplets at different volumes. It can be observed that increasing the volume of the droplet leads to longer evaporation time at the same ambient conditions. Overall, agreement between the measured evaporation time and model predictions are very good with deviations of less than 5% as the droplet volume increases.

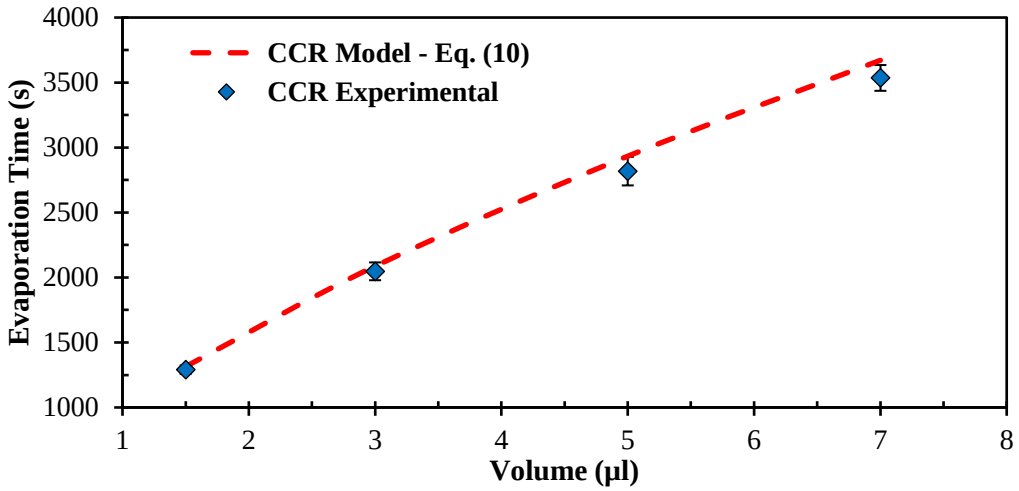

Figure 2-4 Variation of evaporation time for a pair of water sessile droplets (L/d= 1.741) on a coated glass substrate for different droplet volumes. The relative humidity was 40%.

Figure 2-5 shows the experimental evaporation time has a direct proportionality with the relative humidity (RH). This is reasonable and expected, because an increase in the amount of water vapor in the ambient air leads to a decrease in the concentration difference (difference in water vapor concentration) between the surface of the droplets and the ambient air. This leads to a decrease in the evaporation rate and an increase in evaporation time. Also, as shown in **Figure 2-5**, there is a good agreement between the model and the experimental results with differences of less than 9%. Increasing relative humidity to more than 40% slows evaporation, confirms the

purely diffusive mass transfer assumption, and improves model-experimental agreement. Therefore, we did not need to test the evaporation process for relative humidity higher than 40%. While the number of data points in **Figure 2-4** and **Figure 2-5** are limited, we can observe that the trends are reasonable and expected from a physics perspective and we do not expect any sudden change in trend between the data reported. While increasing the number of data points may enhance visualization, the existing trends remain consistent and align with theoretical expectations.

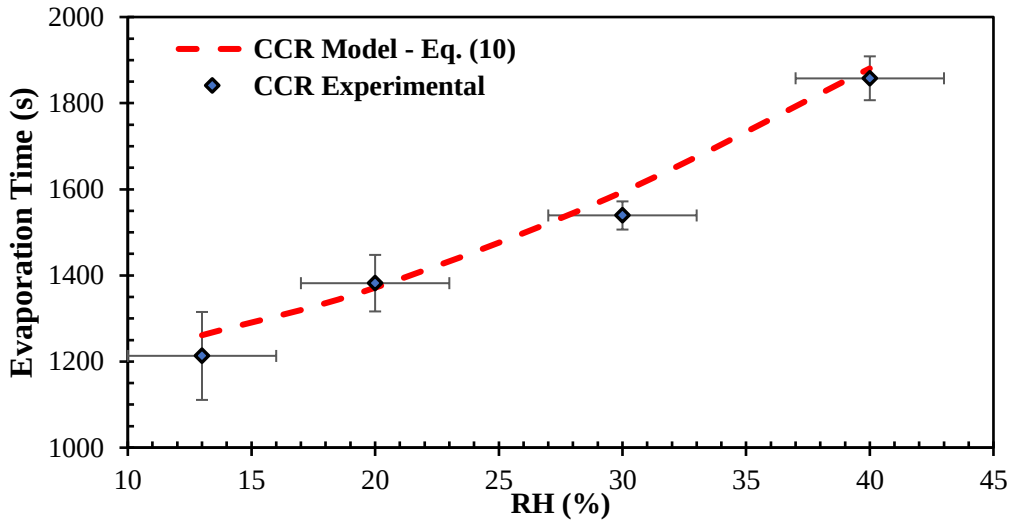

Figure 2-5 Variation of evaporation time for a pair of water sessile droplets (V= 3.0 µL) separated by constant L/d value of (2.064) on a coated glass substrate at different relative humidities.

Regarding the effect of the surface wettability, it was found that water droplets on Teflon and the pre-treated glass do not completely evaporate in CCR mode. As the evaporation takes place, the contact angle of the droplet decreases while its contact line is pinned. The CCR evaporation mode ends when the droplet's contact angle reaches the receding contact angle value, and the contact line begins to move. It was found that 70% of the evaporation time for water droplets on the pre-treated glass surface occurs in CCR mode; this was 58% for Teflon. Therefore, the

evaporation times for water droplets evaporating on these surfaces are measured from the beginning of the evaporation process until the occurrence of depinning.

Figure 2-6 shows a comparison between experimental evaporation time and predicted values. **Figure 2-6** was obtained by measuring experimentally, the evaporation times of a pair of sessile water droplets on the three surfaces mentioned in Section-03 and comparing them with the model's predictions. The evaporation time was measured from when the droplets were deposited on the surface to when the contact angle reached the receding angle, see Section-03, at which the contact line started to move and the CCR mode ended. Also, it can be observed from **Figure 2-6** that divergence from the model is reduced if the surface is more hydrophobic. This is because a droplet of the same volume on a hydrophobic surface takes longer to evaporate than one on a hydrophilic one. The hydrophobic nature of the substrate results in the creation of an interlocked space in the region near the droplet. As a consequence, the diffusive transport of water vapor is hindered, leading to a decrease in the evaporation flux. Moreover, the presence of a second droplet, especially when their vapor fields strongly interact, further diminishes the evaporation flux. The continuing decrease in the evaporation rate strongly supports the hypothesis of purely diffusive mass transport, while decreasing the contact angle to less than 90 ^{o} increases the evaporation rate. The higher deviation could be attributed to the convective mass transfer that comes into play. This claim is proven in **Figure 2-7**, in which the vapor concentration distributions around two sessile droplets sitting on hydrophilic (**Figure 2-7.a**) and hydrophobic (**Figure 2-7.b**) surfaces for constant L/d_0=3 value are shown. Where d_0 is the initial contact diameter of the droplet. The initial contact angle for each surface was chosen to be 41° and 120° which are the average contact angles in the literature of water droplets on glass and Teflon surfaces, respectively. The concentration contours were obtained by solving the governing

diffusion equation using finite difference method (FDM; see Supplementary Information for more details). It was found that the average vapor concentration in the wedge area between the two droplets on the hydrophobic surface was 22.7 μg/cm^3, while it was 20.9 μg/cm^3 for the hydrophilic one. It can be concluded that increasing the hydrophobicity of the surface leads to a nearly 9% rise in the evaporation concentration in the wedge area, thereby slowing down the evaporation process. So, **Figure 2-7.a** and **Figure 2-7.b** alongside **Figure 2-6** enhance the comprehensiveness of our analysis and provide a more nuanced understanding of the interplay between surface wettability and evaporation dynamics.

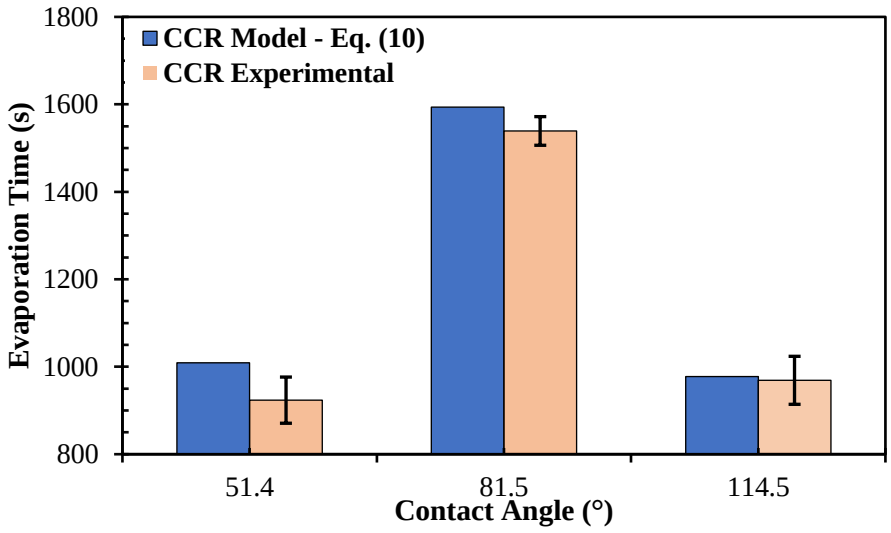

Figure 2-6 Variation of evaporation time for a pair of water sessile droplets (V= 3.0 μL) on different substrates at a constant separating distance L=5 mm. The relative humidity is 30%.

(a) **(b)**

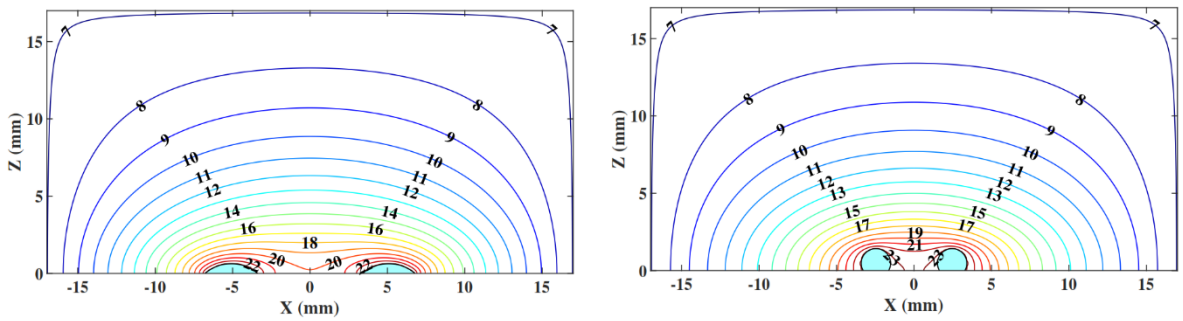

Figure 2-7 Vapor concentration distribution at the midplane around a pair of sessile water droplets of V = 3 µL on a hydrophilic substrate (a), θ_0 = 41°, and a hydrophobic substrate (b), θ_0 = 120° at (L/d_0 =3). All concentration values have units of µg/cm^3.

2.4.2 Model Results

The system used here consisted of a pair of sessile water droplets with initial contact radius and contact angle of 0.2 cm and 45º, respectively. The saturated vapor concentration and the diffusion coefficient were taken to be C_s=2.32x10^{-5} g/cm^3 and D=0.261 cm^2/s, respectively, at an ambient temperature of 25°C [46]. The relative humidity of the ambient was set to 40%.

2.4.2.1 The Effect of the Separation Distance Between the Droplets

Figure 2-8 shows the variation of the normalized evaporation rate ($\frac{\dot{m}_{iso}-\dot{m}_{int}}{\dot{m}_{iso}}$ %) as a function of (L/ d_0). **Figure 2-8** has been standardized to be applicable for any liquid type, any droplet volume, and any ambient relative humidity (RH) value. It is evident that an increase in the separation distance between two droplets results in a decrease in the normalized evaporation rate. This decline is attributed to the increase of the initial evaporation rate ($\dot{m}_{int}$), bringing it closer to that of a single isolated droplet, i.e., ($\dot{m}_{iso} - \dot{m}_{int}$) diminishes. Also, as the distance between the droplets decreases, the vapor concentration in the wedge area increases, leading to a reduction in the evaporation rate of the droplets. Furthermore, **Figure 2-8** illustrates a critical separation

distance, denoted by $L/d_0 \geq 10$, at which the evaporation transitions from a pair of droplets to a single isolated droplet mode, with a difference of less than 5%.

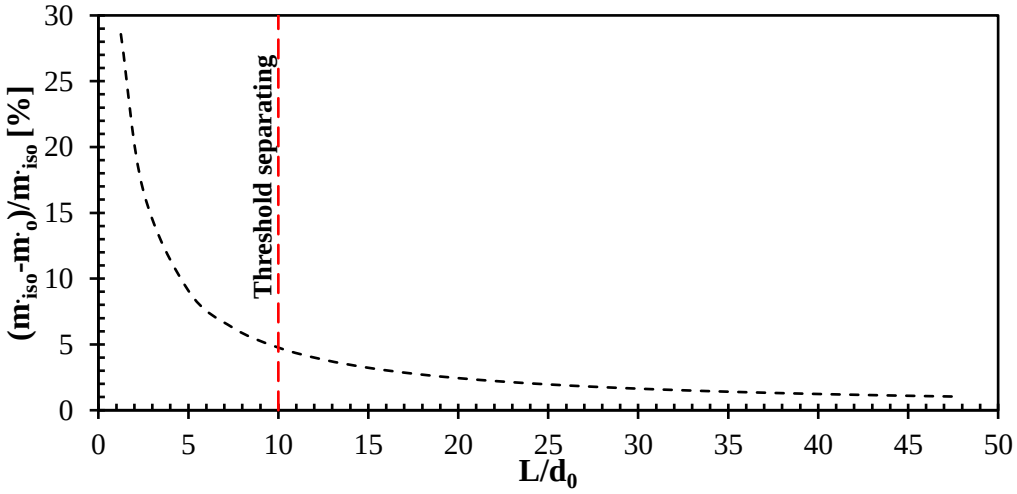

Figure 2-8 Normalized initial evaporation rate for a pair of sessile droplets as a function of L/d_0 as predicted by the proposed model.

2.4.2.2 Effect of Contact Angle and Contact Radius on Evaporation Time.

The objective of this section is to study the variation in the droplet's contact radius and contact angle with evaporation time under CCA and CCR evaporation modes, respectively.

The evaporation time can be calculated using Equation (2-8) or (2-10), depending on the mode of evaporation, by setting a=0 in Eq. (2-8) or θ_f =0 in Eq. (2-10). For each step in time from t=0 until the completion of the evaporation, $t=t_e$, the instantaneous contact angle or contact radius is computed, using either Eq. (2-8) or Eq. (2-10), depending on the evaporation mode.

Figure 2-9.a shows the linear decrease of $(a/a_0)^2$ with normalized instantaneous evaporation time (t/t_e) for a pair of water sessile droplets under CCA evaporation mode at different separating distances. It can be observed that all data (symbols) are aligned with the linear trend line (dashed line). This trend can be attributed to the linear decrease in droplet surface area with evaporation

time (**Figure 2-10**). In other words, the surface area of the droplets decreases linearly with the evaporation time.

On the other hand, **Figure 2-9.b** shows the variation of (θ / θ_0) under CCR evaporation mode with evaporation time (t/t_e) for different values of initial contact angles, θ_0. It can be observed that increasing the hydrophobicity of the substrate delays the decreasing rate of the contact angle and distorts its linear decrease. The reason for this non-linear behavior is that when the contact angle is greater than 90°, a restricted area near the contact line of the droplet is formed. This area leads to a higher amount of trapped vapor near the contact line. This vapor hinders the evaporation process. Also, the effect of the second droplet will lead to a further reduction in evaporation near the substrate. It was proven in Section-4.1 that increasing the hydrophobicity of the surface leads to a higher vapor concentration in the wedge are between the droplets (see **Figure 2-7.a** and **Figure 2-7.b**). Therefore, it can be concluded that increasing the vapor concentration in this wedge area decreases the evaporation rate and distorts the linear decrease of the contact angle of a droplet on a hydrophobic surface.

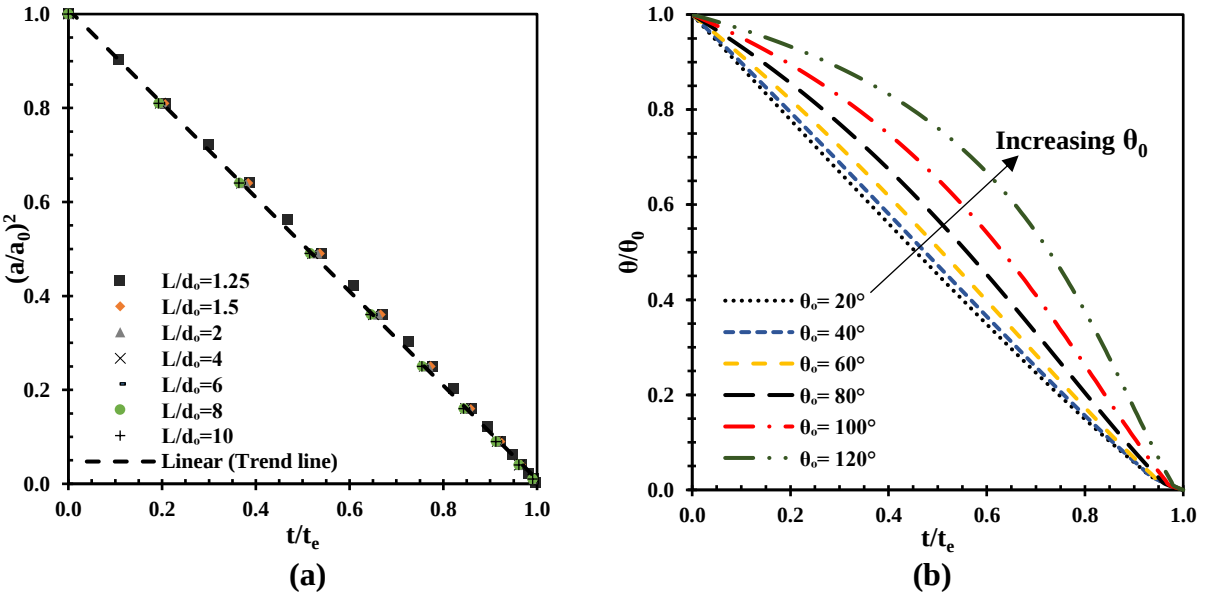

Figure 2-9 Variation of the model normalized contact radius (a) and normalized contact angles (b) with the normalized evaporation time for a pair of identical liquid droplets on a substrate under CCA and CCR modes, respectively. Data shown are for different L/d_0 values (symbols) with the fitting trend line (dashed line) for (a) and at different initial droplet contact angles for (b).

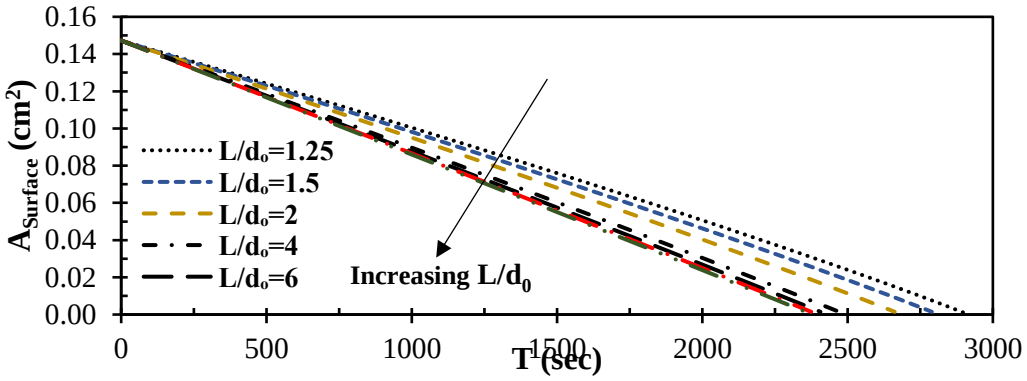

Figure 2-10 Variation of the droplet surface area with the evaporation time for a pair of water sessile droplets of V = 5.5 µL under CCA mode at different initial L/d_0 values.

2.4.3 Model Limitations

The effect of liquid volatility on the evaporation behavior of a pair of sessile droplets as predicted by the model was also studied. Despite significant disparities between the experimental findings and the model predictions shown in **Figure 2-11.a** and **Figure 2-11.b**, the model accurately captures the main trend. Also, it can be observed in **Figure 2-11.a** that the model overestimates the experimental evaporation times by almost a constant value of 62% for all experimental sets. Knowing this value, we can estimate the correct experimental value precisely. Moreover, this disparity provides insight into the impact of an additional factor that increases evaporation in real-life scenarios. The violation of the purely diffusive mass transfer assumption for the proposed model can account for this effect. Ethanol has a vapour pressure of 5.95 kPa at 20 °C 154% higher than that of water (2.34 kPa at the same temperature). Thus, the evaporation rate of an ethanol droplet is significantly higher than that of a water droplet. Furthermore, we can assume that the ethanol concentration in the ambient is zero (i.e., $C_\infty = 0$). This leads to a substantial increase in the driving potential ($C_s - C_\infty$) of the mass transfer between the droplet and

the ambient. From **Figure 2-5** we can conclude that decreasing the ambient vapor concentration increases the evaporation rate and decreases the evaporation time. Therefore, it may not be the case that diffusion alone determines the evaporation rate of ethanol droplets, and the convective term should be considered. This point was also stated by Kelly-Zion et al. [47] and Gurrala et al. [48]. Therefore, it becomes apparent that a reassessment of our model or other models in the literature is needed to incorporate the convective term to accurately capture the intricate dynamics of evaporation. Our results especially highlight such scenarios for highly volatile substances like ethanol.

Despite notable discrepancies between the experimental findings and the predictions of our model, it's important to highlight that the model successfully captures the overarching trend. Specifically, we observe that reducing the distance between droplets correlates with longer evaporation times, regardless of the absolute value. This trend is consistent with the principle that decreasing the distance between droplets results in a higher vapour concentration within the wedge area, thereby diminishing the evaporation rate of the droplets. Consequently, the model effectively accounts for the influence of the wedge area between droplets on evaporation time.

To clarify the above point, we introduce **Figure 2-11.b**, which presents a comparison between experimental evaporation times and model predictions for a pair of sessile 1-Propanol droplets. Remarkably, despite the substantial errors, our model continues to accurately capture the underlying trend and its slope, with deviations between experimental and predicted values remaining relatively constant.

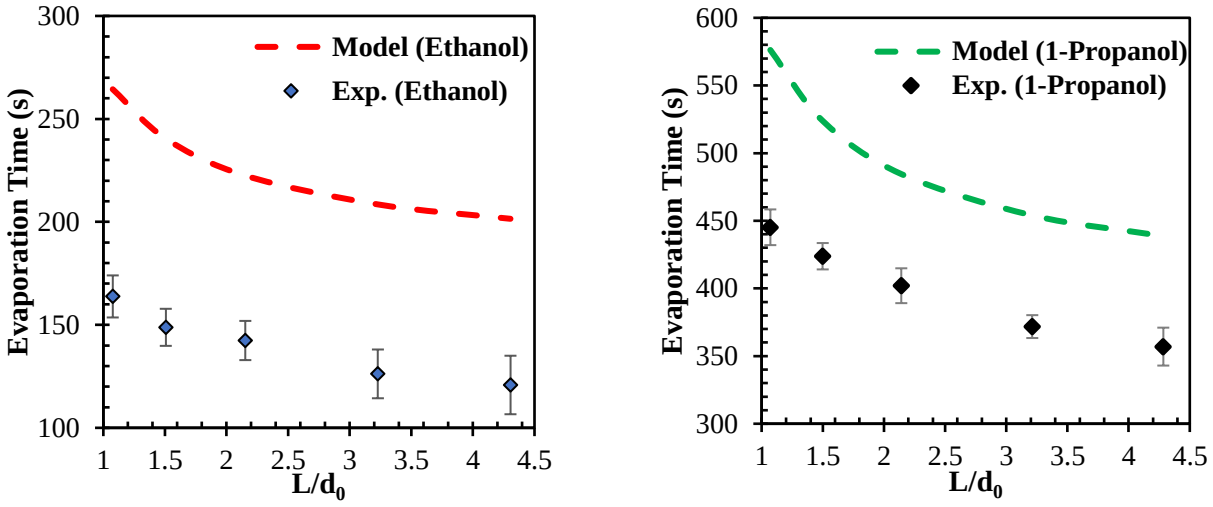

(a) (b)

Figure 2-11 Variation of evaporation time for a pair of (a) Ethanol and (b) 1-Propanol sessile droplets (V= 3.0µL) on a coated glass substrate at different separating distances (L/d_0).

To support the claim above about possible convective effect, we did tests to examine the impact of liquid volatility on evaporation time, 1-propanol (C3H8O) is utilized, **Figure 2-11.b**. At 25 °C, 1-Propanol has a C_s value of 74 µg/cm^3, which is higher than the value for water (23 µg/cm^3) and lower than the value for ethanol (147 µg/cm^3). This indicates that the evaporation rate of 1-Propanol liquid droplets is slower than that of ethanol liquid droplets, but faster than that of water droplets of equal volume. **Figure 2-12** compares the proposed model's calculated evaporation times with the three liquids' experimental evaporation times. The water, 1-Propanol, and ethanol droplets deviate from the model by 9.2%, 29.4%, and 61.4%, respectively. Therefore, it can be concluded that the liquid's volatility affects the evaporation rate and the deviation from the diffusion model.

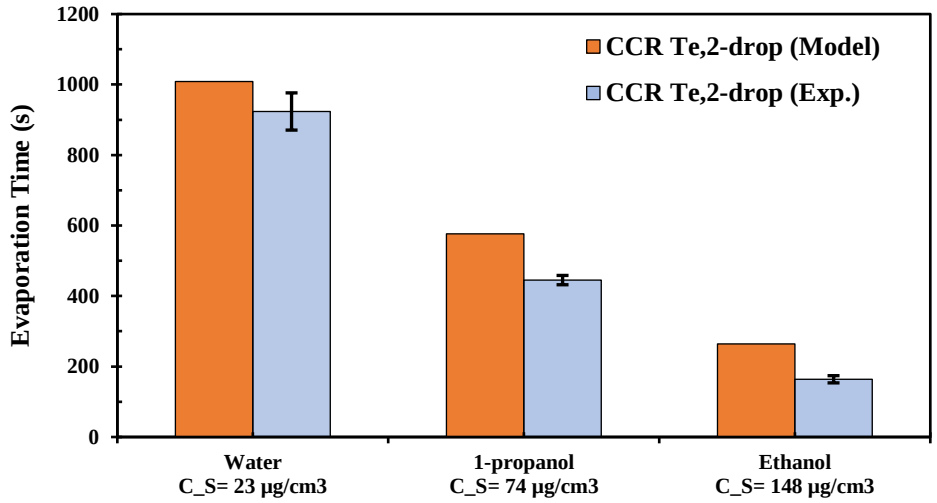

Figure 2-12 Variation of evaporation time for a pair of sessile droplets (V= 3.0 µL) of different liquids at a constant separating distance (L=5 mm). The ambient temperature is 24°C.

2.5 Conclusion

A point source model was developed to characterize the evaporation process of a pair of droplets on a substrate surface surrounded by quiescent air in an isothermal system. The droplet is considered to be a point mass source located at its center. The evaporation is assumed to be a purely diffusive, quasi-steady-state process.

The model presents an expression that determines the evaporation rate of a droplet in a system of a pair of droplets. From the evaporation rate expression, it was found that when the separation distance between two droplets is ten times the droplet diameter, the two droplets act as if they are isolated. Furthermore, it has been shown that the square of the contact radius of a droplet under the CCA evaporation mode exhibits a linear decrease with the evaporation time. This finding provides evidence for the linear decrease in the droplet's surface area during evaporation. Also, when a droplet on hydrophilic surfaces undergoes evaporation under CCR mode, the contact angle of the droplet decreases linearly with evaporation time. In contrast, the contact angle of a droplet on a hydrophobic surface experiences a non-linear decrease. It is shown that

this can be attributed to increasing the vapor concentration of the wedge area between the two droplets.

The proposed model is validated experimentally, and it shows excellent agreement with the experimental results. The deviation between the experimental results and those predicted from the model is less than 5% on average. Also, the effect of the water droplet's volume, surface wettability, or the ambient's relative humidity led to a deviation of less than 10% from the model's predictions. By testing three different liquids (water, 1-propanol, and ethanol) of different volatility, it was found that the model captures the correct trend of the experimental results with a constant deviation of 62%. The accurate trend and the consistent deviation enable the model to be utilized for estimating correct experimental values in future applications. Also, it can be concluded that increasing the liquid volatility speeds up the evaporation process which leads to the convective effect and leads to higher deviation from the predictions of the purely diffusive proposed model.

2.6 References

[1] K. Annamalai, W. Ryan, and S. Chandra, "Evaporation of multicomponent drop arrays," *J. Heat Transfer*, vol. 115, no. 3, pp. 707–716, 1993, doi: 10.1115/1.2910742.

[2] S. Chakraborty, M. A. Rosen, and B. D. MacDonald, "Analysis and feasibility of an evaporative cooling system with diffusion-based sessile droplet evaporation for cooling microprocessors," *Appl. Therm. Eng.*, vol. 125, pp. 104–110, Oct. 2017, doi: 10.1016/j.applthermaleng.2017.07.006.

[3] W. Wang, J. Lin, and D. C. Schwartz, "Scanning force microscopy of DNA molecules elongated by convective fluid flow in an evaporating droplet," *Biophys. J.*, vol. 75, no. 1, pp. 513–520, Jul. 1998, doi: 10.1016/S0006-3495(98)77540-X.

[4] P. He and B. Derby, "Controlling Coffee Ring Formation during Drying of Inkjet Printed 2D Inks," *Adv. Mater. Interfaces*, vol. 4, no. 22, p. 1700944, Nov. 2017, doi: 10.1002/admi.201700944.

[5] J. T. Delaney, P. J. Smith, and U. S. Schubert, "Inkjet printing of proteins," *Soft Matter*, vol. 5, no. 24, pp. 4866–4877, 2009, doi: 10.1039/b909878j.

[6] Y. O. Popov, "Evaporative deposition patterns: Spatial dimensions of the deposit," *Phys. Rev. E - Stat. Nonlinear, Soft Matter Phys.*, vol. 71, no. 3, pp. 1–17, 2005, doi: 10.1103/PhysRevE.71.036313.

[7] A. S. Dimitrov, C. D. Dushkin, H. Yoshimura, and K. Nagayama, “Observations of Latex Particle Two-Dimensional-Crystal Nucleation in Wetting Films on Mercury, Glass, and Mica,” *Langmuir*, vol. 10, pp. 300–326, 1994, Accessed: Jul. 13, 2021. [Online]. Available: https://pubs.acs.org/sharingguidelines

[8] R. G. Picknett and R. Bexon, “The evaporation of sessile or pendant drops in still air,” *J. Colloid Interface Sci.*, vol. 61, no. 2, pp. 336–350, 1977, doi: 10.1016/0021-9797(77)90396-4.

[9] C. Bourges-Monnier and M. E. R. Shanahan, “Influence of Evaporation on Contact Angle,” *Langmuir*, vol. 11, pp. 2820–2829, 1995, Accessed: Jul. 13, 2021. [Online]. Available: https://pubs.acs.org/sharingguidelines

[10] G. McHale, S. M. Rowan, M. I. Newton, and M. K. Banerjee, “Evaporation and the wetting of a low-energy solid surface,” *J. Phys. Chem. B*, vol. 102, no. 11, pp. 1964–1967, 1998, doi: 10.1021/jp972552i.

[11] K. S. Birdi, D. T. Vu, and A. Winter, “A study of the evaporation rates of small water drops placed on a solid surface,” *J. Phys. Chem.*, vol. 93, no. 9, pp. 3702–3703, 1989, doi: 10.1021/j100346a065.

[12] S. M. Rowan, I. Newton, and G. McHale, “Evaporation of Microdroplets and the Wetting of Solid Surfaces,” *J. Phys. Chem*, vol. 99, pp. 13268–13271, 1995, Accessed: Jul. 13, 2021. [Online]. Available: https://pubs.acs.org/sharingguidelines

[13] S. Dash and S. V. Garimella, “Droplet evaporation dynamics on a superhydrophobic surface with negligible hysteresis,” *Langmuir*, vol. 29, no. 34, pp. 10785–10795, 2013, doi: 10.1021/la402784c.

[14] H. Y. Erbil, G. McHale, and M. I. Newton, “Drop evaporation on solid surfaces: Constant contact angle mode,” *Langmuir*, vol. 18, no. 7, pp. 2636–2641, 2002, doi: 10.1021/la011470p.

[15] S. A. Kulinich and M. Farzaneh, “Effect of contact angle hysteresis on water droplet evaporation from super-hydrophobic surfaces,” *Appl. Surf. Sci.*, vol. 255, no. 7, pp. 4056–4060, 2009, doi: 10.1016/j.apsusc.2008.10.109.

[16] T. A. H. Nguyen, A. V. Nguyen, and V. Hampton, Marc A. Xu, Zhi Ping Huang, Longbin Rudolph, “Theoretical and experimental analysis of droplet evaporation on solid surfaces,” *Chem. Eng. Sci.*, vol. 69, no. 1, pp. 522–529, Feb. 2012, doi: 10.1016/j.ces.2011.11.009.

[17] J. M. Stauber, S. K. Wilson, B. R. Duffy, and K. Sefiane, “On the lifetimes of evaporating droplets,” *J. Fluid Mech.*, vol. 744, pp. 1–12, 2014, doi: 10.1017/jfm.2014.94.

[18] A. Shaikeea, S. Basu, S. Hatte, and L. Bansal, “Insights into vapor-mediated interactions in a nanocolloidal droplet system: Evaporation dynamics and affects on self-assembly topologies on macro- to microscales,” *Langmuir*, vol. 32, no. 40, pp. 10334–10343, 2016, doi: 10.1021/acs.langmuir.6b03024.

[19] J. P. and J. Moon, “Control of Colloidal Particle Deposit Patterns within Picoliter Droplets Ejected by Ink-Jet Printing,” *Langmuir*, vol. 22, no. 8, pp. 3506–3513, Apr. 2006, doi: 10.1021/LA053450J.

[20] R. W. Style *et al.*, “Patterning droplets with durotaxis,” *Proc. Natl. Acad. Sci.*, vol. 110, no. 31, pp. 12541–12544, Jul. 2013, doi: 10.1073/PNAS.1307122110.

[21] H. Hu and R. G. Larson, “Evaporation of a sessile droplet on a substrate,” *J. Phys. Chem. B*, vol. 106, no. 6, pp. 1334–1344, 2002, doi: 10.1021/jp0118322.

[22] X. Chen *et al.*, “Evaporation of droplets on superhydrophobic surfaces: Surface roughness

and small droplet size effects," *Phys. Rev. Lett.*, vol. 109, no. 11, p. 116101, Sep. 2012, doi: 10.1103/PhysRevLett.109.116101.
[23] M. Labowsky, "The effects of nearest neighbor interactions on the evaporation rate of cloud particles," *Chem. Eng. Sci.*, vol. 31, no. 9, pp. 803–813, 1976, doi: 10.1016/0009-2509(76)80054-1.
[24] A. J. D. Shaikeea and S. Basu, "Evaporating sessile droplet pair: Insights into contact line motion, flow transitions and emergence of universal vaporisation pattern," *Appl. Phys. Lett.*, vol. 108, no. 24, 2016, doi: 10.1063/1.4953836.
[25] A. J. D. Shaikeea and S. Basu, "Insight into the Evaporation Dynamics of a Pair of Sessile Droplets on a Hydrophobic Substrate," *Langmuir*, vol. 32, no. 5, pp. 1309–1318, 2016, doi: 10.1021/acs.langmuir.5b04570.
[26] T. K. Pradhan and P. K. Panigrahi, "Deposition pattern of interacting droplets," *Colloids Surfaces A Physicochem. Eng. Asp.*, vol. 482, pp. 562–567, 2015, doi: 10.1016/j.colsurfa.2015.07.013.
[27] R. D. Deegan, O. Bakajin, T. F. Dupont, G. Huber, S. R. Nagel, and T. A. Witten, "Capillary flow as the cause of ring stains from dried liquid drops," *Nature*, vol. 389, no. 6653, pp. 827–829, 1997, doi: 10.1038/39827.
[28] L. Chen and J. R. G. Evans, "Arched structures created by colloidal droplets as they dry," *Langmuir*, vol. 25, no. 19, pp. 11299–11301, 2009, doi: 10.1021/la902918m.
[29] S. Hatte and S. Pandey, Keshav Pandey, Khushboo Chakraborty, Suman Basu, "Universal evaporation dynamics of ordered arrays of sessile droplets," *J. Fluid Mech.*, vol. 866, pp. 61–81, 2019, doi: 10.1017/jfm.2019.105.
[30] S. Malcolm, A. Azzam, and A. Amirfazli, "Point source modelling approach for sessile droplet evaporation," *Phys. Fluids*, vol. 36, no. 1, 2024, doi: 10.1063/5.0180908.
[31] J. E. Castillo and J. A. Weibel, "A point sink superposition method for predicting droplet interaction effects during vapor-diffusion-driven dropwise condensation in humid air," *Int. J. Heat Mass Transf.*, vol. 118, pp. 708–719, 2018, doi: 10.1016/j.ijheatmasstransfer.2017.11.045.
[32] D. Khilifi, W. Foudhil, K. Fahem, S. Harmand, and S. Ben Jabrallah, "Study of the phenomenon of the interaction between sessile drops during evaporation," *Therm. Sci.*, vol. 23, no. 2, pp. 1105–1114, 2019, doi: 10.2298/TSCI180406188K.
[33] M. H. Yildirim Erbil, And Dogan, "Determination of Diffusion Coefficient−Vapor Pressure Product of Some Liquids from Hanging Drop Evaporation," *Langmuir*, vol. 16, no. 24, pp. 9267–9273, Nov. 2000, doi: 10.1021/LA000721B.
[34] S. F. Chini and A. Amirfazli, "Understanding the evaporation of spherical drops in quiescent environment," *Colloids and Surfaces*, vol. 432, pp. 82–88, 2013, doi: 10.1016/j.colsurfa.2013.05.013.
[35] C. Poulard, G. Guéna, and A. M. Cazabat, "Diffusion-driven evaporation of sessile drops," *J. Phys. Condens. Matter*, vol. 17, no. 49, p. S4213, Nov. 2005, doi: 10.1088/0953-8984/17/49/015.
[36] S. F. Chini and A. Amirfazli, "Resolving an ostensible inconsistency in calculating the evaporation rate of sessile drops," *Adv. Colloid Interface Sci.*, vol. 243, pp. 121–128, 2017, doi: 10.1016/j.cis.2016.05.015.
[37] I. Langmuir., "The Evaporation of Small Spheres," *Phys. Rev.*, vol. 12, no. 5, p. 368, Nov. 1918, doi: 10.1103/PhysRev.12.368.

[38] M. A. Saada, S. Chikh, and L. Tadrist, “Numerical investigation of heat and mass transfer of an evaporating sessile drop on a horizontal surface,” *Phys. Fluids*, vol. 22, no. 11, p. 112115, Nov. 2010, doi: 10.1063/1.3488676.
[39] Maxwell JC, “Collected Scientific Papers - 1st ed. ; 1890 628 [Cambridge, UK].”
[40] V. Devarakonda and A. K. Ray, “Effect of inter-particle interactions on evaporation of droplets in a linear array,” *J. Aerosol Sci.*, vol. 34, no. 7, pp. 837–857, 2003, doi: 10.1016/S0021-8502(03)00065-X.
[41] S. M. Rowan, M. I. Newton, and G. McHale, “Evaporation of microdroplets and the wetting of solid surfaces,” *J. Phys. Chem.*, vol. 99, no. 35, pp. 13268–13271, 1995, doi: 10.1021/j100035a034.
[42] S. Hatte, K. Pandey, K. Pandey, S. Chakraborty, and S. Basu, “Universal evaporation dynamics of ordered arrays of sessile droplets,” *J. Fluid Mech.*, vol. 866, pp. 61–81, 2019, doi: 10.1017/jfm.2019.105.
[43] A. W. Wray, B. R. Duffy, and S. K. Wilson, “Competitive evaporation of multiple sessile droplets,” *J. Fluid Mech.*, vol. 884, 2019, doi: 10.1017/jfm.2019.919.
[44] V. I. Fabrikant, “On the potential flow through membranes,” *ZAMP Zeitschrift für Angew. Math. und Phys.*, vol. 36, no. 4, pp. 616–623, 1985, doi: 10.1007/BF00945301.
[45] S. Tonini and G. E. Cossali, “Analytical modeling of the evaporation of sessile drop linear arrays,” *Phys. Rev. E*, vol. 105, no. 5, pp. 1–13, 2022, doi: 10.1103/PhysRevE.105.054803.
[46] E. E. Ray Bolz, D. Eng, G. L. Tuve, and B. Raton London New York Washington, *CRC Handbook of Tables for Applied Engineering Science*. CRC Press, 1970. doi: 10.1201/9781315214092.
[47] P. L. Kelly-Zion, C. J. Pursell, S. Vaidya, and J. Batra, “Evaporation of sessile drops under combined diffusion and natural convection,” *Colloids Surfaces A Physicochem. Eng. Asp.*, vol. 381, no. 1–3, pp. 31–36, 2011, doi: 10.1016/j.colsurfa.2011.03.020.
[48] K. C. Gurrala, Pradeep Katre, Pallavi Balusamy, Saravanan Banerjee, Sayak Sahu, “Evaporation of ethanol-water sessile droplet of different compositions at an elevated substrate temperature,” *Int. J. Heat Mass Transf.*, vol. 145, 2019, doi: 10.1016/j.ijheatmasstransfer.2019.118770.

Chapter 3 Modelling of the Evaporation Process of a Pair of Sessile Droplets on a Heated Substrate [1]

3.1 Introduction

Sessile droplet evaporation is a complex process involving mass and heat transfer at the interface, a moving liquid/vapor interface, and non-uniform evaporation flux across the droplet's surface. This phenomenon has been extensively studied in numerous research works due to its significant applications in various fields, such as spray drying, DNA analysis [1], inkjet technology [2], combustion processes [3], thermal management in electronics [4], and cooling mechanisms [5]. It is also important in printing on hydrophobic substrate in electronic printing [6], [7].

The evaporation of a droplet is dynamic, with its shape changing during the process. Picknett and Bexon [8] were among the first to observe three evaporation modes: constant contact angle (CCA) mode, constant contact radius (CCR) mode, and mixed mode. In CCA mode, the contact radius shrinks while the contact angle remains constant [9], while in CCR mode, the contact angle decreases with a fixed contact line [10], [11]. The mixed mode involves both a decrease in contact angle and contact line [8]. The difference between the advancing (θ_{Adv}) and receding (θ_{Recd}), contact angles, known as contact angle hysteresis (CAH), helps determine the evaporation mode [11]. If $\theta_{Recd} \approx 0$, evaporation is purely CCR. Otherwise, the droplet initially follows CCR mode until the contact angle equals θ_{Recd}, then shifts to CCA mode [12], [13].

When a single, isolated droplet of a non-volatile liquid is placed on an unheated surface, it can be assumed that mass transport from the sessile droplet occurs primarily through diffusion, with

[1] *This chapter has been published as a peer-reviewed journal article under the same title in the Physics of Fluids journal.*

which molecules transfer across the liquid-vapor interface (phase change) or by how quickly saturated vapor molecules diffuse from the droplet surface into the surrounding air [14], [15]. The molecular transfer rate happens on a timescale of about 10^{-10} seconds, while the diffusion-based transport rate has a characteristic time of a^2/D (where D is the diffusion coefficient for vapor in air and, a, is the droplet's contact radius). For water, under normal evaporation conditions, this timescale is approximately in the range of seconds. The transport of vapor molecules away from the droplet surface occurs via diffusion, convection, or a combination of both [16]. However, experimental results have shown that the evaporation of non-volatile droplets at room temperature is predominantly governed by diffusion rather than convection [10], [17]–[19].

Maxwell [20] was the first to set assumptions to determine the evaporation rate of single isolated sessile drops. Later, many researchers proposed models describing the evaporation process of a sessile droplet on unheated substrate [8], [15], [21]–[25]. These classical models assume the evaporation process is steady-state and controlled by diffusion, with the system at the ambient temperature. Recent studies show that diffusive models work well for unheated surfaces, however, when the substrate temperature is higher than the ambient, convection becomes significant, and these models underestimate the evaporation rate [22], [26]–[32]. As the substrate temperature increases the natural convection effect increases the mass transfer (evaporation rate) in the vapour phase, through the flow around the droplet [33]. Kelly-Zion *et al.* [32] and Carle *et al.* [26] proposed empirical correlations for the evaporation rate of a single isolated droplet on a heated substrate, taking into account the combined effects of diffusion and convection in mass transfer. All these authors carried out their works for the evaporation behaviour of a single isolated droplet on a heated substrate.

Most real-world and practical cases of droplet evaporation involve arrays of droplets rather than a single isolated droplet [34]–[36]. The behavior of droplet arrays can be partially understood by studying individual sessile droplets, which has led to extensive research on the evaporation process of single droplets [8]–[10], [12], [15], [17], [23], [37]. While these studies provide valuable insights, the transfer rate of energy, mass, or momentum from an array of droplets is different due to interactions between the droplets [38]. A first approach to understand evaporation of droplet arrays is to examine the evaporation of two adjacent droplets [34], [39]–[41]. When two droplets are positioned close together on a substrate surface, a "wedge" region forms between them (see

Figure 3-1). Within this region, the accumulation of vapor reduces the evaporation rate, a phenomenon initially observed in [42]. As a result of the higher vapor concentration in the wedge region, the droplet's lifetime is extended [43].

Shaikeea *et al*. [39], [40], proposed semi-analytical models for the evaporation process of a pair of sessile droplets placed on a hydrophobic substrate was limited in scope to specific contact angles (115°), fluid type (water), with unclear evaporation modes. Similar limitations are observed in the semi-analytical model of linear arrays of sessile droplets proposed by Hatte *et al.* [44], where certain factors are contingent on specific experimental conditions. Wilson *et al.* [45] introduced an asymptotic analytical model for the evaporation of multiple sessile droplets, leveraging the integral approach proposed in [46]. However, their model's complexity and restriction to thin droplets pose limitations. Tonini and Cossali [47] proposed analytical and numerical models for the evaporation of sessile droplet linear arrays. Their analytical model involves solving Laplace's equation to determine concentration values at specific locations,

introducing complexity with terms such as the Legendre function of the first kind with complex index. For their numerical solution, they adopted a 3D numerical approach utilizing COMSOL Multiphysics. None of these studies considered the effect of substrate temperature on the evaporation behaviour of an array of sessile droplets. Moreover, their proposed models are based solely on the assumption of diffusive mass transfer, without accounting for the combined effect of convection in the case of a heated substrate.

In our previous study [48], we proposed a simplified point source model (PSM) to simulate the evaporation of a pair of sessile droplets on a substrate surface, surrounded by still air,

Figure 3-1. The model is for a purely diffusive isothermal quasi-steady-state evaporation process to find the diffusive evaporation rate (E_d) as a function of the separation distance (L) between two droplets; Equation (3-1) was found as:

$$E_d = \frac{1-\frac{a}{L}}{1-\frac{a^2}{L^2}} \times \left[-2\pi\, a\, D\, \frac{sin\theta}{1+cos\theta}\, (C_s - C_\infty)\, 56.561\theta^{-0.892}\right] \tag{3-1}$$

where (θ) is the contact angle of the droplet, and (C_s) and (C_∞) are the vapor concentration at the droplet surface and far field, respectively. In Equation (2-6), we assumed that the evaporation process is quasi-steady state. For non-volatile liquids like water, the time needed for the concentration field to adapt to changes in droplet size is approximately (a^2/D). The ratio of this adjustment time (a^2/D) to the droplet's evaporation time (t_e) is around $a^2/D \cdot t_e \approx 10^{-5}$ [23]. Given these conditions, it is reasonable to assume that the evaporation process can be considered quasi-steady state. The model was validated through experimental work and demonstrated agreement with the experimental results across various conditions, including different droplet volumes,

ambient humidity levels, and surface wettability. This model also addressed the challenges of the droplet interface motion, evaporation mode, coupled mass and heat transfer dynamics, and the non-uniformity of evaporative flux within a computationally light framework.

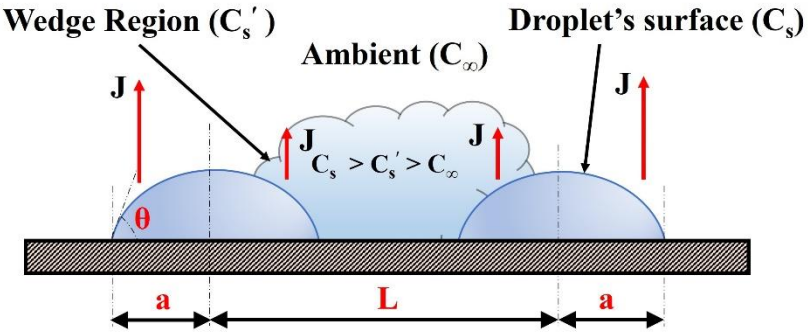

Figure 3-1 Schematics of a central (midplane) sectional plane of a pair of sessile droplets considered as spherical cap drying on a substrate surface; L is the separation distance between the droplets, a is the droplet's contact radius, and θ is the droplet contact angle.

In this study, we build on our previous work by expanding the previous model to allow for examining the impact of substrate temperature on the evaporation behavior of a pair of sessile water droplets. The key question we seek to answer is whether our proposed diffusive (PSM) model remains valid under heated substrate conditions. Also, we aim to determine the limits of the proposed diffusive model based on experimental works. Lastly, our goal is to develop an empirical correlation that accurately predicts the evaporation rate of a pair of sessile droplets on a heated substrate, considering the combined effects of diffusion and convection.

In this study, convection is primarily driven by the concentration difference between the droplet surface and the surrounding ambient, denoted as $(C_s - C_\infty)$ in Eq. (2-6). This concentration difference, $(C_s - C_\infty)$, is influenced mainly by the liquid's volatility and the temperature gradient $(T_s - T_\infty)$. However, since we utilized a non-volatile liquid (water) and

maintained an almost constant ambient temperature, T_∞, the concentration difference $(C_s - C_\infty)$ is predominantly governed by the substrate temperature.

3.2 Experimental Apparatus

An experimental apparatus was designed and constructed to study the evaporation behavior of a pair of sessile water droplets sitting on a heated aluminium substrate, see **Figure 3-2**. The droplets were placed on the substrate by using a motorized syringe pump (KD Scientific-788111) with a volume accuracy of ±0.5%. The distance between the droplets was controlled by using a linear X-stage with an accuracy of ± 0.01 mm. For image processing, two cameras (**Figure 3-2**, Camera I and Camera II) were employed to capture the variation in droplet contact angle and contact radius during evaporation. Camera I and Camera II (Plugable, 2MP, 250x Magnification) were vertically and horizontally mounted, respectively. The Contact Angle plugin in Image J was used to measure the contact angle of the droplets.

All experiments were conducted within a humidity-controlled chamber (dimensions: L=28 cm, W=32 cm, H=41 cm). Humidity levels were regulated by a programmable humidity controller (IHC200, Inkbird), capable of maintaining relative humidity between 5% and 99%, with an accuracy of ±3%. Throughout the experiment, the mass of the droplets was continuously monitored using an analytical balance (ML304T, Mettler Toledo Ltd.) with a resolution of 0.1 mg and an accuracy of ±0.2 mg.

The substrate was a clean mirror polished aluminium substrate with dimensions of 25mm by 50mm. The surface was, firstly, washed by ethanol; then, it was rinsed with deionized water before it was heated in an oven at 65°C for two hours. The surface was left overnight before it was used in the experiments. The corresponding average initial contact angle for all experiments

was (62° ± 4.7°). The aluminium substrate was heated by Polyimide Heat Pad (12V, 7W). The temperatures of the substrate and the ambient were always monitored with a K-type thermocouple having an accuracy of ± 0.1°C. A constant substrate temperature was maintained using an Arduino-based PID controller.

The experiments were carried out at the substrate temperatures of: 40°C, 50°C, 60°C, 70°C, and 80°C, and with varying separation distances between the droplets: 4 mm, 8 mm, 15 mm, and 20 mm. The initial droplets volume of 5 µL was used for all experiments; correspondingly, by considering the contact angle of the droplets, the L/d, where *d* is the droplet's contact diameter, values were determined to be 1.23, 2.43, 4.63, and 6.24, respectively. The relative humidity inside the chamber was kept at 25% ± 3%. The experiments were carried out in a laboratory temperature of 22–23°C. The contact lines of the droplets were pinned nearly through 85% of the total evaporation time for all experiments (CCR evaporation mode).

The evaporation rate of the droplet, $E_{measured}$, was calculated using the formula $E_{measured} = \frac{\Delta m}{2.\Delta t}$, where Δm represents the change in droplets mass (two droplets) over a specific time interval, Δt, set to 30 seconds for all experiments. The total evaporation rate was obtained by averaging the values of $E_{measured}$ over the entire evaporation period. Also, the evaporation heat flux, q'', was determined using the formula $q'' = \frac{\Delta m}{2.\Delta t.A_s} h_{fg}$, where h_{fg} is the latent heat of evaporation of water at the substrate temperature, and A_s is the represents surface area of the droplet at the given time at which the mass change is measured.

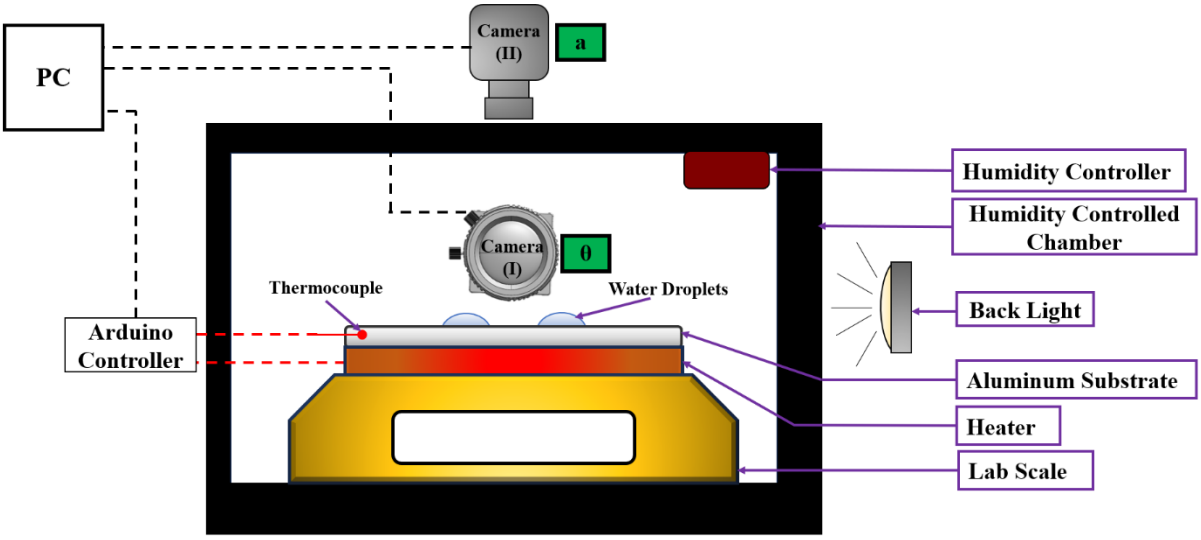

Figure 3-2 Schematic of the experimental apparatus.

3.3 Assumptions and Range of Applicability

For this part of the study, we assume the following:

1. As previously noted, that the evaporation process is treated as quasi-steady, based on the fact that the concentration field adapts much more rapidly than the droplet evaporates. Specifically, for non-volatile liquids like water, the characteristic diffusion time a^2/D is several orders of magnitude smaller than the evaporation timescale t_e , with their ratio approximately10^{-5}, validating the quasi-steady approximation.
2. The system is assumed to be isothermal, neglecting any variation in droplet surface temperature. This assumption is introduced for simplification, given the absence of experimental means to accurately measure surface temperatures. Moreover, it remains valid under the premise that temperature gradients induced by latent heat of vaporization are negligible.
3. For the proposed PSM model, it was assumed diffusion-dominated evaporation by neglecting convection effects. In this section, we revisit this assumption to evaluate its validity under heated substrate conditions.

3.4 Natural Convection Validity

The evaporation rate described in Equation (3-1) accounts solely for the diffusion component and neglects any vapor/air convection effects. Because vapor is less dense than liquid, the evaporation process at the liquid-air interface not only causes diffusion but also induces an outward convective mass flow in the surrounding air, referred to as Stefan flow, which is not captured in purely diffusive models. Moreover, when a droplet rests on a heated surface, two natural convection mechanisms emerge. The first is thermodynamically driven by buoyancy forces resulting from density differences between the heated droplet surface and the surrounding air. The second mechanism is associated with the airflow induced by the temperature gradient, where warmer air rises from the droplet surface and is replaced by cooler ambient air, creating a convective circulation around the droplet. The vapor density gradients $(C_s - C_\infty)$ corresponding to the first mechanism (concentration-driven) and the second mechanism (thermally driven) can be calculated using Equations (3-2), and(3-3), respectively. In these equations, P_{vs} represents the saturation vapor pressure; RH_s, and RH_∞ are the relative humidities at the droplet surface (assumed to be 100%) and in the ambient air, respectively; $\overline{RH}$ is the average of RH_s, and RH_∞; Pa is the atmospheric pressure; and Ra is the specific gas constant for air.

$$(C_S - C_\infty)_{CD} = RH_s \times \frac{P_{vs}(T_s)}{R.T_s} - RH_\infty \times \frac{P_{vs}(T_\infty)}{R.T_\infty} \tag{3-2}$$

$$(C_S - C_\infty)_{TD} = \overline{RH} \times \frac{P_a}{R_a} \times \left(\frac{1}{T_\infty} - \frac{1}{T_s}\right) \tag{3-3}$$

Figure 3-3 shows the variation of both thermally driven and concentration-driven vapor density gradients for droplets evaporating at ambient of RH=40%. It can be observed that for $T_s - T_\infty < 30\ ^\circ C$, the concentration-driven and thermally driven vapor density gradients are of

comparable magnitude. While the concentration-driven gradient remains consistently higher than the thermally driven one for $T_s - T_\infty > 30\ °C$, the contribution of the thermally driven gradient remains considerable.

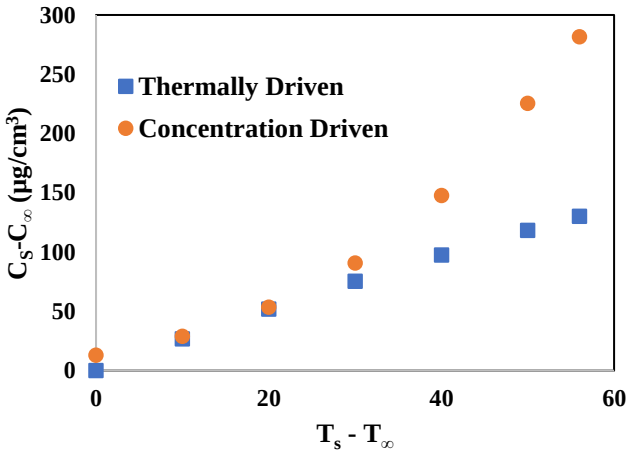

Figure 3-3 Calculated thermally driven and concentration driven Concentration gradient of water droplet as a function of the temperature difference between the substrate and the ambient at RH=40 %

In the previous paragraph, the contributions of two different natural convection mechanisms for a pair of sessile droplets on a heated substrate were analysed. We now turn our attention to evaluating the influence of Stefan flow on convection in the case of sessile droplets resting on an unheated substrate. To do that, we evaluated the vapor density gradient $(C_s - C_\infty)$ under two distinct scenarios.

In the first scenario, the droplets are placed on an unheated substrate while the ambient relative humidity varies from 60% to 0%. This setup is used to examine how changes in ambient humidity influence the vapor density gradient and, consequently, the potential for vapor/air convection. In the second scenario, the substrate temperature is increased from 24°C (unheated) to 44°C (heated), while maintaining a constant ambient relative humidity of 0%. This allows us to isolate and assess the effect of thermally driven concentration gradients on natural convection. Together,

these cases help distinguish the role of thermal effects from concentration-driven convection during the evaporation process.

Figure 3-4 illustrates that reducing the ambient relative humidity leads to an increase in the vapor concentration gradient $(C_s - C_\infty)$. This supports the idea that lower humidity enhances the driving force for vapor diffusion and may promote vapor/air convection. Additionally, the figure shows that increasing the substrate temperature has a more pronounced impact on the concentration gradient than lowering the relative humidity. Specifically, reducing the RH from 60% to 0% results in at most a 1.5-time increase in the gradient, whereas raising the substrate temperature by 20°C leads to nearly a 5-times increase. This clearly demonstrates that heating the substrate significantly amplifies the vapor concentration gradient at the droplet interface, thereby encouraging the onset of natural convection driven by buoyancy effects more than Stefan flow.

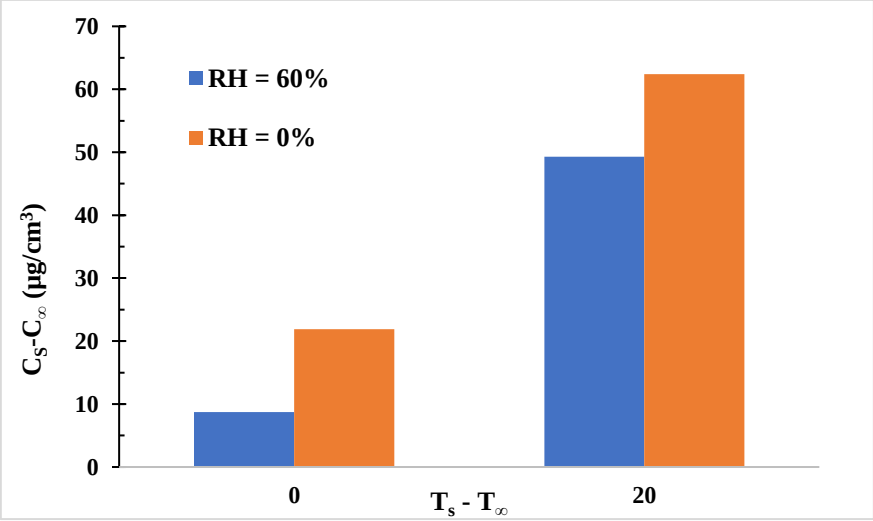

Figure 3-4 Calculated concentration gradient of water droplet as a function of the temperature difference between the substrate and the ambient at RH=60 % and 0%.

3.5 Results and Discussion

3.5.1 Experimental Results

In our previous study [48], we introduced Eq. (2-6) to describe the evaporation rate of a pair sessile droplets on unheated substrate, $T_s = T_\infty$. To account for the influence of a heated substrate, $T_s > T_\infty$, Eq. (2-6) is modified, leading to Eq. (3-4). This can be done by replacing the term $(C_s - C_\infty)$ in Eq. (2-6), which is $C_S\,(T_s)(1 - RH)$, to be $\left(C_S\,(T_s) - RH.\,C_S\,(T_\infty)\right)$ in Eq. (3-4). Also, for any liquids other than water, RH in Eq. (2-6) and Eq. (3-4) should be zero. It is important to note that Eq. (3-4) describes the evaporation rate of a pair of sessile droplets, but it remains based solely on the assumption of purely diffusive evaporation. Also, in Eq. (3-4), it is assumed that the droplets are isothermal with the substrate temperature. As discussed in the Introduction section, the evaporation process can be assumed to be quasi-steady state.

$$E_d = \frac{1 - \frac{a}{L}}{1 - \frac{a^2}{L^2}} \times \left[-2\pi\, a\, D\, \frac{sin\theta}{1 + cos\theta}\, \left(C_S\,(T_s) - RH.\,C_S\,(T_\infty)\right) 56.561\theta^{-0.892}\right] \qquad (3\text{-}4)$$

Figure 3-5 shows the experimental evaporation rate as a function of the temperature difference between the substrate temperature (T_s) and the ambient temperature (T_∞) for various L/d values. The results indicate that regardless of the separation distance, the evaporation rate consistently increases with increasing the substrate temperature. This is expected, as higher surface temperatures increase the vapor pressure at the droplet surface, isothermal assumption above, thereby increasing the concentration gradient between the droplet surface (C_s) and the ambient (C_∞). Consequently, this larger concentration difference increases the evaporation rate. A similar conclusion can be observed in **Figure 3-6**, that increasing the distance between the droplets increases the evaporation rate. This finding aligns with our previous study [48], in which

we concluded that increasing the distance between the droplets decreases the effect of the wedge area thereby enhancing the evaporation rate.

The experimental results from **Figure 3-5** and **Figure 3-6** are compared with the quasi-steady-state, diffusion-controlled evaporation model described by Eq. (3-4) (represented by black triangles). It is observed that the experimental evaporation rates closely match the predictions of the diffusion model as the substrate temperature decreases to the lab value [22], [25], [33], [49]. However, as the substrate temperature rises above the ambient, the evaporation rates exceed those predicted by the diffusion-controlled model. **Figure 3-5** also shows that regardless of the separation distance between the droplets, the difference between the experimental evaporation rate and the diffusion model predictions remains less than 20% when T_s - T_∞ is less than 30°C. **Figure 3-6** shows increasing the distance between the droplets, increases the deviation from the predictions from the diffusion model for a given substrate temperature. These deviations point to the existence of an additional mechanism, beyond diffusion, that enhances the evaporation rate. The influence of this mechanism becomes more significant as the substrate temperature increases. The mechanism responsible is suggested to be natural convection in the vapor phase, driven by buoyancy forces. Also, It is worth noting that, as shown in **Figure 3-5**, even for unheated substrate conditions where $\Delta T = T_s - T_\infty = 0$, the evaporation rate is not zero. This is because the driving force for evaporation is the concentration gradient rather than the temperature difference. Therefore, as long as the relative humidity (RH) is below 100%, evaporation will occur, even in the absence of a temperature gradient.

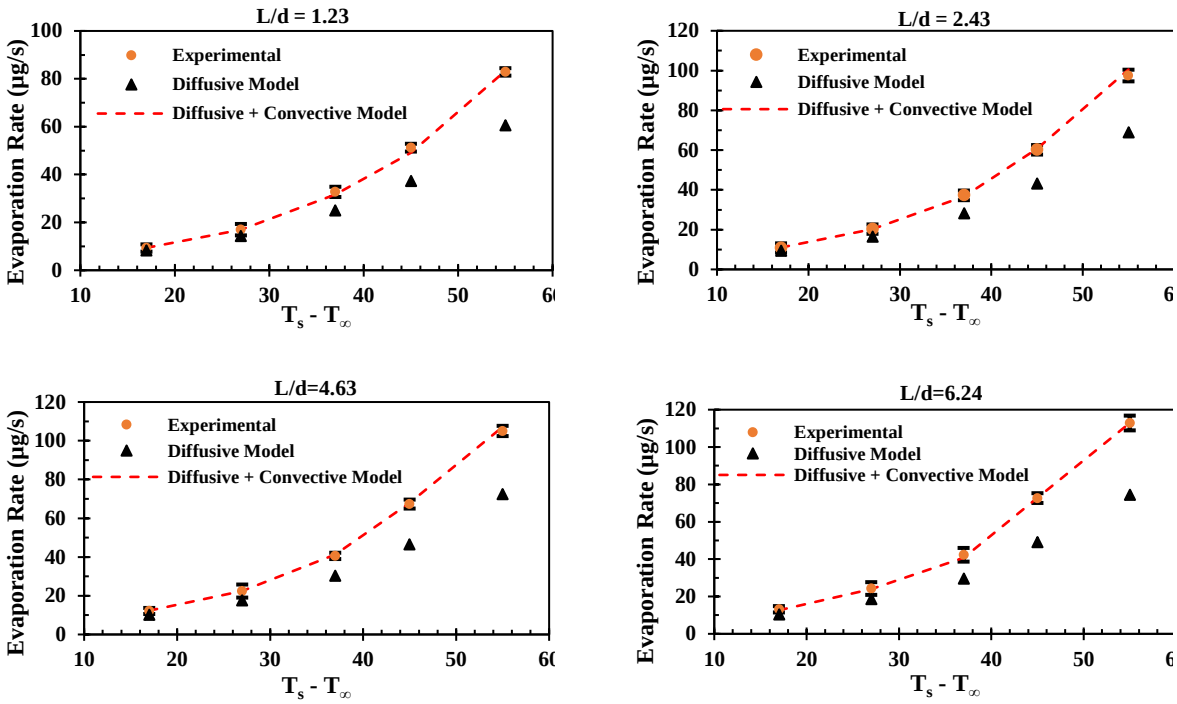

Figure 3-5 Variation of evaporation rate for a pair of water sessile droplets (V= 5.0 µL) as a function of the temperature difference between the substrate and the ambient at different separation distances (L/d = 1.23, 2.43, 4.63, and 6.24).

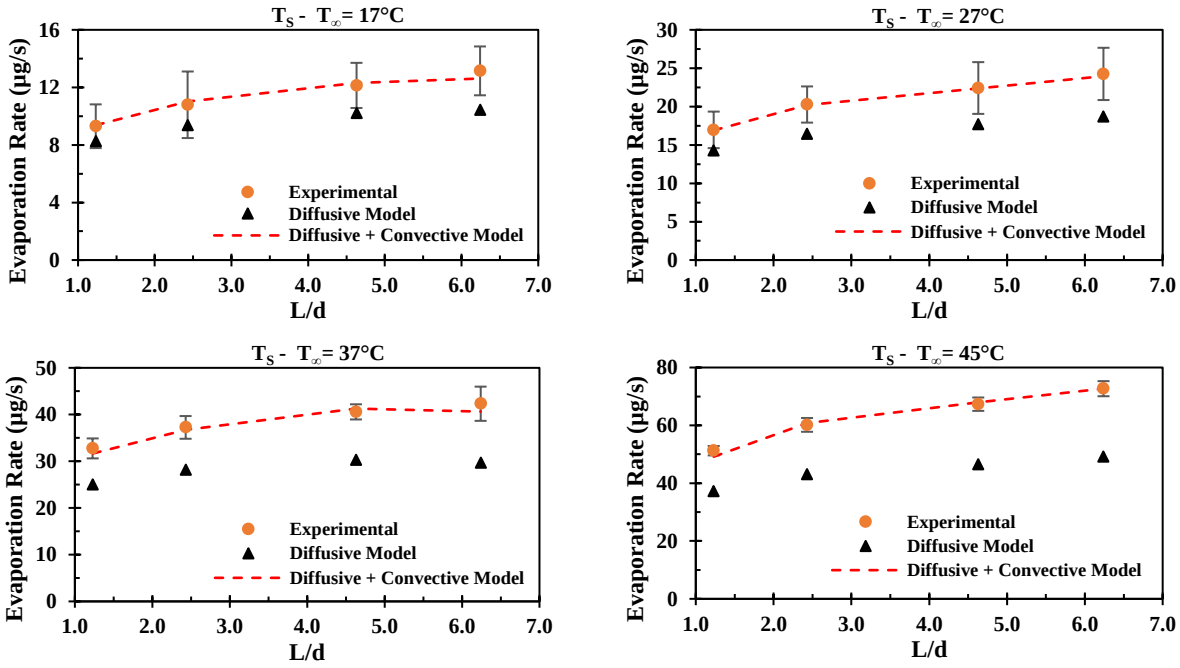

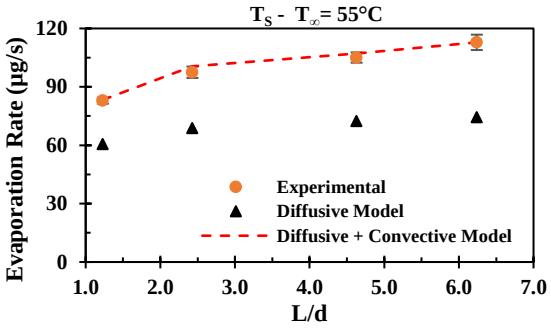

Figure 3-6 Effect of the separation distances between a pair of sessile water droplets on the evaporation rate at different separation distances

To examine the deviation of experimental evaporation rates from the diffusion model, a dimensionless diffusion evaporation rate number, E_d^*, is introduced. This represents the ratio between the diffusion evaporation rate, calculated using Eq. (3-4), and the total measured evaporation rate. Additionally, a dimensionless convection evaporation rate number, E_C^*, is introduced to represent the ratio between the convection evaporation rate and the total measured evaporation rate. Since both diffusion and convection contribute to the evaporation process, the total evaporation rate can be considered as the sum of the diffusive and convective components: $E_{Total} = E_d + E_C$. The dimensionless evaporation rates can then be expressed as $E_d^* + E_C^* = 1$.

Also, it is important to note that the Rayleigh number is typically used to describe natural convection processes and generally includes the Prandtl number (ν/α), which (ν) is the momentum diffusivity and (α) is the thermal diffusivity, which is relevant for thermally induced convection. However, since our study focuses on natural convection-driven mass transfer, we substituted the Prandtl number with the Schmidt number (ν/D), replacing thermal diffusivity (α) with mass diffusivity (D). As discussed in **section 3.4** although the concentration-driven vapor density gradient remains consistently higher than the thermally driven gradient when T_s - T_∞ is higher than 30°C, the contribution of the thermally driven component is still significant. However, for the sake of simplicity, the thermally driven gradient will be neglected in this study,

and only the concentration-driven gradient will be considered. Accordingly, the Rayleigh number used in the analysis is defined by Equation (3-5).

$$R_a = Gr.Sc = \frac{(C_S - C_\infty)}{C_\infty}.\frac{g.a^3}{v.D} \quad (3\text{-}5)$$

However, Ra alone does not account for the influence of an adjacent droplet. Incorporating the separation distance (L) into Ra is challenging since Ra typically uses a single characteristic length, a, to describe the geometry of the droplet. To address this limitation, we combined Ra with the dimensionless separation distance, L/d, forming a new dimensionless group that better captures the effects of droplet interactions. As such, in our study, we chose Ra·(L/d) as a dimensionless group because the Rayleigh number (Ra) represents the ratio of convective to diffusive mass transfer over the surface of a single droplet.

Figure 3-7 shows the dimensionless evaporation rates plotted against the product of the Rayleigh number and L/d (Ra·L/d). The results indicate that as (Ra·L/d) increases, the dimensionless diffusive evaporation rate decreases, while the convective evaporation rate increases. Also, It is evident that when Ra.L/d is less than 400, the diffusive evaporation rate accounts for more than 80% of the total evaporation. This finding can be explained by the fact that, as the substrate temperature decreases or the droplets come closer together, evaporation slows down significantly. This finding can be explained by utilizing the findings from our previous study [48] i.e., when the distance between droplets decreases, the vapor concentration in the wedge region rises, resulting in a lower evaporation rate for the droplets. Under these conditions, in the wedge area, the evaporation occurs primarily through diffusion.

However, as the substrate temperature rises or the distance between the droplets increases (for 400 < Ra.L/d < 2400), the evaporation rate accelerates, and the contribution of convective

evaporation becomes more prominent. Additionally, when Ra.L/d exceeds 2400, the contributions of diffusive and convective evaporation rates stabilize, with diffusion accounting for about 70% of total. This can be explained by solving the governing diffusion equation, $\nabla^2 C = 0$, by using the finite difference method (FDM) described in our previous study [48] to generate the concentration contours. **Figure 3-8** illustrates the vapor concentration distributions around two sessile water droplets positioned on a heated substrate at varying temperatures, with an L/d of 2.43. It is evident that increasing the substrate temperature leads to a rise in the vapor concentration within the wedge area. Furthermore, the rate of change of vapor concentration in the wedge area (dC_s'/dT) becomes more pronounced as the substrate temperature increases, as depicted by the slope in **Figure 3-9**. Therefore, increasing the substrate temperature has two opposing effects on the evaporation process. On one hand, higher temperatures enhance evaporation by increasing the difference,$(C_s - C_\infty)$, which in turn generates convective streams over the droplet surfaces. On the other hand, the elevated substrate temperature also increases the vapor concentration in the wedge area, leading to a reduction in the evaporation rate. This reduction promotes a stronger reliance on diffusion-driven mechanisms for the evaporation process. So, due to these two effects, the contribution of the convective and diffusive evaporation rates stabilize at higher substrate temperatures (i.e. higher Ra.L/d).

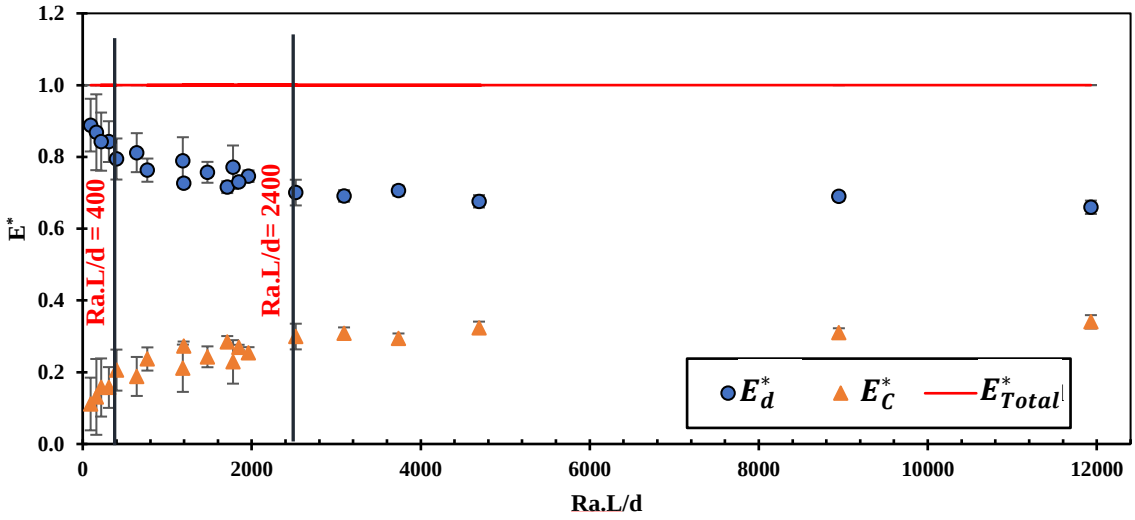

Figure 3-7 Variation of the dimensionless diffusive and convective evaporation rates as a function of the dimensionless number Ra.L/d from all experiments in **Figure 3-5**.

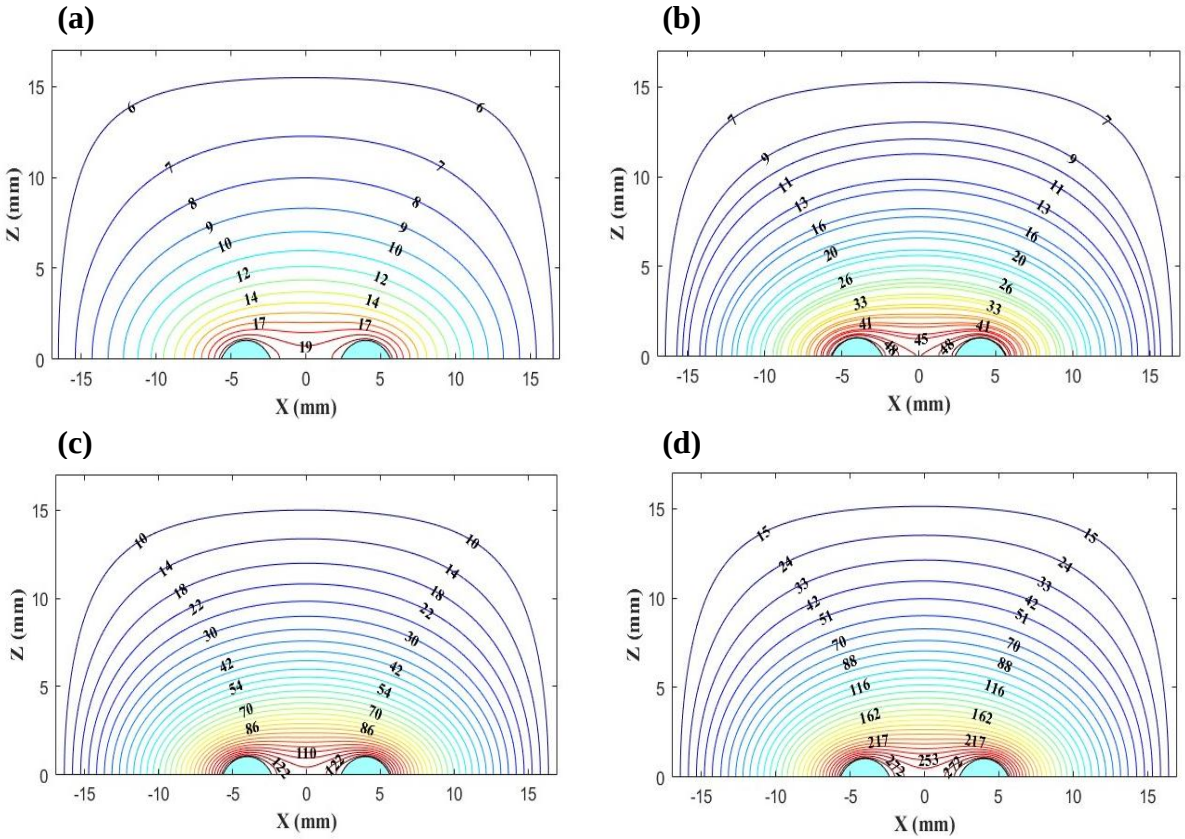

Figure 3-8 Vapor concentration distribution at the midplane around a pair of sessile water droplets of V = 5 µL on a heated substrate (θ = 64° and L/d =2.43) at (a) T_s - T_∞ = 0, (b) T_s - T_∞ = 17°C, (c) T_s - T_∞ = 37°C, and (d) T_s - T_∞ = 55°C. All concentration values have units of µg/cm^3.

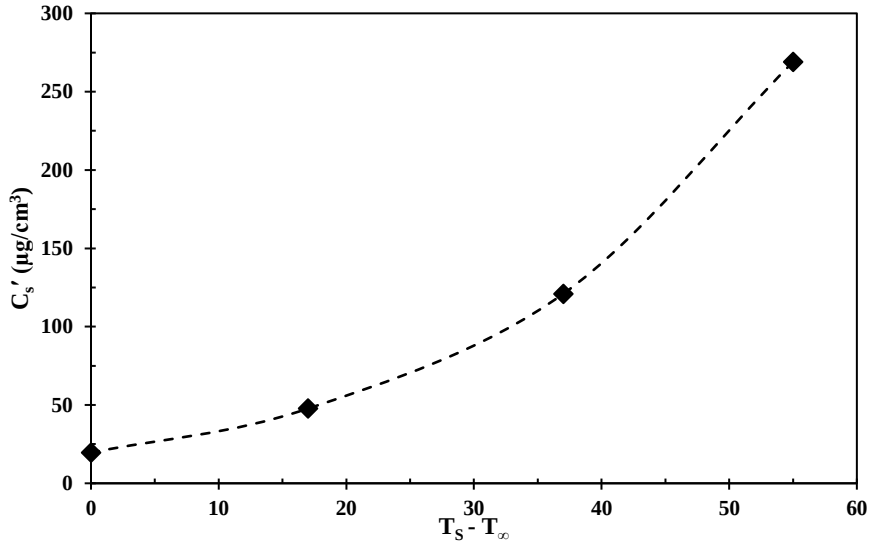

Figure 3-9 Average vapor concentration in the wedge area between two water droplets of V = 5 µL on a heated substrate at θ = 64° and L/d =2.43 as a function of the temperature difference between the substrate and the ambient.

3.5.2 Convective – Diffusive Correlation:

3.5.2.1 Concentration-Driven Convection Only

Considering Figure 5 that shows the parameter Ra.L/d can be used to delineate the importance of diffusive versus convective evaporation regimes, we will use this parameter to construct an empirical correlation to for total evaporation rate. Given that Ra.L/d is a compound parameter that is included by concentration gradient , distance between droplets and their size, etc., using there appropriate definitions (as shown in Eq. (3-6)), the term Ra.L/d is unbundled to experimentally relevant parameters. By doing so, we independently evaluate the influence of each term on the importance of diffusive versus convective evaporation. This is so as the term $\left(\frac{C_S - C_\infty}{C_\infty}\right)$ shows the influence of the concentration difference between the droplet surface and the surrounding environment. The term $\left(\frac{g.a^3}{v^2}\right)$ is denotes the droplet size and the substrate temperature effect; the effect of the diffusivity is captured by the term $\left(\frac{v}{D}\right)$, which is dependent

on the substrate temperature, T_s (droplet temperature given the isothermal assumption in this work); and finally, the influence of droplet separation distance is reflected in the term $\left({}^{L}/_{d}\right)$.

$$R_a.{}^{L}/_{d} = Gr.Sc.{}^{L}/_{d} = \left(\frac{C_S - C_\infty}{C_\infty}\right) \times \left(\frac{g.a^3}{v^2}\right) \times \left(\frac{v}{D}\right) \times \left({}^{L}/_{d}\right) \quad (3\text{-}6)$$

Given above, one can build an empirical correlation for the total evaporation rate, incorporating both diffusion and convection effects, as shown by Eq. (3-7). In Eq. (3-7), E_{Cd}^* represents the ratio of the dimensionless convection evaporation rate number, E_C^*, to the dimensionless diffusive evaporation rate number, E_d^* (i.e., $E_{Cd}^* = \frac{E_C^*}{E_d^*}$). This approach ensures that the influence of each term is independent of the others, meaning the exponents C_2 to C_5 are not restricted by the effects of the other terms [32], [50]. This contrasts with the case where all parameters are combined within Ra and subjected to the same exponent. The Solver plugin in Excel was utilized to perform nonlinear regression, determining the coefficients and exponents, C_1 to C_5, for Eq. (3-7). This process involved fitting E_{Cd}^* from Eq. (3-7) to the one computed from $\left(\frac{E_{Total}}{E_d} - 1\right)$, where E_{Total} is the total measured evaporation rates, the data shown in **Figure 3-5**, and E_d is the computed diffusive evaporation rate from Eq. (3-4). The resulting correlation constants are presented in **Table 3-1** along with a root mean square RMS relative error of 6.1%.

As discussed in **section 3.4**, the proposed correlation is based on thermally induced natural convection, which is appropriate for analysing the evaporation of non-volatile liquids such as water on a heated substrate. However, in the case of volatile liquids like ethanol, natural convection driven by concentration gradients must also be taken into account, as it plays a significant role in the evaporation process. Furthermore, as Ra depends on the concentration gradient $(C_s - C_\infty)$, its mathematical form remains the same regardless of whether the gradient

is driven by temperature differences or concentration variations. The proposed correlation in Equation (3-7) is specifically developed for thermally driven natural convection, making it suitable for non-volatile liquids. However, in the case of volatile liquid droplets evaporating on heated substrates, the diffusive evaporation rate given by Equation (3-4), E_d, must be adjusted to incorporate the effects of natural convection induced by Stefan flow, an outward convective mass flux generated by evaporation. This adjustment can be achieved by applying the *Spalding model*, which accounts for the influence of Stefan flow on the overall evaporation rate. Specifically, the diffusive evaporation rate E_d, in Equation (3-7) is replaced by E_{dc} from equation (3-8) where E_{dc}, which accounts for both diffusive and convective contributions on an unheated substrate. In Equation (3-8), $C_a(T_\infty)$ represents the air density at ambient temperature, and B_m is the Spalding mass transfer number, which captures the enhancement in mass transfer resulting from Stefan flow. The Spalding number is calculated using Equation (3-9), where Y_{vs} and $Y_{v\infty}$ are the vapor mass fractions at the droplet surface and in the ambient environment, respectively.

$$E_{Total} = E_d[1 + E_{cd}^*] = E_d\left\{1 + C_1 \times \left[\left(\frac{C_S - C_\infty}{C_\infty}\right)^{C_2} \times \left(\frac{g.a^3}{v^2}\right)^{C_3} \times \left(\frac{v}{D}\right)^{C_4} \times \left({}^{L}/_{d}\right)^{C_5}\right]\right\} \quad (3\text{-}7)$$

Table 3-1 Coefficients and exponents used in the correlation from Eq.(3-7) for the measured evaporation rates, along with the resulting RMS error in calculating the evaporation rate compared to the measured values.

C_1	C_2	C_3	C_4	C_5	RMS (%)
0.008	0.014	1.078	1.334	0.264	6.1

$$E_{dC} = \frac{1 - \frac{a}{L}}{1 - \frac{a^2}{L^2}} \times \left[-2\pi\, a\, D\, \frac{sin\theta}{1 + cos\theta}\left(C_S(T_s) + C_a(T_\infty)\right) 56.561\theta^{-0.892} \times ln(1 + B_m)\right] \quad (3\text{-}8)$$

$$B_m = \frac{Y_{vs} - Y_{v\infty}}{1 - Y_{vs}} \quad (3\text{-}9)$$

3.5.2.2 Combined Concentration- and Thermally Driven Natural

As discussed in **section 3.4**, the thermally driven component of the vapor density gradient is less significant compared to the concentration-driven component. However, to incorporate its contribution, the Rayleigh number term Ra.L/d must be modified from the form presented in Equation. (3-6) to that given in Equation (3-10). In Equation (3-10), an additional term $\left(\frac{T_S - T_\infty}{T_f}\right)$, where T_f is the film temperature defined as $\left(\frac{T_S + T_\infty}{2}\right)$, is introduced to account for the influence of the thermally induced concentration gradient. The modified empirical correlation for the total evaporation rate, incorporating both diffusion, concentration and thermally driven convection effects, as shown by Equation (3-11). The resulting correlation constants are presented in **Table 3-2** along with a root mean square RMS relative error of 6.1%.

$$R_a.{}^{L}/_{d} = \left[\left(\frac{C_S - C_\infty}{C_\infty}\right) + \left(\frac{T_S - T_\infty}{T_f}\right)\right] \times \left(\frac{g.a^3}{v^2}\right) \times \left(\frac{v}{D}\right) \times \left({}^{L}/_{d}\right) \tag{3-10}$$

$$E_{Total} = E_d \left\{1 + C_1 \times \left[\left[\left(\frac{C_S - C_\infty}{C_\infty}\right)^{C_2} + \left(\frac{T_S - T_\infty}{T_f}\right)^{C_3}\right] \times \left(\frac{g.a^3}{v^2}\right)^{C_4} \times \left(\frac{v}{D}\right)^{C_5} \times \left({}^{L}/_{d}\right)^{C_6}\right]\right\} \tag{3-11}$$

Table 3-2 Coefficients and exponents used in the correlation from Eq.(3-11) for the measured evaporation rates, along with the resulting RMS error in calculating the evaporation rate compared to the measured values.

C_1	C_2	C_3	C_4	C_5	C_6	RMS (%)
1.3 X 10^{-5}	0.172	1.094	1.131	1.480	0.261	6.3

3.5.3 Droplet Heat Transfer

Since our study involves both heat and mass transfer, it is essential to quantify the amount of heat absorbed by the droplets during evaporation. To achieve this, the evaporation heat flux is

calculated using Eq. (3-12), where E_i represents the temporal evaporation rate, A_{si} denotes the temporal surface area of the droplets, and t_e is the total evaporation time.

$$q^{"} = \frac{1}{t_e}\int \frac{\Delta m_i \times h_{fg}}{\Delta t_i \times A_{si}}\, dt \approx \frac{1}{t_e}\sum \frac{E_i \times h_{fg}}{A_{si}} \tag{3-12}$$

Figure 3-10 shows the evaporation heat flux calculated using Eq. (3-12) for all conditions considered in our study, compared with the evaporation heat flux obtained from the diffusive model using Eq (3-4). It can be observed that as the substrate temperature increases, the heat flux absorbed by the droplets also increases. This is consistent with the increased evaporation rate shown in **Figure 3-5**. As the evaporation rate increases, the droplet's surface temperature temporarily decreases. To maintain equilibrium with the substrate, the droplet then absorbs more heat to restore its surface temperature. Additionally, at a given surface temperature, increasing the separation distance between droplets leads to higher heat flux by enhancing the evaporation rate. This is attributed to the reduced vapor concentration in the wedge region as the separation distance increases, thereby promoting faster evaporation. This suggests that a higher evaporation rate, induces more recirculation streams over the surface of the droplets. These streams induce a convective effect over the surface of the droplets, which in turn raises the evaporation heat flux.

This study addresses a critical gap in the literature regarding the evaporation behavior of a pair of sessile droplets on heated substrates, where the combined effects of diffusion and convection have not been comprehensively modelled or experimentally validated. Previous studies primarily focused on isolated droplets, or on arrays of droplets with limited consideration of substrate heating effects. By extending the Point Source Model (PSM) to incorporate the influence of substrate temperature, this work demonstrates the interplay between diffusion and natural convection, providing a robust framework for understanding and predicting droplet

evaporation under varying thermal and spatial conditions. The empirical correlation developed here connects theory with experimental results, providing a useful tool for applications in thermal management and microfluidics.

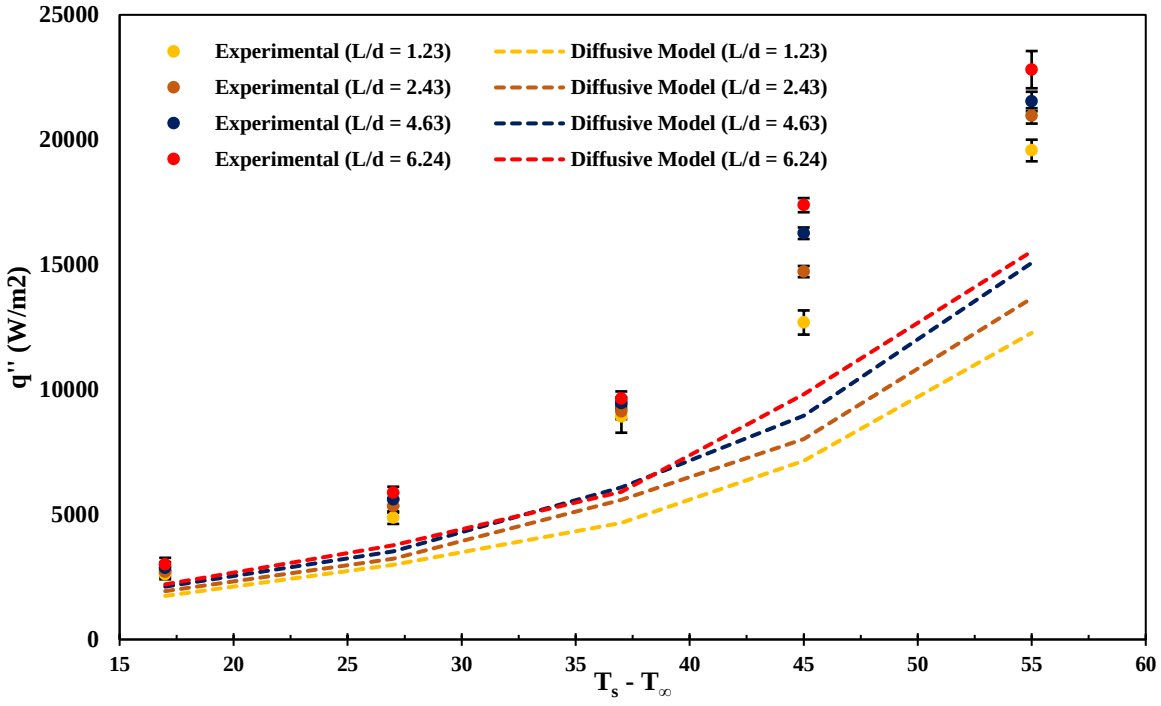

Figure 3-10 Evaporation heat flux for a pair of sessile water droplets on a heated substrate under different conditions of substrate temperatures and separation distances.

3.6 Conclusion

This study investigated the evaporation behavior of a pair of sessile water droplets on a heated aluminium substrate, highlighting the interplay between diffusion and convection. At lower substrate temperatures, evaporation is predominantly diffusive, with the proposed diffusive model showing good agreement with experimental data. However, as substrate temperatures rise, natural convection driven by buoyancy forces significantly enhances evaporation, particularly when the temperature difference exceeds 30°C.

The findings reveal that diffusion dominates evaporation when (Ra·L/d), the Rayleigh number product the (*L/d*), is below 400, contributing over 80% of the total rate. As Ra·L/d increases with higher substrate temperatures or greater droplet separations, convection becomes more influential, eventually stabilizing at approximately 30% contribution when Ra·L/d exceeds 2400. A dimensionless model combining the effects of diffusion and convection predicts evaporation rates with less than 5% error across the tested conditions.

This work provides valuable insights into droplet evaporation dynamics, offering a simple yet accurate tool for understanding heat and mass transfer during evaporation. These findings have potential applications in thermal management and microfluidic systems.

3.7 References

[1] W. Wang, J. Lin, and D. C. Schwartz, "Scanning force microscopy of DNA molecules elongated by convective fluid flow in an evaporating droplet," *Biophys. J.*, vol. 75, no. 1, pp. 513–520, 1998, doi: 10.1016/S0006-3495(98)77540-X.

[2] T. Kawase, H. Sirringhaus, R. H. Friend, and T. Shimoda, "Inkjet printed via-hole interconnections and resistors for all-polymer transistor circuits," *Adv. Mater.*, vol. 13, no. 21, pp. 1601–1605, 2001, doi: 10.1002/1521-4095(200111)13:21<1601::AID-ADMA1601>3.0.CO;2-X.

[3] M. Saito, M. Sato, and I. Suzuki, "Evaporation and combustion of a single fuel droplet in acoustic fields," *Fuel*, vol. 73, no. 3, pp. 349–353, 1994, doi: 10.1016/0016-2361(94)90086-8.

[4] A. Bar-Cohen, M. Arik, and M. Ohadi, "Direct liquid cooling of high flux micro and nano electronic components," *Proc. IEEE*, vol. 94, no. 8, pp. 1549–1570, 2006, doi: 10.1109/JPROC.2006.879791.

[5] Z. Chen, Q. Xie, G. Chen, Y. Yu, and Z. Zhao, "Numerical simulation of single-nozzle large scale spray cooling on drum wall," *Therm. Sci.*, vol. 22, no. 1, pp. 359–370, 2018, doi: 10.2298/TSCI170920243C.

[6] P. Naderi, B. R. Sheuten, A. Amirfazli, and G. Grau, "Inkjet printing on hydrophobic surfaces: Controlled pattern formation using sequential drying," *J. Chem. Phys.*, vol. 159, no. 2, 2023, doi: 10.1063/5.0149663.

[7] M. J. Docherty, P. Naderi, G. Grau, K. Sefiane, and A. Amirfazli, "Inkjet Printing on Hydrophobic Surface: Practical Implementation of Stacked Coin Strategy," *Adv. Eng. Mater.*, vol. 26, no. 11, Jun. 2024, doi: 10.1002/adem.202400237.

[8] R. G. Picknett and R. Bexon, "The evaporation of sessile or pendant drops in still air," *J. Colloid Interface Sci.*, vol. 61, no. 2, pp. 336–350, 1977, doi: 10.1016/0021-9797(77)90396-4.

[9] G. McHale, S. M. Rowan, M. I. Newton, and M. K. Banerjee, “Evaporation and the wetting of a low-energy solid surface,” *J. Phys. Chem. B*, vol. 102, no. 11, pp. 1964–1967, 1998, doi: 10.1021/jp972552i.
[10] K. S. Birdi, D. T. Vu, and A. Winter, “A study of the evaporation rates of small water drops placed on a solid surface,” *J. Phys. Chem.*, vol. 93, no. 9, pp. 3702–3703, 1989, doi: 10.1021/j100346a065.
[11] S. M. Rowan, I. Newton, and G. McHale, “Evaporation of Microdroplets and the Wetting of Solid Surfaces,” *J. Phys. Chem*, vol. 99, pp. 13268–13271, 1995, Accessed: Jul. 13, 2021. [Online]. Available: https://pubs.acs.org/sharingguidelines
[12] T. A. H. Nguyen, A. V. Nguyen, and V. Hampton, Marc A. Xu, Zhi Ping Huang, Longbin Rudolph, “Theoretical and experimental analysis of droplet evaporation on solid surfaces,” *Chem. Eng. Sci.*, vol. 69, no. 1, pp. 522–529, 2012, doi: 10.1016/j.ces.2011.11.009.
[13] J. M. Stauber, S. K. Wilson, B. R. Duffy, and K. Sefiane, “On the lifetimes of evaporating droplets,” *J. Fluid Mech.*, vol. 744, pp. 1–12, 2014, doi: 10.1017/jfm.2014.94.
[14] S. F. Chini and A. Amirfazli, “Understanding the evaporation of spherical drops in quiescent environment,” *Colloids and Surfaces*, vol. 432, pp. 82–88, 2013, doi: 10.1016/j.colsurfa.2013.05.013.
[15] Y. O. Popov, “Evaporative deposition patterns: Spatial dimensions of the deposit,” *Phys. Rev. E - Stat. Nonlinear, Soft Matter Phys.*, vol. 71, no. 3, pp. 1–17, 2005, doi: 10.1103/PhysRevE.71.036313.
[16] S. F. Chini and A. Amirfazli, “Resolving an ostensible inconsistency in calculating the evaporation rate of sessile drops,” *Adv. Colloid Interface Sci.*, vol. 243, pp. 121–128, 2017, doi: 10.1016/j.cis.2016.05.015.
[17] H. Y. Erbil, G. McHale, and M. I. Newton, “Drop evaporation on solid surfaces: Constant contact angle mode,” *Langmuir*, vol. 18, no. 7, pp. 2636–2641, 2002, doi: 10.1021/la011470p.
[18] I. Langmuir, “The evaporation of small spheres,” *Phys. Rev.*, vol. 12, no. 5, pp. 368–370, 1918, doi: 10.1103/PhysRev.12.368.
[19] M. Ait Saada, S. Chikh, and L. Tadrist, “Numerical investigation of heat and mass transfer of an evaporating sessile drop on a horizontal surface,” *Phys. Fluids*, vol. 22, no. 11, 2010, doi: 10.1063/1.3488676.
[20] JC Maxwell, “Collected Scientific Papers - 1st ed. ; 1890 628 [Cambridge, UK].”
[21] R. D. Deegan, O. Bakajin, T. F. Dupont, G. Huber, S. R. Nagel, and T. A. Witten, “Capillary flow as the cause of ring stains from dried liquid drops,” *Nature*, vol. 389, no. 6653, pp. 827–829, 1997, doi: 10.1038/39827.
[22] H. Gelderblom *et al.*, “How water droplets evaporate on a superhydrophobic substrate,” *Phys. Rev. E - Stat. Nonlinear, Soft Matter Phys.*, vol. 83, no. 2, pp. 1–6, 2011, doi: 10.1103/PhysRevE.83.026306.
[23] H. Hu and R. G. Larson, “Evaporation of a sessile droplet on a substrate,” *J. Phys. Chem. B*, vol. 106, no. 6, pp. 1334–1344, 2002, doi: 10.1021/jp0118322.
[24] S. Semenov, V. M. Starov, R. G. Rubio, and M. G. Velarde, “Instantaneous distribution of fluxes in the course of evaporation of sessile liquid droplets: Computer simulations,” *Colloids Surfaces A Physicochem. Eng. Asp.*, vol. 372, no. 1–3, pp. 127–134, 2010, doi: 10.1016/j.colsurfa.2010.10.004.
[25] B. Sobac and D. Brutin, “Triple-line behavior and wettability controlled by nanocoated

substrates: Influence on sessile drop evaporation," *Langmuir*, vol. 27, no. 24, pp. 14999–15007, 2011, doi: 10.1021/la203681j.
[26] F. Carle, S. Semenov, M. Medale, and D. Brutin, "Contribution of convective transport to evaporation of sessile droplets: Empirical model," *Int. J. Therm. Sci.*, vol. 101, pp. 35–47, 2016, doi: 10.1016/j.ijthermalsci.2015.10.012.
[27] W. Wang, J. Lin, and D. C. Schwartz, "Scanning force microscopy of DNA molecules elongated by convective fluid flow in an evaporating droplet," *Biophys. J.*, vol. 75, no. 1, pp. 513–520, Jul. 1998, doi: 10.1016/S0006-3495(98)77540-X.
[28] P. Gurrala, P. Katre, S. Balusamy, S. Banerjee, and K. C. Sahu, "Evaporation of ethanol-water sessile droplet of different compositions at an elevated substrate temperature," *Int. J. Heat Mass Transf.*, vol. 145, 2019, doi: 10.1016/j.ijheatmasstransfer.2019.118770.
[29] S. Dash and S. V. Garimella, "Droplet evaporation on heated hydrophobic and superhydrophobic surfaces," *Phys. Rev. E - Stat. Nonlinear, Soft Matter Phys.*, vol. 89, no. 4, pp. 1–8, 2014, doi: 10.1103/PhysRevE.89.042402.
[30] E. Y. Gatapova, A. A. Semenov, D. V. Zaitsev, and O. A. Kabov, "Evaporation of a sessile water drop on a heated surface with controlled wettability," *Colloids Surfaces A Physicochem. Eng. Asp.*, vol. 441, pp. 776–785, 2014, doi: 10.1016/j.colsurfa.2013.05.046.
[31] B. Sobac and D. Brutin, "Thermal effects of the substrate on water droplet evaporation," *Phys. Rev. E - Stat. Nonlinear, Soft Matter Phys.*, vol. 86, no. 2, pp. 1–10, 2012, doi: 10.1103/PhysRevE.86.021602.
[32] P. L. Kelly-Zion, C. J. Pursell, S. Vaidya, and J. Batra, "Evaporation of sessile drops under combined diffusion and natural convection," *Colloids Surfaces A Physicochem. Eng. Asp.*, vol. 381, no. 1–3, pp. 31–36, 2011, doi: 10.1016/j.colsurfa.2011.03.020.
[33] F. Carle, B. Sobac, and D. Brutin, "Experimental evidence of the atmospheric convective transport contribution to sessile droplet evaporation," *Appl. Phys. Lett.*, vol. 102, no. 6, 2013, doi: 10.1063/1.4792058.
[34] A. Shaikeea, S. Basu, S. Hatte, and L. Bansal, "Insights into vapor-mediated interactions in a nanocolloidal droplet system: Evaporation dynamics and affects on self-assembly topologies on macro- to microscales," *Langmuir*, vol. 32, no. 40, pp. 10334–10343, 2016, doi: 10.1021/acs.langmuir.6b03024.
[35] J. P. and J. Moon, "Control of Colloidal Particle Deposit Patterns within Picoliter Droplets Ejected by Ink-Jet Printing," *Langmuir*, vol. 22, no. 8, pp. 3506–3513, Apr. 2006, doi: 10.1021/LA053450J.
[36] R. W. Style *et al.*, "Patterning droplets with durotaxis," *Proc. Natl. Acad. Sci.*, vol. 110, no. 31, pp. 12541–12544, Jul. 2013, doi: 10.1073/PNAS.1307122110.
[37] X. Chen *et al.*, "Evaporation of droplets on superhydrophobic surfaces: Surface roughness and small droplet size effects," *Phys. Rev. Lett.*, vol. 109, no. 11, p. 116101, Sep. 2012, doi: 10.1103/PhysRevLett.109.116101.
[38] M. Labowsky, "The effects of nearest neighbor interactions on the evaporation rate of cloud particles," *Chem. Eng. Sci.*, vol. 31, no. 9, pp. 803–813, 1976, doi: 10.1016/0009-2509(76)80054-1.
[39] A. J. D. Shaikeea and S. Basu, "Evaporating sessile droplet pair: Insights into contact line motion, flow transitions and emergence of universal vaporisation pattern," *Appl. Phys. Lett.*, vol. 108, no. 24, 2016, doi: 10.1063/1.4953836.
[40] A. J. D. Shaikeea and S. Basu, "Insight into the Evaporation Dynamics of a Pair of Sessile

Droplets on a Hydrophobic Substrate," *Langmuir*, vol. 32, no. 5, pp. 1309–1318, 2016, doi: 10.1021/acs.langmuir.5b04570.
[41] T. K. Pradhan and P. K. Panigrahi, "Deposition pattern of interacting droplets," *Colloids Surfaces A Physicochem. Eng. Asp.*, vol. 482, pp. 562–567, 2015, doi: 10.1016/j.colsurfa.2015.07.013.
[42] L. Chen and J. R. G. Evans, "Arched structures created by colloidal droplets as they dry," *Langmuir*, vol. 25, no. 19, pp. 11299–11301, 2009, doi: 10.1021/la902918m.
[43] S. Hatte and S. Pandey, Keshav Pandey, Khushboo Chakraborty, Suman Basu, "Universal evaporation dynamics of ordered arrays of sessile droplets," *J. Fluid Mech.*, vol. 866, pp. 61–81, 2019, doi: 10.1017/jfm.2019.105.
[44] S. Hatte, K. Pandey, K. Pandey, S. Chakraborty, and S. Basu, "Universal evaporation dynamics of ordered arrays of sessile droplets," *J. Fluid Mech.*, vol. 866, pp. 61–81, 2019, doi: 10.1017/jfm.2019.105.
[45] A. W. Wray, B. R. Duffy, and S. K. Wilson, "Competitive evaporation of multiple sessile droplets," *J. Fluid Mech.*, vol. 884, 2019, doi: 10.1017/jfm.2019.919.
[46] V. I. Fabrikant, "On the potential flow through membranes," *ZAMP Zeitschrift für Angew. Math. und Phys.*, vol. 36, no. 4, pp. 616–623, 1985, doi: 10.1007/BF00945301.
[47] S. Tonini and G. E. Cossali, "Analytical modeling of the evaporation of sessile drop linear arrays," *Phys. Rev. E*, vol. 105, no. 5, pp. 1–13, 2022, doi: 10.1103/PhysRevE.105.054803.
[48] A. Azzam, R. Kempers, and A. Amirfazli, "Modeling of the evaporation process of a pair of sessile droplets using a point source model (PSM)," *Int. Commun. Heat Mass Transf.*, vol. 157, p. 107733, 2024, doi: 10.1016/j.icheatmasstransfer.2024.107733.
[49] R. D. Deegan, O. Bakajin, T. F. Dupont, G. Huber, S. R. Nagel, and T. A. Witten, "Contact line deposits in an evaporating drop," *Phys. Rev. E - Stat. Physics, Plasmas, Fluids, Relat. Interdiscip. Top.*, vol. 62, no. 1 B, pp. 756–765, 2000, doi: 10.1103/PhysRevE.62.756.
[50] P. L. Kelly-Zion, C. J. Pursell, G. N. Wassom, B. V. Mandelkorn, and C. Nkinthorn, "Correlation for sessile drop evaporation over a wide range of drop volatilities, ambient gases and pressures," *Int. J. Heat Mass Transf.*, vol. 118, pp. 355–367, 2018, doi: 10.1016/j.ijheatmasstransfer.2017.10.129.

Chapter 4 Vapor-Induced Motion of a Pure Droplet by a Mixture Droplet on a Heated Substrate

4.1 Introduction

The controlled movement of droplets across surfaces is involved in numerous applications, including microfluidics [1], biology [2], and heat transfer [3].

Various methods have been employed to achieve controlled droplet movement on different surfaces, as well as the merging of sessile droplets [4–6]. These techniques include surface energy gradients [7], surface modifications [8, 9], and the application of external fields such as thermal, acoustic and others [10–12] to facilitate droplet transport. Any of these approaches require overcoming contact line pinning caused by contact angle hysteresis causing droplet to adhere to the surface.

Recently, it was found that the influence of nearby droplets through vapor field can be sufficiently strong to induce droplet movement on high-energy surfaces by overcoming contact line pinning. Droplet interactions are driven by evaporation-induced surface tension gradients, leading to motion. In binary liquid droplets, this behavior is primarily governed by the solutal Marangoni effect, while in pure liquid droplets, differences in evaporation rates can also induce movement. Cira et al. [13] studied interactions between two droplets using mixtures of propylene glycol (PG) and water. Based on their experiments, they concluded that the presence of the other droplet causes uneven evaporation across the surface of the droplets. This uneven evaporation generates a concentration gradient within the droplets, which in turn induces Marangoni flow, ultimately driving the motion of the droplets. However, their findings did not provide insight into how the droplet motion could be controlled, for instance, by accelerating or decelerating it.

When two adjacent propylene glycol (PG)-water droplets with different compositions are placed within three contact diameters of each other, their interaction is divided in two "sequential" main stages, see **Figure 4-1**. In the first stage (**Figure 4-1.a**), which is called long-range interaction, droplets will attract or repulse each other depending on the composition of the droplets. In the second stage (**Figure 4-1.b**), known as short-range interaction, the droplets will coalesce or chase each other [14–18]. Droplets with similar concentrations will coalesce, while those with different concentrations will chase each other.

Water has a significantly higher vapor pressure than PG, by approximately three orders of magnitude, causing it to evaporate much faster. As a result, during the evaporation process, a wedge region enriched with water vapor forms between the droplets (**Figure 4-1.a**). This causes the surfaces of the droplets exposed to this wedge region, proximal sides, to experience higher water vapor enrichment compared to other areas, distal sides. Since water has a higher surface tension, this creates a surface tension imbalance, which generates a force pulling the droplets toward each other [14, 16]. When the two droplets come close, a small amount of mass exchange occurs through the precursor film or direct contact. If the droplets have similar concentrations, they merge upon initial contact. However, for droplets with different concentrations, small regions of the droplet surface become contaminated by the liquid from neighboring droplets, as indicated by γ_{AC} in **Figure 4-1.b**, while the remaining surface retains the original liquid composition, represented by, γ_{BC}. This behavior can be understood by considering that the diffusion coefficient of (PG) in water is on the order of 10^{-5} cm²/s [19], and the surface area of a small droplet (volume < 5 μL) is approximately 10^{-1} cm². Based on this, the estimated time for PG to diffuse across the entire surface of the water droplet is around 10^{4} seconds—long enough that γ_{BC} remains largely unchanged during the interaction. As a result, this mass exchange creates

concentration gradients, and surface tension gradient force represented by the dashed arrows in **Figure 4-1.b**, causing the droplet with lower surface tension to chase the one with higher surface tension [14].

Besides the interaction between binary droplets, theoretical work in [20], later confirmed experimentally by [21] and [15], shows that vapor-mediated motion can also occur with nearby pure liquid droplets, even without the solutal Marangoni effect. Man et al. [20], using the Onsager principle, theoretically predicted the motion of two pure droplets and introduced a new mechanism for droplet movement. They demonstrated that droplet motion can occur without the Marangoni effect, driven by a gradient in the evaporation rate. The uneven evaporation rate causes droplets to move from high evaporation side (distal side) to low evaporation one (proximal side) to minimize energy dissipation associated with the fluid flow generated by evaporation. Also, Sadafi et al. [15] identified additional mechanisms that could explain the motion of two droplets of the same liquid. These mechanisms include the thermocapillary effect resulting from temperature variations across the substrate and changes in contact angles due to evaporation. However, it remains unclear whether the solutal Marangoni effect or the thermocapillary effect plays a more dominant role in controlling droplet motion, warranting further investigation.

(a)

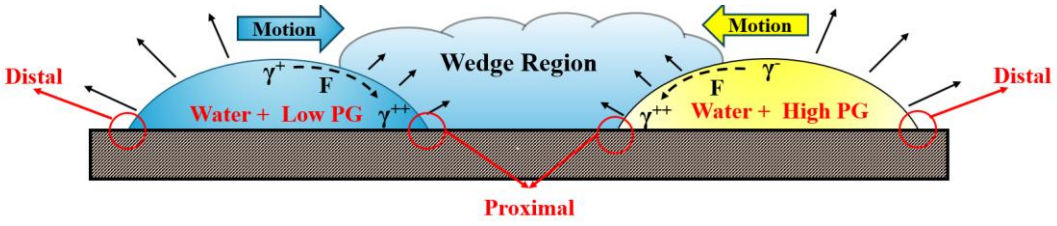

(b)

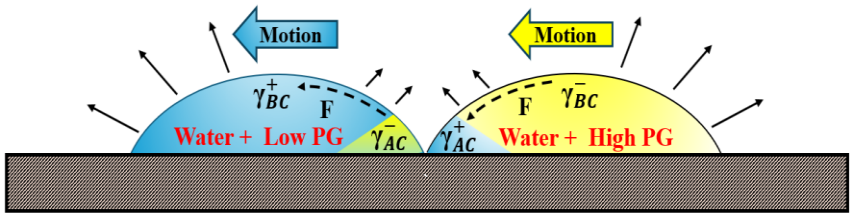

Figure 4-1 Schematics of a central (midplane) sectional plan of a pair of adjacent propylene glycol (PG)-water droplets of different PG concentrations during: **(a)** long-range interaction, and **(b)** short-range interaction. The solid arrows represent the interfacial mass flux. The dotted arrows represent the direction of the driving force from low surface tension regions to the higher ones; γ_{BC}, and γ_{AC} are the surface tensions before and after contact of the droplets, respectively.

While these studies offer valuable insights into the motion mechanisms of sessile droplets on an inert substrate, many questions remain unanswered. In applications such as heat exchangers and 3D printers, substrate temperature significantly influences the wetting behavior of liquids and, consequently, droplet movement. Previous experimental and theoretical studies [13, 15–17, 20, 21], have focused solely on unheated inert substrates and have not explored the impact of substrate temperature on droplet motion.

The surface tension of any liquid is inversely proportional to temperature [22]. Therefore, increasing the substrate temperature reduces the surface tension of the liquids, which in turn lowers the driving force on the droplet and decreases its velocity. At the same time, a higher substrate temperature increases the evaporation rate of one droplet and can enhance the condensation rate on the other droplet, creating a larger surface tension gradient across the droplet's surface and thereby increasing its velocity. Therefore, increasing the substrate temperature causes two opposing effects: it can reduce the droplet's velocity by lowering the liquid's surface tension, while simultaneously cause an increasing in the velocity by increasing the evaporation-condensation process and the resulting surface tension gradient. The net effect depends on the relative dominance of these two opposing mechanisms. A hypothesis can be

proposed that varying the substrate temperature may either increase or decrease the velocity of droplets. This characteristic offers a versatile approach for controlling droplet motion, which is advantageous for practical applications such as heat exchangers and surface cleaning processes, where controllable droplet dynamics are needed.

The above hypothesis can be further clarified using the empirical correlation introduced in our previous study [23] for the evaporation of a pair of sessile droplets on a heated substrate, see Eq. (4-1). The total evaporation rate ($\dot{m}_{evap}$) as a function of the separation distance (L) between two droplets was given as a function of contact angle of the droplet, θ, the diffusion coefficient for vapor in air, D, the momentum diffusivity, v, the droplet's contact radius, a, and (C_s) and (C_∞), i.e. the vapor concentration at the droplet surface (T_s) and far field (T_∞), respectively.

$$\dot{m}_{evap} = \frac{1-\frac{a}{L}}{1-\frac{a^2}{L^2}} \times \left[-2\pi\, a\, D\, \frac{sin\theta}{1+cos\theta}\left(C_S\left(T_s\right) - RH.C_S\left(T_\infty\right)\right) 56.561\theta^{-0.892}\right] \times \left\{1 + 0.008 \times \left[\left(\frac{C_S - C_\infty}{C_\infty}\right)^{0.014} \times \left(\frac{g.a^3}{v^2}\right)^{1.078} \times \left(\frac{v}{D}\right)^{1.334} \times \left({}^{L}/_{d}\right)^{0.264}\right]\right\} \quad (4\text{-}1)$$

According to Eq. (4-1), increasing the substrate temperature, T_s, increases the evaporation-condensation rates of the droplets which leads to a higher surface tension gradient and, consequently, higher droplets velocities. It is worth mentioning that Eq. (4-1), was originally formulated to determine the evaporation rate for a pair of pure liquid sessile droplets. However, the same physical principles apply to a pair of sessile droplets with different compositions. As such, increasing the substrate temperature will yield similar results, due to increasing C_s on the surface of the droplets, leading to an enhanced evaporation rate for the droplets. So, the droplet motion behavior of droplets on a substrate can be fine-tuned by adjusting the substrate temperature.

Additionally, as shown in **Figure 4-1**, during the second stage of interaction, known as short-range interaction (**Figure 4-1.b**), the driving force becomes more affected by the droplet composition. The droplets contact, exchanging mass and forming contaminated regions with surface tensions (γ_{AC}) dependent on the neighboring droplet's composition. Depending on the composition, this interaction can create either a strong or weak surface tension gradient, which subsequently affects the velocity of the droplets. The effect of varying droplet composition on droplet velocity also remains unanswered in the literature. Although Cira et al. [13] made significant contributions, their velocity experiments only involved droplets with 10% PG. Similarly, studies in [17] and [16] examined droplets with concentrations of 20% PG and 10% PG, respectively, for velocity experiments.

The objective of this study is to examine how substrate temperature and droplet composition influence the droplet velocities at short range. This is examined using one water droplet and one propylene glycol (PG)-water mixture droplet with varying compositions. The droplets rest on a heated glass substrate at different temperatures.

4.2 Experimental Apparatus

An experimental apparatus was designed and constructed to study the motion of a pair of sessile droplets sitting on a heated glass substrate, see **Figure 2-2**. The droplets were placed on the substrate by using a motorized syringe pump (KD Scientific-788111) with a volume accuracy of ±0.5%. The distance between the droplets was controlled by using a linear X-stage with an accuracy of ± 0.01 mm. Two cameras (**Figure 2-2**, Camera I and Camera II) were employed to capture position of the droplet at each moment. Camera I and Camera II (Plugable, 2MP, 250x Magnification) were vertically and horizontally mounted, respectively. The recorded images and videos were captured at a scale of 36 pixels per millimeter. During the experiments, the needles

were carefully aligned to be on one horizontal plane parallel to Camera I. The tests were repeated 5-10 times to ensure that the droplet motion occurred in this horizontal plane. This approach ensured the accuracy of the droplet positions, eliminating any influence from motion perpendicular to the imaging plane. All experiments were conducted within a humidity-controlled chamber constructed from 10 mm thick transparent acrylic, with dimensions of 28 cm (L) × 32 cm (W) × 41 cm (H). Humidity was regulated by a programmable humidity controller (IHC200, Inkbird), capable of maintaining the relative humidity between 5% and 99%, with an accuracy of ±3%. The substrate was untreated glass with dimensions of 75mm by 50mm. The glass substrate was heated by a polyimide heater (12V, 7W). The substrate temperature was maintained using an Arduino-based PID controller. The temperatures of the substrate and the ambient were monitored using K-type thermocouples with an accuracy of ± 0.1°C.

Experiments were carried out at substrate temperatures ranging from 24 to 135°C. We observed that coalescence occurs when the distance between the droplets is slightly less than 3.5 mm. Therefore, a separation distance of 3.5 mm was chosen for all experiments. For the propylene glycol (PG)-water droplet, the actuating droplet, PG concentrations ranged from 20 to 100% by volume. An initial droplet volume of 3.5 μL was used for all experiments. Volumes larger than 3.5 μL caused distortion of the contact line, preventing the droplet from maintaining a spherical cap shape. The relative humidity inside the chamber was fixed at 47% ± 3% and ambient temperatures was approximately 24°C.

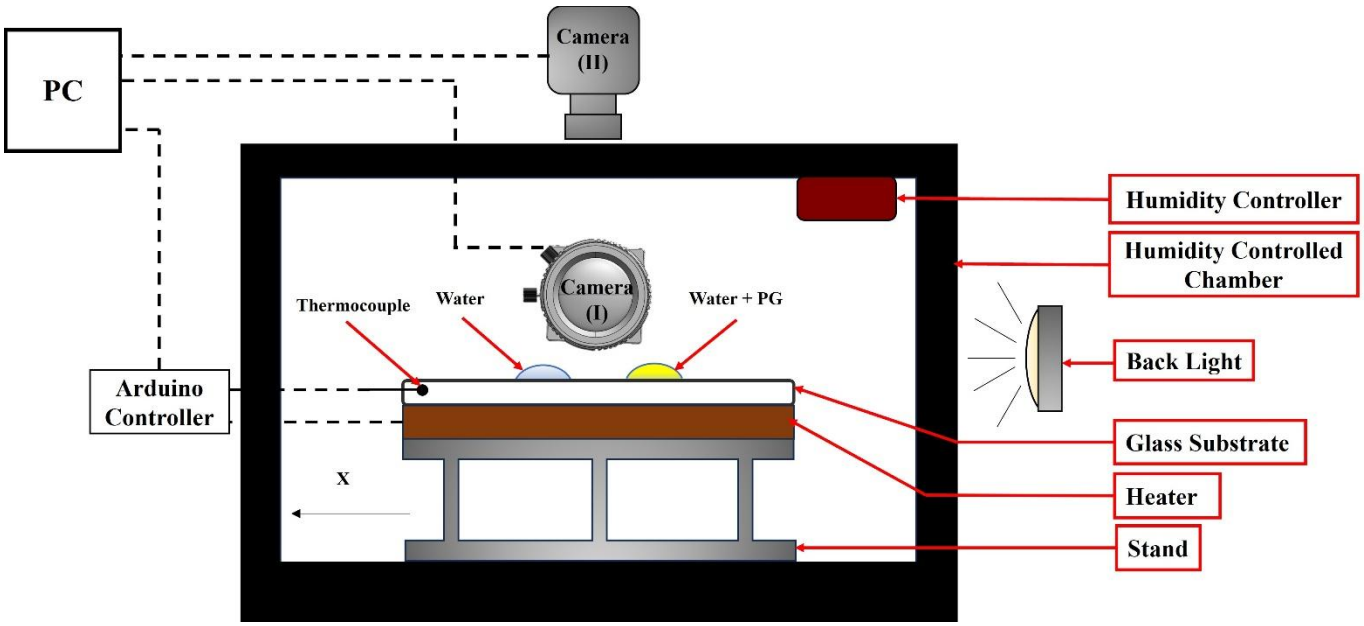

Figure 4-2 Schematic of the experimental apparatus (the droplet sizes are exaggerated for clarity).

4.3 Assumptions and Range of Applicability

For this part of the study, we assume the following:

1. The system is assumed to be isothermal, neglecting any variation in droplet surface temperature. This assumption is introduced for simplification, given the absence of experimental means to accurately measure surface temperatures.
2. In chapter 03, we proposed an empirical correlation for the evaporation rate of a pair of sessile droplets on a heated substrate combining both diffusive and convective effects. Although, this correlation was originally derived to calculate the evaporation rate for a pair of pure liquid sessile droplets, it can be employed for a pair of sessile droplets with different compositions since it holds the same physical principles.

4.4 Results and Discussion

Here first the effect of substrate temperature on the droplet motion of a pair of water and PG-water mixture droplets is investigated. This is followed by the effect of composition on the motion, and finally the combined effect of changing temperature and composition for the PG-water droplet.

4.4.1 Substrate Temperature Effect on Droplet Motion

The effect of substrate temperature was examined using a pair of initially sessile droplets: one consisting of pure water and the other of pure propylene glycol (PG) (the actuating droplet). As discussed in the Introduction section, when two droplets of different surface tensions become sufficiently close, mass exchange occurs between them, causing the surface tensions of the contaminated regions to change from γ_{BC} to γ_{AC} as illustrated in **Figure 4-1.b**. This surface tension gradient drives the droplet with the lower surface tension to chase the droplet with the higher surface tension [14]. This was seen experimentally, see **Figure 4-3** and (**Supplementary Video-01**), in which the lower surface tension PG droplet chases the higher surface tension water droplet. This observation is consistent with the previous study [24]. Furthermore, higher substrate temperatures (up to the boiling point of the liquid with the lowest boiling temperature (100 °C for water) result in increased droplet velocities as shown in **Figure 4-3** and the video in **Supplementary Video-01**.

Furthermore, the velocity of the water droplet was quantified by tracking its X-position, the linear distance travelled along the direction of motion, the over a fixed time interval, Δt, of 0.25 seconds (fixed for all experiments) and is plotted in **Figure 4-4.a**. The droplet's velocity was then calculated by averaging the measured velocities throughout the entire motion period, **Figure 4-4.b**. This shows that substrate temperature significantly increases the droplet velocity. When

the temperature increases by 20°C, from T_S = 24°C (unheated condition) to T_S = 45°C, the droplet velocity more than doubles. Furthermore, when the temperature exceeds 45°C, the velocity increase reaches approximately 7 times at T_S = 90°C.

The effect of substrate temperature can be explained using Eq. (3-4), which indicates that the evaporation rate is directly proportional to the substrate temperature. As the substrate temperature increases, vapor concentration at the droplet surface, C_s, increases, i.e. $(C_s - C_\infty)$ increases. The increase of concentration potential, $(C_s - C_\infty)$, the evaporation rate increases, that results in a higher condensation rate of PG vapour on the water droplet's surface. Such condensation leads to a steeper surface tension gradient, that propels the droplet faster.

To provide a simplified representation of this finding, an order-of-magnitude model was constructed analysing the data in **Figure 4-4.b**, see Eq. (4-2). The temperature-dependent diffusion coefficient can be expressed in Eq. (4-3), where D_{ref} is the reference diffusion coefficient at a reference temperature T_{ref} [25, 26]. Furthermore, according to kinetic theory, the mean molecular speed, $\bar{u}$, is proportional to $T^{1.5}$ [25]. This indicates that both the mass diffusivity and the mean molecular speed are proportional to the substrate temperature raised to the power of 1.5, assuming thermal equilibrium between the substrate and the droplet surfaces. Physically, this means that as the substrate temperature increases, molecular diffusion accelerates with a power-law dependence of 1.5. This enhanced diffusion strengthens the surface tension gradient, thereby increasing the droplet velocity, which agrees with our experimental findings. This approximation captures the key scaling behavior of the system, offering insight into the change of U_{avg} with the changing of the substrate temperature.

$$U_{avg} \sim 10^{-3}.T_S^{1.5} \tag{4-2}$$

$$D(T) = D_{ref}\left(\frac{T}{T_{ref}}\right)^{1.5} \quad (4\text{-}3)$$

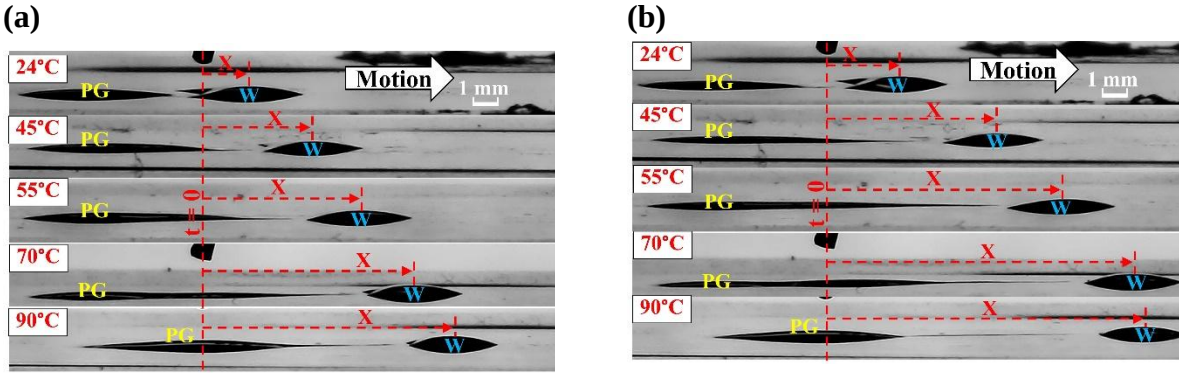

Figure 4-3 Picture sequence showing side view of the motion of a 3.5 µL water droplet (Right) induced by a 3.5 µL PG droplet (Left) in each frame, for: **(a)** t=2.5 s, and **(b)** t=5 seconds of the interaction at different substrate temperatures.

Notably, when the substrate temperature rises above 100°C (the boiling point of water), the droplet velocity increases. At T_S = 110°C, the velocity is 9 times higher than that of the unheated condition, while at T_S = 135°C, it reaches 20 times higher (**Supplementary Video-01**). However, the droplet travels a shorter distance in these cases compared to all other conditions, **Figure 4-5**. The reason the droplet travels a shorter distance is the boiling during its motion. Boiling reduces the amount of water on the droplet's distal side, where surface tension is higher. This reduction is attributed to the better mixing between the water and PG, due to boiling, smooths the surface tension gradient over the surface of the droplet, weakening the driving force and ultimately causing the droplet to come to a stop.

The shorter traveling distances of droplets on substrates heated above 100°C can be further analysed using the model proposed in our previous study [27]. According to the literature, the evaporation of water sessile droplets on glass substrates is primarily governed by the CCR evaporation mode. Therefore, Eq. (4-4) from our previous study [27] can be used to estimate the evaporation time for a pair of sessile water droplets on a glass substrate under the CCR mode.

Although, Eq. (4-4), was originally derived to calculate the evaporation time for a pair of pure liquid sessile droplets, it can be employed for a pair of sessile droplets with different compositions since it holds the same physical principles.

$$\int_{\theta_0}^{\theta_f} \frac{\theta^{0.892}}{56.561\ sin\theta\ \ (1+cos\theta)}\ d\theta = \frac{-2LD\left(C_S\left(T_s\right) - RH.\,C_S\left(T_\infty\right)\right)}{(a+L)\ \ a^2\ \rho_L}\ t_e \qquad (4\text{-}4)$$

where θ is the instantaneous contact angle of the droplet at any given time $0 < t < t_e$, and θ_0 is the initial contact angle of the droplet, and θ_f is the droplet's final contact angle. Form Eq. (4-4)(2-10), it can be determined that for a pair of sessile water droplet with a volume of 3.5 µl on a heated substrate at 100°C, the time, t_e, required to lose half of their mass is in order of 1-2 seconds. As shown in **Figure 4-5**, the droplets lost approximately half of their mass within a 2.5-second time span under both temperature conditions (110°C, and 135°C). Therefore, the increased mass loss of water from the droplet leads to a smoother surface tension gradient, ultimately causing the droplet's motion to stop.

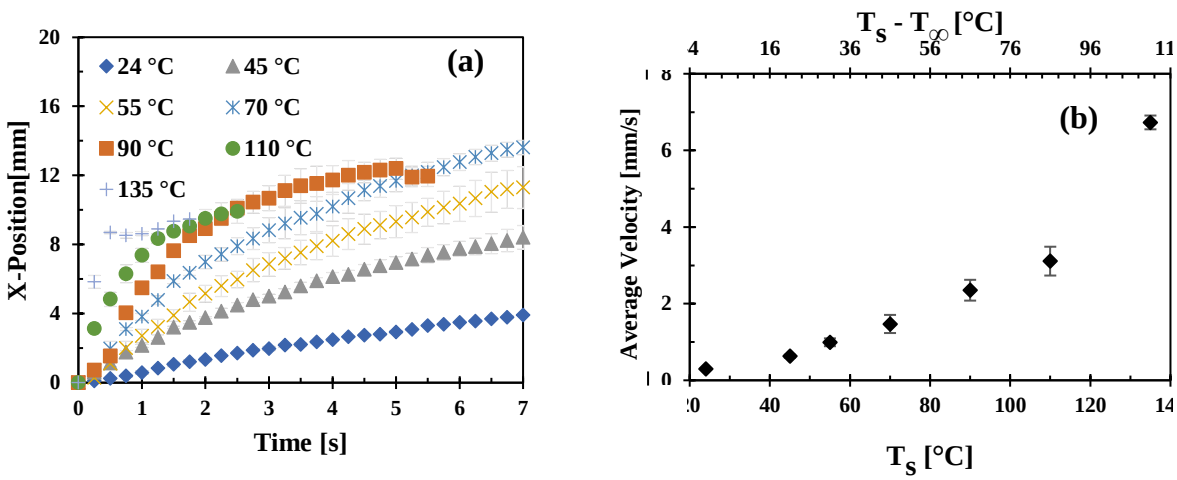

Figure 4-4 Position **(a)**, and velocity **(b)** of the water droplet movement induced by 100% PG droplet under different substrate temperatures

(a) **(b)**

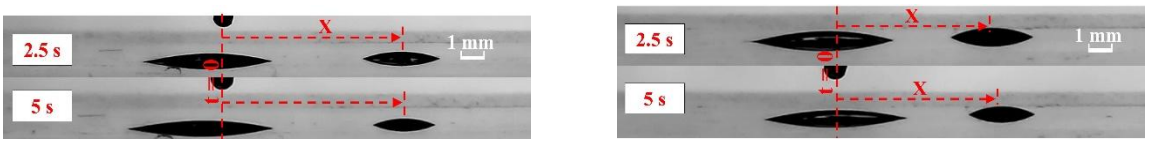

Figure 4-5 Picture sequence showing side view of the motion of a 3.5 µL water droplet (Right) induced by a 3.5 µL PG droplet (left) at **(a)** T_S=110 °C, and **(b)** T_S=135 °C, for various times shown on each frame

4.4.2 Droplet Composition Effect on Droplet Motion

To quantify how the actuating droplet's composition affects the velocity of a water droplet at uniform substrate temperature, we placed a droplet of water and a PG mixture with varying PG concentrations on an unheated glass substrate.

Figure 4-6 and **Supplementary Video-02** shows that decreasing the PG concentration, increases the velocity of the water droplet. This finding is consistent with the model proposed by Sellier et al. [24, 28], in which they showed that the velocity of the water droplet is proportional to $(\gamma_{\text{distal}} - \gamma_{\text{proximal}})$ when they used a pure ethanol droplet as an actuating droplet. When the actuating droplet has lower PG concentration and contacts the water droplet, mass exchange creates a lower PG concentration at the proximal side (lower $\gamma_{proximal}$) of the water droplet compared to cases with higher PG levels. This results in a steeper concentration gradient across the droplet's surface, higher $(\gamma_{\text{distal}} - \gamma_{\text{proximal}})$, which generates a stronger driving force and, consequently, a higher droplet velocity. To better understand the impact of PG concentration on the surface tension of W–PG mixture droplets, **Figure 4-7.a** illustrates this relationship using surface tension data from [29, 30]. It can be observed that the effect of PG concentration is more pronounced for concentrations below 50%. In contrast, for PG concentrations above 50%, the variation in the mixture's surface tension becomes less significant. So, by decreasing the PG concentrations of the actuating droplet, the amount of the PG left on the proximal side of the

water droplet after contact decreases and creates a stronger surface tension gradient along the droplet's surface.

Another possible explanation for this phenomena, proposed by Sadafi et al. [15], is the vapor-induced thermal gradient (VTG) mechanism. In this mechanism, when two droplets are placed adjacent to each other, a wedge area with higher vapor concentration forms between them [27]. This wedge reduces the evaporation flux on the proximal side of the droplet, while the distal side experiences higher evaporation flux. The increased evaporation on the distal side lowers its interface temperature, around 3-4 °C for water droplets [31], leading to a higher surface tension (γ_{distal}). Conversely, reduced evaporation on the proximal side raises its interface temperature, decreasing ($\gamma_{proximal}$). Therefore, when the actuating droplet has a higher water concentration (or lower PG), the wedge area's concentration increases, which further reduces the evaporation flux on the proximal side of the water droplet. This increases the surface tension gradient $(\gamma_{\text{distal}} - \gamma_{\text{proximal}})$, thereby increasing the driving force and, consequently, the droplet velocity [24, 28].

However, our experimental findings align more closely with **Figure 4-7.a**, which demonstrates that the variation in PG concentration has a more dominant effect on the surface tension of the mixture than the VTG mechanism. Additionally, the temperature gradients caused by the latent heat of vaporization are relatively small, around 3-4 °C for water droplets [31], which aligns with the experimental findings of approximately 2°C reported by Sadafi et al. [15]. A comparison of **Figure 4-7.a**, and **Figure 4-7.b** reveals that reducing the PG concentration by 10% (e.g., from 50% to 40%, as shown in **Figure 4-7.a**) increases the surface tension by nearly 9%. In contrast, achieving a similar change by reducing the temperature (as shown in **Figure 4-7.b**) would require a temperature decrease of approximately 30°C, which is unlikely to occur

under normal conditions. As a result, the contribution of the VTG mechanism is less significant compared to the effect of surface tension variation with PG concentration.

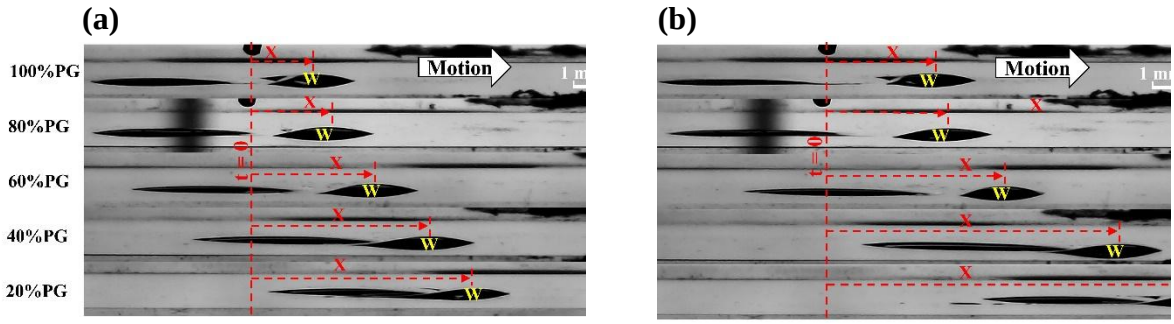

Figure 4-6 Picture sequence showing side view for the motion of a 3.5 µL water droplet (Right) induced by a 3.5 µL PG droplet of different concentration (Left) after **(a)** t=5s, and **(b)** t=10 seconds of the interaction on an unheated glass substrate ($T_s = T_\infty$ =24°C).

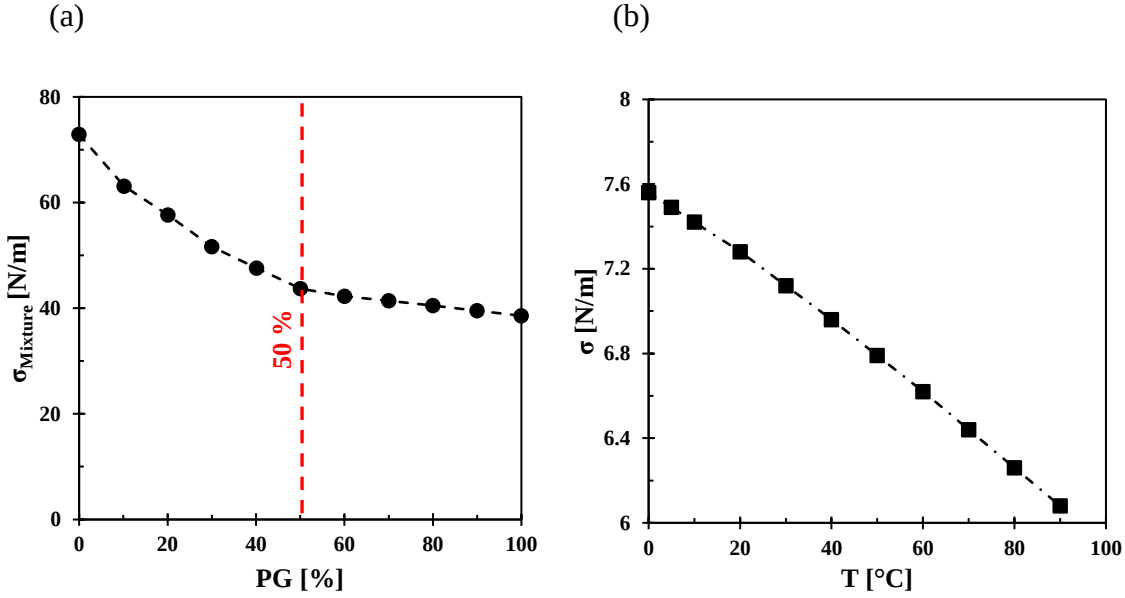

Figure 4-7 (a) Variation of the surface tension of water–propylene glycol (PG) mixtures with PG concentration in water at 20 °C. Data extracted from references [29, 30]. (b) Variation of the surface tension of water as a function of temperature; data extracted from [32].

The position versus time traces for the cases of changing the PG concentrations, are plotted in **Figure 4-8.a**, and the average velocities in **Figure 4-8.b**. These results show that when the

actuating droplet's PG concentration is above 50%, the velocity rises by about 90% as the PG concentration decreases from 100% to 60%. However, when the PG concentration of the actuating droplet is lower than 50%, the velocity of the water droplet increases by around 3 and 6 times when the PG concentration of the actuating droplet decreases to 40% and 20%, respectively. Moreover, the trend observed in **Figure 4-8.b** aligns closely with that in **Figure 4-7.a**. It shows that the effect of PG concentration on the surface tension of the mixture becomes more pronounced at PG concentrations below 50% (9-16%). In contrast, at PG concentrations above 50%, the variation in surface tension is less significant (2-3.5%). To simplify this finding, an order-of-magnitude model was developed using the data from **Figure 4-8.b**, see Eq.(4-5). Interestingly, the molar volume of PG in a PG-W mixture varies as: $PG_{\%}^{1.4}$, based on experimental findings from [30]. This indicates that increasing the PG concentration increases the volume occupied by PG on the proximal side of the water droplet by a power of 1.4. Consequently, this leads to a lower surface tension gradient, $\left(\gamma_{\text{distal}} - \gamma_{\text{proximal}}\right)$, and a reduced droplet velocity, decreasing by a power of 1.3 (where 1.3 ≈ 1.4). Conversely, reducing the PG concentration decreases the PG volume on the proximal side of the droplet, thereby enhancing the surface tension gradient and increasing the droplet velocity.

$$U_{avg} \sim 10^2 . PG_{\%}^{-1.3} \tag{4-5}$$

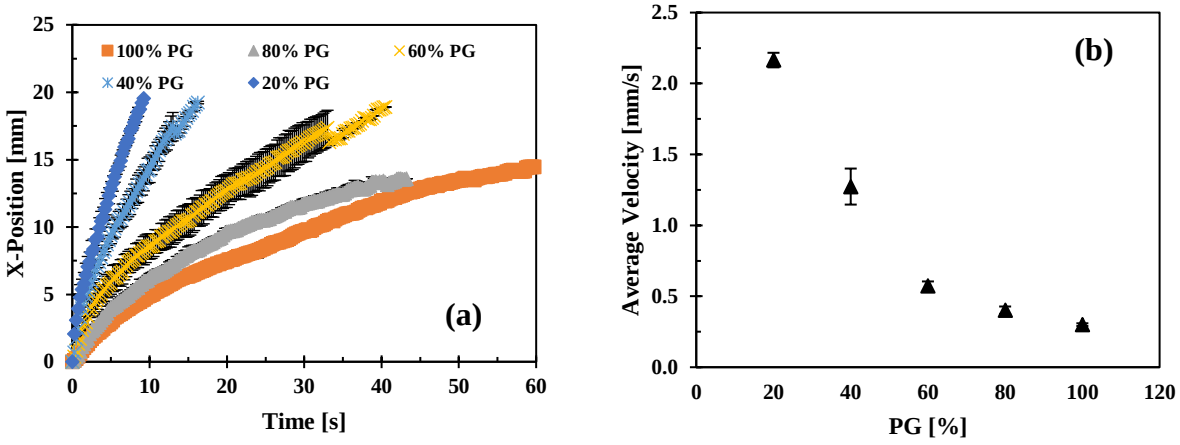

Figure 4-8 Position **(a)**, and velocity **(b)** of the water droplet movement induced by PG droplet of different concentrations on an unheated glass substrate ($T_s = T_\infty = 24°C$).

4.4.3 Combined Temperature and Droplet Composition Effect

Figure 4-9 shows the effects of the composition of the actuating droplet and the substrate temperature on the average velocity of the water droplet. Reducing the concentration of the actuating droplet from 100% to 80% does not significantly increase the water droplet's velocity at any of the substrate temperatures tested. This suggests that even at 80% concentration, the actuating droplet remains sufficiently rich in PG, resulting in minimal change in the surface tension on the distal side of the water droplet. The effect of PG concentration becomes more pronounced at concentrations of 40% and 20%. As the actuating droplet becomes leaner in PG, the reduced surface tension on the distal side of the water droplet consequently increases its average velocity. This finding is compatible with the fact that decreasing the PG concentration increases the surface tension substantially, especially for concentration less than 50% **Figure 4-7.a** (i.e. 40% and 20% in **Figure 4-9**) for any substrate temperature. However, increasing the PG concentration more than 50%, leads to less surface tension gradient with less driving force and lower droplet velocity. Considering that droplet velocity increases as PG concentration decreases ($U_{avg} \alpha\ PG_{\%}^{-1.3}$), Eq.(4-5), due to the molar volume of PG increasing by a power of

1.4, it can be concluded that further reducing PG concentration will further enhance droplet velocity.

The effect of changing the actuating droplet's composition is not as significant as altering the substrate temperature. **Figure 4-9** shows that even a slight increase in substrate temperature, at a constant concentration, boosts the water droplet's velocity more significantly than changes in PG concentration at the same temperature. The effect of the actuating droplets concentration becomes more significant at higher substrate temperatures, while this effect is modest for unheated substrate condition.

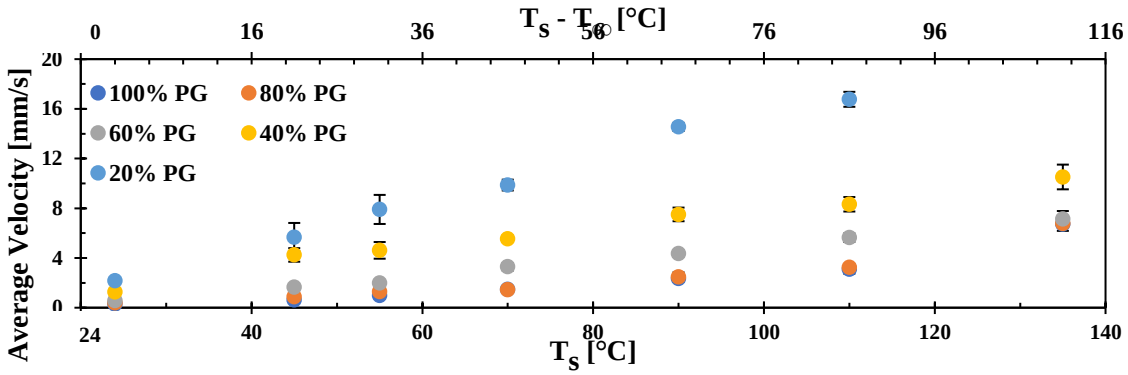

Figure 4-9 The average velocity of the water droplet movement induced by PG droplet of different concentrations under different substrate temperatures

When the actuating droplet contains 20% propylene glycol (PG) under heated substrate condition, the movement of the water droplet becomes very chaotic. This chaotic motion resulted in the formation of smaller droplets during the motion of the water droplet. This phenomenon is illustrated in **Figure 4-10** where the water droplet begins to fragment into smaller droplets as soon as movement starts. This chaotic motion suggests that combining a heated substrate with a lower PG concentration in the actuating droplet significantly enhances the surface tension gradient across the water droplet's surface. This high surface tension gradient, $(\gamma_{\text{proximal}} -$

γ_{distal}), becomes strong enough to overcome the cohesive forces within the water droplet, causing it to split into smaller droplets. After separation, these smaller droplets, with unknown concentrations and surface tension gradients, exhibit random motion in both magnitude and direction. Each droplet develops its own surface tension gradient based on its composition post-separation. This unique surface tension gradient drives the droplets to move in various directions at different velocities, resulting in chaotic motion.

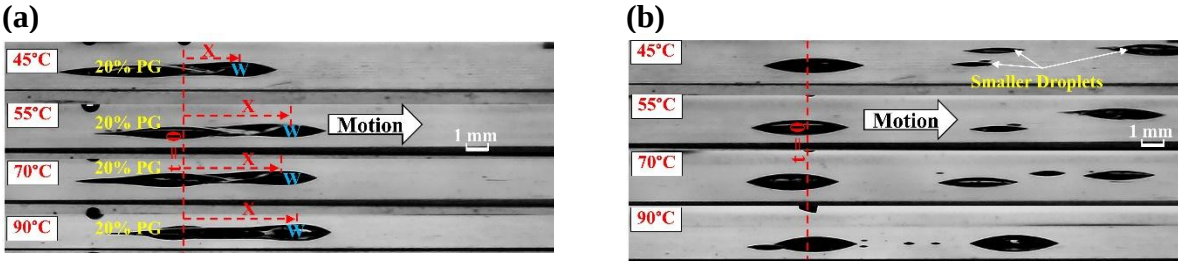

Figure 4-10 Picture sequence showing side view of the motion of a 3.5 µL water droplet (Right) induced by a 3.5 µL 20% PG droplet (Left) at **(a)** t=0.25 s, and **(b)** final state of the interaction at different substrate temperatures.

In all cases examined in this study, the actuating droplet consistently chases the water droplet. However, two instances of coalescences were observed and are illustrated in **Figure 4-11**. Coalescence occurs when the actuating droplet has a concentration of 20% and the substrate temperatures are 110°C and 135°C. At 110°C, the coalescent droplet continues to move after coalescence, whereas at 135°C, the coalescent droplet remains stationary after coalescence. Given that water constitutes 80% of the actuating droplet, the coalescence of the two droplets is more likely to occur [14–18]. Additionally, at a substrate temperature of 135°C, evaporation rate on the distal side of the coalesced droplet is higher than that when it is at 110°C. This increase in evaporation rate causes a more rapid reduction in surface tension on the distal side, γ_{distal}, at 135°C, leading the coalesced droplet to stop earlier.

(a) **(b)**

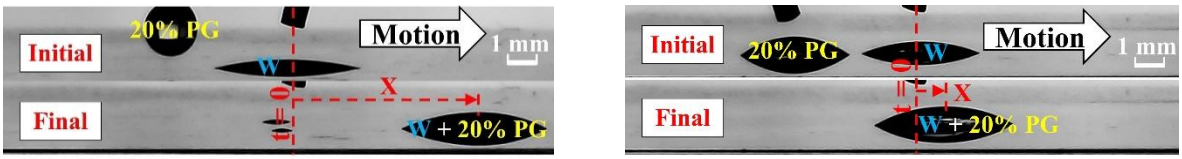

Figure 4-11 Picture sequence showing side view of initial and finale states of a 3.5 µL water droplet (Right) induced by a 3.5 µL 20% PG droplet (Left) at **(a)** T_s=110°C, and **(b)** T_s=135°C.

4.5 Conclusion

This study investigated the vapor-induced motion of a water droplet in proximity to a propylene glycol (PG)-water mixture droplet on a heated substrate to understand into how substrate temperature and PG concentration influence droplet velocity and movement.

The experiments demonstrated that substrate temperature plays a significant role in driving droplet velocity: As substrate temperature increases, the evaporation rate rises, leading to a more substantial condensation rate on the water droplet and, consequently, an intensified surface tension gradient. This gradient serves as a driving force for motion, accelerating the droplet velocity. The velocity increased dramatically when substrate temperatures exceeded the boiling point of water (100°C), with velocities reaching up to 20 times of those observed under unheated conditions. However, this high-speed movement also corresponded with a decrease in travel distance, as elevated temperatures led to rapid evaporation on the droplet's distal side, reducing the surface tension differential and bringing the droplet to a stop sooner.

The PG-water mixture composition also had an impact on the water droplet's motion, with lower PG concentrations (20%-40%) producing faster droplet speeds. This effect arises because reduced PG concentrations lead to a sharper concentration gradient across the droplet's surface. Additionally, when the substrate is heated and the PG concentration in the actuating droplet is 20%, chaotic motion and fragmentation of the water droplet occur, indicating that the combined effect of low PG content and high substrate temperatures significantly increases the surface

tension gradient, overcoming the cohesive forces within the droplet and causing it to split into smaller droplets.

This research provides understanding of how thermal and compositional parameters can be manipulated to control droplet movement on surfaces. Such insights could inform the design of future fluidic devices and systems where precise droplet motion control is essential, such as in cooling systems, chemical assays, and self-cleaning applications. Furthermore, investigating the effects of dynamic changes in substrate temperature and composition gradients across larger surfaces could offer additional avenues to control and optimize droplet behavior in practical applications.

4.6 References

1. Chou WL, Lee PY, Yang CL, et al (2015) Recent advances in applications of droplet microfluidics. Micromachines 6:1249–1271. https://doi.org/10.3390/mi6091249
2. Schneider T, Kreutz J, Chiu DT (2013) The potential impact of droplet microfluidics in biology. Anal Chem 85:3476–3482. https://doi.org/10.1021/ac400257c
3. Bonab MS, Wijnperle D, Mugele F, et al (2024) Electrowetting assisted shedding of droplets by a shearing airflow in dropwise condensation. Int J Heat Mass Transf 220:124925. https://doi.org/10.1016/j.ijheatmasstransfer.2023.124925
4. Karpitschka S, Hanske C, Fery A, Riegler H (2014) Coalescence and noncoalescence of sessile drops: Impact of surface forces. Langmuir 30:6826–6830. https://doi.org/10.1021/la500459v
5. Karpitschka S, Riegler H (2010) Quantitative experimental study on the transition between fast and delayed coalescence of sessile droplets with different but completely miscible liquids. Langmuir 26:11823–11829. https://doi.org/10.1021/la1007457
6. Borcia R, Menzel S, Bestehorn M, et al (2011) Delayed coalescence of droplets with miscible liquids: Lubrication and phase field theories. Eur Phys J E 34:1–9. https://doi.org/10.1140/epje/i2011-11024-9
7. Chowdhury IU, Sinha Mahapatra P, Sen AK (2019) Self-driven droplet transport: Effect of wettability gradient and confinement. Phys Fluids 31:. https://doi.org/10.1063/1.5088562
8. Zhang P, Peng B, Wang J, Jiang L (2019) Bioinspired Self-Propulsion of Water Droplets at the Convergence of Janus-Textured Heated Substrates. Adv Funct Mater 29:1–8. https://doi.org/10.1002/adfm.201904535
9. Li P, Cao M, Bai H, et al (2019) Unidirectional Liquid Manipulation Via an Integrated Mesh with Orthogonal Anisotropic Slippery Tracks. Adv Funct Mater 29:1–7. https://doi.org/10.1002/adfm.201904446
10. Irajizad P, Ray S, Farokhnia N, et al (2017) Remote Droplet Manipulation on Self-Healing

Thermally Activated Magnetic Slippery Surfaces. Adv Mater Interfaces 4:1–7. https://doi.org/10.1002/admi.201700009
11. Wixforth A, Strobl C, Gauer C, et al (2004) Acoustic manipulation of small droplets. Anal Bioanal Chem 379:982–991. https://doi.org/10.1007/s00216-004-2693-z
12. Brunet P, Eggers J, Deegan RD (2007) Vibration-induced climbing of drops. Phys Rev Lett 99:3–6. https://doi.org/10.1103/PhysRevLett.99.144501
13. Cira NJ, Benusiglio A, Prakash M (2015) Vapour-mediated sensing and motility in two-component droplets. Nature 519:446–450. https://doi.org/10.1038/nature14272
14. Wang Z, Orejon D, Takata Y, Sefiane K (2022) Wetting and evaporation of multicomponent droplets. Phys Rep 960:1–37. https://doi.org/10.1016/j.physrep.2022.02.005
15. Sadafi H, Dehaeck S, Rednikov A, Colinet P (2019) Vapor-Mediated versus Substrate-Mediated Interactions between Volatile Droplets. Langmuir 35:7060–7065. https://doi.org/10.1021/acs.langmuir.9b00522
16. Benusiglio A, Cira N, Lai AW, Prakash M (2017) Two-component self-contracted droplets: long-range attraction and confinement effects. 2:1–8
17. You A, Be MAY, In I (2020) Evaporation-induced transport of a pure aqueous droplet by an aqueous mixture droplet Evaporation-induced transport of a pure aqueous droplet by an aqueous mixture droplet. 032003: https://doi.org/10.1063/1.5139002
18. Shi S, Man X, Russell TP (2019) Soft Matter. 15:. https://doi.org/10.1039/c8sm02584c
19. Wang MH, Soriano AN, Caparanga AR, Li MH (2010) Binary mutual diffusion coefficient of aqueous solutions of propylene glycol and dipropylene glycol. J Taiwan Inst Chem Eng 41:279–285. https://doi.org/10.1016/j.jtice.2009.09.001
20. Man X, Doi M (2017) Vapor-Induced Motion of Liquid Droplets on an Inert Substrate. Phys Rev Lett 119:44502. https://doi.org/10.1103/PhysRevLett.119.044502
21. Wen Y, Kim PY, Shi S, et al (2019) Vapor-induced motion of two pure liquid droplets. Soft Matter 15:2135–2139. https://doi.org/10.1039/C8SM02584C
22. Education P (1976) The effect of temperature on surface tension
23. Azzam A, Amirfazli A, Kempers R (2024) Modelling of the Evaporation Process of a Pair of Sessile Droplets on a Heated Substrate. Under Rev
24. Sellier M, Nock V, Gaubert C, Verdier C (2013) Droplet actuation induced by coalescence: Experimental evidences and phenomenological modeling. Eur Phys J Spec Top 219:131–141. https://doi.org/10.1140/epjst/e2013-01788-0
25. Bird RB, W.E. Stewart, E.N. Lightfoot (1960) Transport Phenomena Title No Title No Title
26. Pan Z, Dash S, Weibel JA, Garimella S V. (2013) Assessment of water droplet evaporation mechanisms on hydrophobic and superhydrophobic substrates. Langmuir 29:15831–15841. https://doi.org/10.1021/la4045286
27. Azzam A, Kempers R, Amirfazli A (2024) Modeling of the evaporation process of a pair of sessile droplets using a point source model (PSM). Int Commun Heat Mass Transf 157:107733. https://doi.org/10.1016/j.icheatmasstransfer.2024.107733
28. Sellier M, Nock V, Verdier C (2011) Self-propelling, coalescing droplets. Int J Multiph Flow 37:462–468. https://doi.org/10.1016/j.ijmultiphaseflow.2011.01.001
29. Townsend DF, Ross S (1986) Surface Activity of the System Poly (propylene glycol) + Water. 284–287
30. Khattab IS, Bandarkar F, Khoubnasabjafari M, Jouyban A (2012) Density , viscosity , surface tension , and molar volume of propylene glycol + water mixtures from 293 to 323

K and correlations by the Jouyban – Acree model. Arab J Chem. https://doi.org/10.1016/j.arabjc.2012.07.012
31. Erbil HY, Dogan M (2000) Determination of Diffusion Coefficient - Vapor Pressure. 9267–9273
32. Gittens GJ (1969) Variation of surface tension of water with temperature. J Colloid Interface Sci 30:406–412. https://doi.org/10.1016/0021-9797(69)90409-3

Chapter 5 Modeling of the Evaporation Process of an Array of Three Sessile Droplets Using a Point Source Model (PSM)

5.1 Introduction

In **Section 2.2.1**, the analytical model for a pair of sessile droplets, PSM, was introduced. A correction factor, η, was proposed to account for the interaction between droplets. This factor is defined as the ratio of the evaporation rate for a pair of interacting droplets ($\dot{m}_{sys}$) to that for single isolated droplet ($\dot{m}_{iso}$). The correction factor, η, is expressed as a function of *L/d*, where, *L*, represents the separation distance between the droplets, and, *d*, denotes the droplet's contact diameter, as described in Eq. (5-1).

$$\eta = \frac{2\ (L/d)}{2\ (L/d) + 1} \tag{5-1}$$

5.2 Modelling Procedure

The evaporation of an array of N-droplets can be simplified by representing it as smaller units, each containing three droplets. Following the same approach used, PSM, to derive Eq. (2-5), the objective here is to determine the new correction factor, η, for a system where a third droplet is added to a pair of sessile droplets. This can be achieved by extending the correction factor formula that was used for a pair of sessile droplets, eq. (5-2), to find the correction factor for an array of three droplets. In Eq. (5-2), i=1, 2,….N represents each droplet location on the substrate, and j=1, 2,….N represents the surrounding sources at each location, **Figure 5-1**.

$$\eta_i + \sum_{j=1, j\neq i}^{N} \eta_j \left(\frac{a}{|\vec{r}_i - \vec{r}_j|} \right) = 1 \tag{5-2}$$

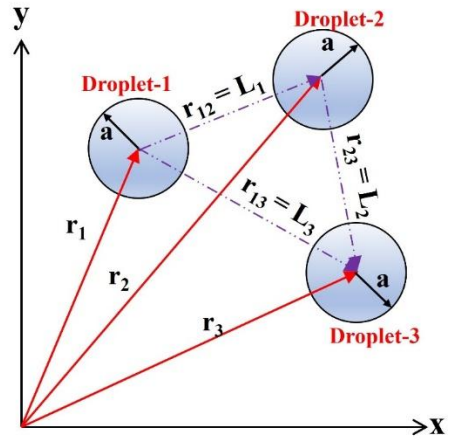

Figure 5-1 Schematic top view of the victor positions for the PSM of three droplets array.

For simplification, let $K_1 = {}^{d}/_{2L_1}$, $K_2 = {}^{d}/_{2L_2}$, and $K_3 = {}^{d}/_{2L_3}$, where K_1, K_2, and K_3 are constants and $d=2a$. By expanding Eq. (5-2), the correction factor of each droplet can be determined from Eq. (5-3), (5-4), and (5-5).

$$\eta_1 = \frac{K_1 + K_3 + K_2^2 - K_1K_2 - K_2K_3 - 1}{K_1^2 - 2K_1K_2K_3 + K_2^2 + K_3^2 - 1} \tag{5-3}$$

$$\eta_2 = \frac{K_1 + K_2 + K_3^2 - K_1K_3 - K_2K_3 - 1}{K_1^2 - 2K_1K_2K_3 + K_2^2 + K_3^2 - 1} \tag{5-4}$$

$$\eta_3 = \frac{K_2 + K_3 + K_1^2 - K_1K_2 - K_1K_3 - 1}{K_1^2 - 2K_1K_2K_3 + K_2^2 + K_3^2 - 1} \tag{5-5}$$

5.3 Assumptions and Range of Applicability

For the proposed model we assume the following:

1. **Quasi-steady evaporation** is assumed for the mass transfer process. This is reasonable because the concentration field adjusts to changes in droplet size over a timescale of approximately a^2/D. For non-volatile liquids like water, the ratio $(a^2/D)/t_e$ <<<1, meaning the concentration field stabilizes much more quickly than the droplet evaporates.
2. **Convective effects are disregarded**, with the assumption that diffusion primarily governs the evaporation process. This is appropriate when the Peclet number (Pe<<1), which compares convective to diffusive mass transport.
3. **An isothermal system is assumed**, meaning any variation in droplet surface temperature is neglected. This is justified for substrates that aren't externally heated, where the evaporation rate is slow enough that the temperature drop from latent heat has minimal effect.

5.4 Results and Discussions

Given the complexity of the derived equations, which limits their ability to provide physical insight, we will introduce certain assumptions to simplify them. To achieve this, we consider three distinct cases, with each case involving a particular assumption to simplify the equations. The cases are as follows:

Case-01: Assume equal spacing between all droplets.

Case-02: Assume that two of the separation distances are equal.

Case-03: Assume unequal spacing between all droplets (Actual case).

5.4.1 Case-01: Assume equal spacing between all droplets

Assuming that $L_1 = L_2 = L_3 = L$, the correction factors in eq. (5-3)-(5-5) can be simplified to eq. (5-6). As shown in **Figure 5-2**, introducing a third droplet to a system of two droplets results in a further reduction in the evaporation rate. This reduction is both reasonable and expected, as each droplet in the array of three equally spaced, identical droplets is influenced by two wedge regions created by the other two droplets. In the first objective of this study, it was established that in a system of two sessile droplets, when the separation distance between the droplets exceeds 10 times the droplet's contact diameter (L/d > 10), the droplets behave as if they are isolated. This can be seen in **Figure 5-2**, for L/d >10, the correction factor (η) for a pair of sessile droplets exceeds 95%, indicating that the deviation from the evaporation behavior of a single isolated droplet is less than 5%. However, in a system of three equally spaced droplets, the threshold value increases to 20 (L/d > 20), as each droplet is now influenced by two wedge regions instead of one.

$$\eta_1 = \eta_2 = \eta_3 = \frac{(L/d)}{(L/d) + 1} \tag{5-6}$$

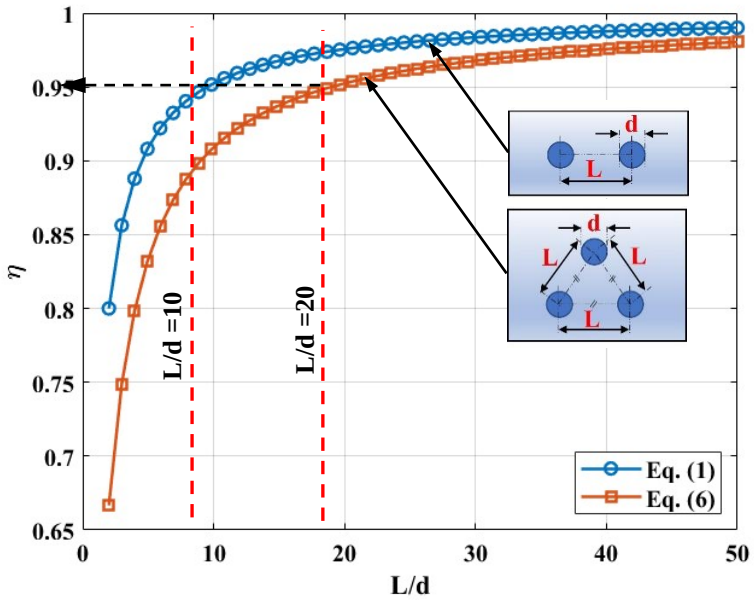

Figure 5-2 Correction factor, η, as a function of *L/d* for a pair of sessile droplets and three identical equally spaced droplets.

5.4.2 Case-02: Assume that two of the separation distances are equal

In this case, the setup is made slightly more complex than in Case-01 to better approximate the actual intricate scenario. It is assumed that $r_{12} = r_{13} = L_1$, and $r_{23} = L_2$, with ψ representing the angle between r_{12}, and r_{13} (as shown in **Figure 5-1**, and **Figure 5-3**). The geometric constraint for this configuration is given by: $(L_2/d) = 2(L_1/d) \times \sin(\frac{\psi}{2})$. For any given L_1/d value, varying the angle, ψ, allows the corresponding L_2/d value to be determined based on this constraint. So, by applying the new assumptions the correction factors in eq. (5-3)-(5-5) can be simplified to eq. (5-7), and eq. (5-8).

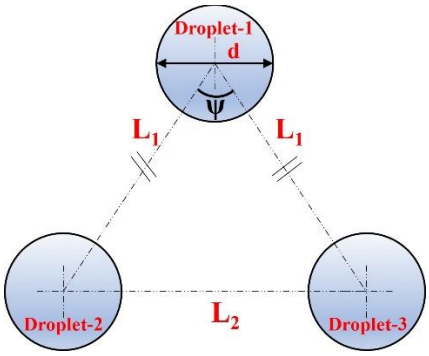

Figure 5-3 Schematics of a top plan of an array of three identical droplets with two equal separation distances

$$\eta_1 = \frac{2K_1 - K_2 - 1}{2K_1^2 - K_2 - 1} \tag{5-7}$$

$$\eta_2 = \eta_3 = \frac{K_1 - 1}{2K_1^2 - K_2 - 1} \tag{5-8}$$

As shown in **Figure 5-4**, for any given rotation angle ψ, increasing the value of L_1/d leads to an increase in the correction factors of all droplets (η_1, η_2, and η_3). This can be attributed to the fact that as droplet 1 moves farther away from droplets 2 and 3, the influence of the wedge regions between droplets (1-2) and (1-3) diminishes, thereby increasing the correction factor for droplet 1. Although the wedge region between droplets (2-3) remains unaffected at a constant ψ value, the reduced influence of droplet 1's wedge region results in an overall increase in the correction factors for droplets 2 and 3 as well.

Furthermore, increasing the angle of rotation ψ for any given L_1/d leads to a decrease in the correction factor for droplet 1 (η_1), while the correction factors for droplets 2 and 3 (η_2, and η_3) increase. This behavior can be explained by the changes in the surface area of each droplet affected by the wedge regions created by neighboring droplets. As illustrated in **Figure 5-5**, increasing the angle of rotation ψ by $\Delta\psi$ increases the affected area on the surface of droplet 1 due to the wedge regions from droplets 2 and 3, while simultaneously reducing the relaxed area

(the surface area not influenced by the wedge regions). This increase in the affected area leads to a reduction in the correction factor η_1 for droplet 1. However, as ψ increases by $\Delta\psi$, the distance L_2 between droplets 2 and 3 increases by ΔL, which reduces the concentration of the wedge region between them. Additionally, the affected areas on the surfaces of droplets 2 and 3 caused by the wedge region of droplet 1 decrease. These two effects, reduced wedge region concentration and smaller affected areas, result in an increase in the correction factors, η_2, and η_3.

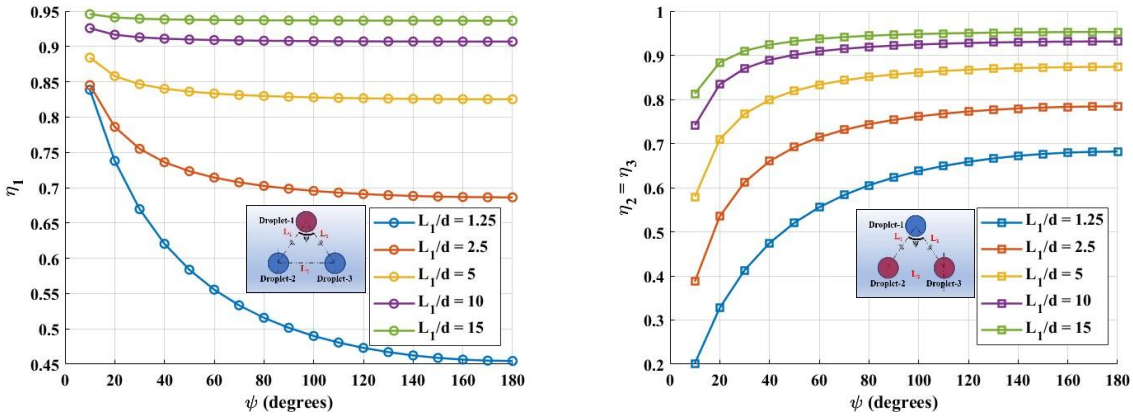

Figure 5-4 Correction factor, η, as a function of angle of rotation, ψ, for Droplet 1 (*left*) and droplets 2 or 3 (*right*), for an array of three identical droplets with two equal separation distances.

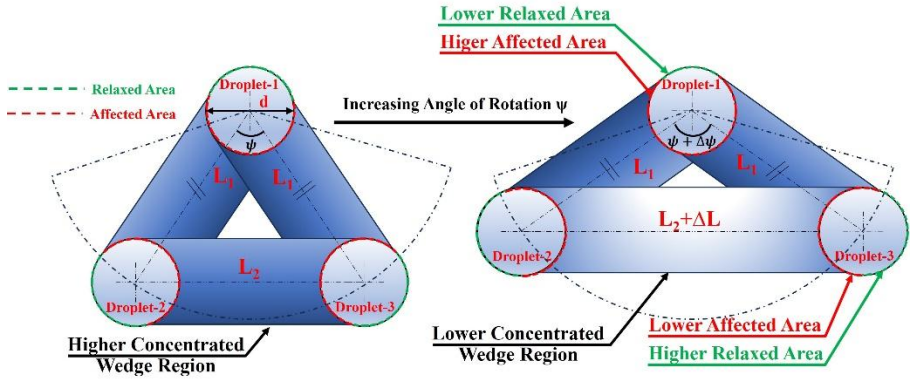

Figure 5-5 Schematic of the effect of increasing the angle of rotation, ψ, at constant L_1/d.

5.4.3 Case-03: Assume unequal spacing between all droplets (Actual case)

In this case, we examine the fully complex scenario without the simplifications applied in Case-01 and Case-02, where $L_1 \neq L_2 \neq L_3$. The simplifications in the earlier cases were introduced to provide a step-by-step understanding of the behavior of an array of three droplets. For this more complex case, we use the geometry illustrated in **Figure 5-6**, where two new geometrical parameters are introduced: the radius of rotation (r) and the azimuthal angle (φ). The geometric constraints for this configuration are defined by eq. (5-9), and eq. (5-10). For any given L_1/d value, varying the angle φ enables the determination of the corresponding L_2/d and L_3/dvalues based on these constraints.

$$L_2/d = \sqrt{(r/d.sin\varphi)^2 + (r/d.cos\varphi - L_1/2d)^2} \tag{5-9}$$

$$L_3/d = \sqrt{(r/d.sin\varphi)^2 + \left(\frac{r}{d}.cos\varphi + L_1/2d\right)^2} \tag{5-10}$$

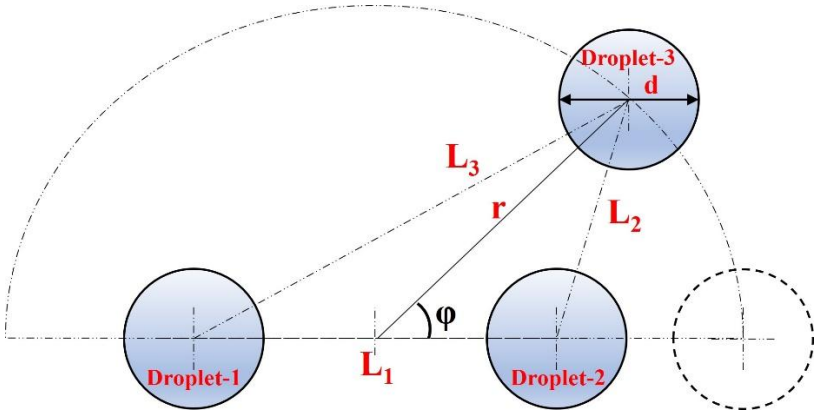

Figure 5-6 Schematics of a top plan of an array of three identical droplets with unequal separation distances.

Using η_1, η_2, and η_3, as defined in eq. (5-3)-(5-5), respectively, we obtained the results presented in **Figure 5-7**. For the given $L_1/d = 1.25$, it can be observed that increasing the azimuthal angle from 0° - 180° leads to a decrease in the correction factor of droplet 1 (η_1). This

behavior is attributed to the expansion of the affected area on the surface of droplet 1 caused by the wedge regions from droplets 2 and 3, as droplet 3 shifts from the right (φ=0) to left (φ=180°). This concept is analogous to the one illustrated in **Figure 5-5**. Conversely, for droplet 2, as droplet 3 moves from the right to the left, the affected area on droplet 2's surface decreases, resulting in an increase in its correction factor (η_2) increases. For droplet 3 as it moved from (φ=0) to (φ=180°), its correction factor, η_3, reaching a maximum at φ=90° before decreasing again. This behavior occurs because at φ=90°, droplet 3 is at its farthest distance from droplets 1 and 2, minimizing the effects of the wedge regions from these droplets and maximizing its correction factor.

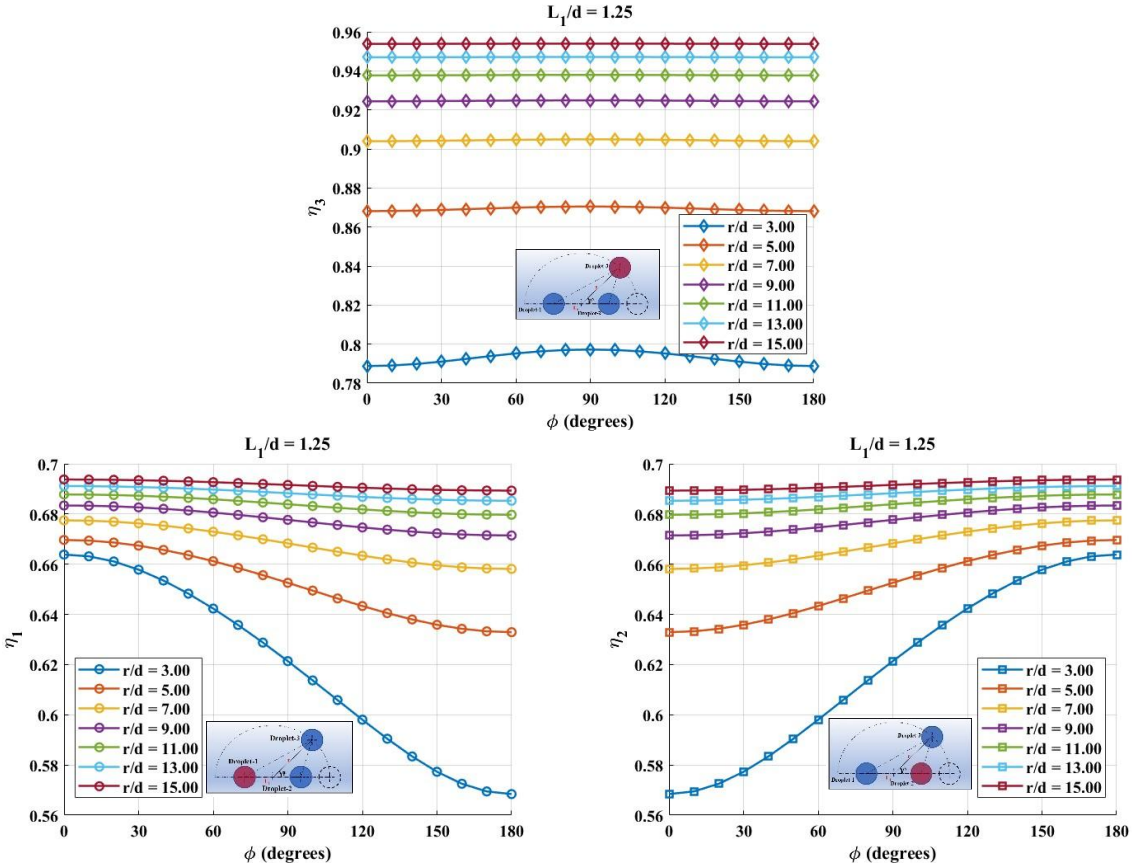

Figure 5-7 Correction factor, η, as a function of the azimuthal angle, φ, for Droplet 1 (*bottom left*), droplets 2 (*bottom left*), and droplet 3 (*top*), for an array of three identical droplets with unequal equal separation distances at $L_1/d=1.25$.

5.5 Conclusion

The study investigated the evaporation dynamics of an array of three sessile droplets using a Point Source Model (PSM) and provided insights into how droplet interactions influence evaporation rates under different spatial configurations. For equally spaced droplets, the correction factor showed a significant reduction in evaporation rates, with the threshold separation distance for isolated droplet behavior increasing from $L/d > 10$ (for two droplets) to $L/d > 20$ (for three droplets).

For partially equal spacing, it was observed that increasing the distance of one droplet from the others (e.g., $L_1 > L_2 = L_3$) reduces its interaction with neighboring droplets, leading to an increase in its evaporation rate. Additionally, the angle of rotation (ψ) affected the correction factors: as ψ increased, droplet 1 experienced a reduction in its evaporation rate due to increased interaction, while droplets 2 and 3 exhibited a rise in their correction factors.

In the most complex scenario of unequal spacing, varying the azimuthal angle (ϕ) revealed dynamic changes in evaporation behavior. For example, droplet 3 achieved its maximum correction factor at $\phi = 90°$, where it was farthest from the other droplets, minimizing interaction effects. Conversely, droplet 1 showed a continuous reduction in its evaporation rate as droplet 3 moved closer.

Chapter 6 Conclusions and Future Works

6.1 Summary and Conclusions

This work investigated both experimentally and analytically the evaporation process of a pair of sessile droplets under various conditions, including droplet volumes, relative humidity, contact angles, and liquid types. Additionally, the effect of substrate temperature on the evaporation rate was examined, along with the combined influence of diffusive and convective evaporation rates. The study further explored the motion behavior of a pair of sessile droplets of different compositions (water and propylene glycol) under heated substrate conditions. Finally, the evaporation behaviour of an array of three droplets was considered in this study.

To achieve the objectives mentioned in the previous paragraph, Firstly, an analytical diffusive model was developed using the Point Source Model (PSM) approach. This model was designed to predict the evaporation rate and evaporation time of a pair of sessile droplets undergoing evaporation in constant contact radius (CCR) and constant contact angle (CCA) modes. The proposed model was validated experimentally using a pair of sessile water droplets evaporating within a humidity-controlled chamber. The validation process included assessing the model's accuracy across various conditions, including droplet volume, ambient relative humidity, substrate wettability (characterized by the droplet’s contact angle), and liquid volatility by examining different liquids with different volatility other than water. The results demonstrated excellent agreement between the model's predictions and the experimental data for these parameters (5-10% deviations), except in the case of highly volatile liquids such as ethanol and 1-propanol. For these liquids, the high evaporation rates introduced significant convective effects that the diffusive model could not capture, unlike the case with less volatile liquids such as water.

To study the effect of substrate temperature on the evaporation rate, a second experimental setup was utilized. This setup included a humidity-controlled chamber equipped with a sensitive laboratory scale to monitor changes in droplet mass during evaporation, enabling the determination of evaporation rates at constant time intervals. Comparison of the experimental evaporation rates with those predicted by the diffusive model revealed underprediction discrepancies at elevated substrate temperatures. The diffusive model was unable to account for the convective effects that became dominant under these conditions and this leads to underpredicted results from the model. Consequently, an empirical correlation was introduced to incorporate the combined effects of diffusion and convection into the evaporation rate predictions.

The same experimental setup, excluding the lab scale, was employed to investigate the motion behavior of a pair of sessile droplets with varying propylene glycol (PG) concentrations on a heated glass substrate. The study found that the velocity of the water droplet was influenced by the composition of the actuating droplet, the PG concentration, and the substrate temperature. For substrate temperatures exceeding 100°C (the boiling point of water), or for actuating droplets with PG concentrations below 50%, the motion behavior became unpredictable. At substrate temperatures above 100°C, the droplet's motion ceased after a very short distance. Similarly, actuating droplets with PG concentrations below 50% exhibited chaotic motion, with the water droplet breaking apart into smaller droplets of varying compositions.

Finally, the proposed PSM model was extended to include the effect of adding a third droplet in a system of two droplets, that the behavior of this small units can represent the behaviour of an array of sessile droplets. This study analyzed the evaporation dynamics of three sessile

droplets using a Point Source Model (PSM) to understand the effects of droplet interactions. Adding a third droplet to a two-droplet system reduced evaporation rates further, with the threshold for isolated behavior increasing from L/d>10 to L/d>20. In partially equal spacing, increasing the distance of one droplet reduced its interaction, raising its evaporation rate, while varying the rotation angle (ψ) shifted the correction factors for all droplets. In unequal spacing, the azimuthal angle (ϕ) influenced evaporation rates dynamically, with droplets achieving peak or minimal rates based on positioning. These findings enhance the understanding of multi-droplet evaporation, benefiting applications requiring precise control.

The findings of this work can be summarized as follows:

A point source model was developed to study the evaporation process of a pair of droplets in quiescent air under isothermal conditions, treating the droplets as point mass sources located at their centres and assuming a purely diffusive, quasi-steady-state process.

The evaporation rate of a droplet depends on the separation distance, with droplets behaving as isolated when the distance is ten times the droplet diameter.

In the CCA (constant contact area) mode, the square of the contact radius decreases linearly with evaporation time, indicating a linear decrease in surface area, while in the CCR (constant contact radius) mode, the contact angle decreases linearly on hydrophilic surfaces but non-linearly on hydrophobic surfaces due to increased vapor concentration in the wedge area between droplets.

The model was experimentally validated, showing excellent agreement with less than 5% deviation on average and less than 10% deviation due to droplet volume, surface wettability, or ambient relative humidity.

For liquids with varying volatility (water, 1-propanol, ethanol), the model captured the experimental trend with a constant deviation of 62%, demonstrating its utility in estimating experimental values for future applications.

The study concluded that higher liquid volatility accelerates evaporation, leading to convective effects and greater deviation from the purely diffusive model predictions.

The evaporation behavior of a pair of sessile water droplets on a heated aluminium substrate was investigated, focusing on the interplay between diffusion and convection.

At lower substrate temperatures, evaporation is primarily diffusive, with the proposed diffusive model aligning well with experimental data. However, as substrate temperatures increase, natural convection driven by buoyancy forces significantly enhances evaporation, especially when the temperature difference exceeds 30°C.

Diffusion dominates evaporation when the Rayleigh number product (Ra·L/d) is below 400, contributing over 80% of the total rate. As Ra·L/d increases with higher substrate temperatures or greater droplet separations, convection becomes more influential, stabilizing at approximately 30% contribution when Ra·L/d exceeds 2400.

A dimensionless model combining diffusion and convection effects predicts evaporation rates with less than 5% error across all tested conditions.

The vapor-induced motion of a water droplet near a propylene glycol (PG)-water mixture droplet on a heated substrate was studied, examining how substrate temperature and PG concentration influence droplet velocity and movement.

Substrate temperature significantly affects droplet velocity: as temperature increases, the evaporation rate rises, leading to higher condensation on the water droplet, which intensifies the surface tension gradient and accelerates the droplet. When substrate temperatures exceed 100°C (the boiling point of water), droplet velocities increase up to 20 times compared to unheated conditions, although the travel distance decreases due to rapid evaporation reducing the surface tension differential.

The PG-water mixture composition also influences droplet motion, with lower PG concentrations (20%-40%) resulting in faster droplet speeds due to a sharper concentration gradient across the droplet surface.

When the substrate is heated and the PG concentration is 20%, chaotic motion and fragmentation of the water droplet occur, indicating that low PG content and high temperatures significantly increase the surface tension gradient, causing the droplet to split into smaller droplets.

Adding a third droplet to a two-droplet system further reduced evaporation rates, increasing the threshold for isolated behavior from $L/d>10$ to 20.

In partially equal spacing, increasing the distance of one droplet reduced its interaction with others, raising its evaporation rate.

In unequal spacing, changes in the azimuthal angle (ϕ) dynamically influenced evaporation rates, with droplets achieving peak or minimal rates based on their relative positions.

6.2 Scope for research and future work

The field of sessile droplet evaporation offers numerous opportunities for further research. Beyond advancing the understanding within the scientific community, the growing range of applications for this phenomenon highlights its potential to improve systems and support more efficient operations. The present study establishes a fundamental framework for experimentally and analytically understanding the evaporation process of sessile droplets. However, a list of potential future works and improvements is still required. This list of future works and enhancements is as follows:

Expanding the proposed PSM model to account for the impact of liquid volatility on the evaporation rate of volatile liquids:

In this study, the proposed diffusive PSM model in Objective-01 demonstrated excellent agreement with experimental results across various droplet volumes, ambient relative humidity levels, and surface wettability. However, the model showed significant discrepancies when applied to droplets of highly volatile liquids, such as 1-propanol and ethanol, with deviations reaching up to 62% compared to experimental results, as discussed in **Section 2.4.3**. Incorporating the effects of convection due to Stefan flow, which occurs during the evaporation of highly volatile liquids, could enhance the model's applicability to industrial processes. Nonetheless, care must be taken to avoid overcomplicating the model and compromising its key advantages of reduced complexity and computational efficiency.

Using infrared temperature sensors to visualize the temperature distribution over the surface of the droplets:

In Objective-02 of the current study, the evaporation heat flux was determined by averaging the variation in droplet mass over the evaporation period. While this method effectively quantified the total heat absorbed by the droplets during evaporation, it did not provide any insight into the temperature distribution across the droplet surface. Understanding this temperature distribution is important, as it reveals the heat flux distribution across the droplet surface, particularly in the presence of neighboring droplets. This knowledge offers a deeper understanding of how droplets influence one another and the impact of the separation distance between them. So, infrared techniques could be used to characterize the evaporation process of sessile droplets on a heated substrate more accurately.

Vapour induced motion of three droplets on a heated and an unheated substrate:

In Objective-03 of the current study, it was demonstrated that the velocity of a water droplet can be precisely controlled by adjusting the substrate temperature and the PG concentration of the actuating droplet. However, in this study, the droplet's motion was restricted to a linear path along the centres of the two droplets, with no control over motion in other desired directions. Introducing a third droplet could enable more precise control by influencing both the velocity and direction of the droplet's motion. The presence of the third droplet would allow directional control through the resultant force generated by the interactions with the other two droplets. Consequently, incorporating a third droplet, combined with careful control of substrate temperature and the concentrations of all droplets, presents a promising study for achieving precise manipulation of droplet motion.

Study the evaporation behaviour of an array of three droplets experimentally:

In Objective-04 of the current study, the PSM approach was utilized to predict the evaporation behaviour of an array of three droplets, analytically. These findings hold considerable importance for industrial applications that demand high levels of control and precision. They are also crucial for advancing research aimed at deepening scientific understanding of multi-droplet evaporation. However, it is important to note that these results are still in the preliminary stages and further experimental validation is required for future studies.

Appendix A

Derivation of The Evaporation Time (t_e) of Two Droplets Under (CCA) Evaporation Mode

For this derivation we start with Eq. (6) form the main text

$$\dot{m}_{sys} = \frac{1-\frac{a}{L}}{1-\frac{a^2}{L^2}} \times \left[-2\pi\ a\ D\ \frac{sin\theta}{1+cos\theta}\ (C_s - C_\infty) \times 56.561\theta^{-0.892}\right] \qquad \text{S - 1}$$

The volume of a spherical cap droplet (in terms of "a" and "θ") is

$$V = \frac{\pi(1-cos\theta)(cos\theta+2)\ a^3}{3\ sin\theta(1+cos\theta)} \qquad \text{S - 2}$$

Recalling that $\dot{m}_{sys} = \rho_L . \frac{dV}{dt}$ and by taking the derivative of Eq. (S-2) with respect to time (the contact angle, θ, is constant during the evaporation process for CCA evaporation mode), one can find

$$\dot{m}_{sys} = \rho_L\ \frac{\pi(1-cos\theta)(cos\theta+2)}{sin\theta(1+cos\theta)}\ a^2\ \frac{da}{dt} \qquad \text{S - 3}$$

By equating Eq. (S - 1) and Eq. (S - 3)

$$\frac{1-\frac{a}{L}}{1-\frac{a^2}{L^2}} \times \left[-2\pi\ a\ D\ \frac{sin\theta}{1+cos\theta}\ (C_s - C_\infty) \times 56.561\theta^{-0.892}\right] = \rho_L\ \frac{\pi(1-cos\theta)(cos\theta+2)}{sin\theta(1+cos\theta)}\ a^2 \frac{da}{dt} \qquad \text{S - 4}$$

Rearranging and simplifying Eq. (S - 4)

$$a.(a+L)\ da = \frac{-2LD}{\rho_L}\ (C_s - C_\infty)\ \frac{1+cos\theta}{(2+cos\theta)} \times 56.561\theta^{-0.892}\ dt \qquad \text{S - 5}$$

Integrating Eq. (S - 5) with respect to a and t

$$\frac{a^3 - a_0^3}{3} - \frac{a^2 - a_0^2}{2} = \frac{-2LD}{\rho_L}\,(C_S - C_\infty)\,\frac{1 + cos\theta}{2 + cos\theta} \times 56.561\theta^{-0.892}\,t_e \qquad \text{S - 6}$$

Where a_o is the initial contact radius of the droplet. Also, the evaporation time te can be determined form Eq. (S - 6) by letting a=0.

Appendix B

Derivation of The Evaporation Time (t_e) of Two Droplets Under (CCR) Evaporation Mode

The volume of a spherical cap droplet in terms of "*a*" and "*h*, the height of the droplet" is

$$V = \frac{\pi h}{6}(3a^2 + h^2) \qquad \text{S - 7}$$

by taking the derivative of Eq. (S - 7) with respect to time, knowing that the contact radius of the droplet, a, is constant during the evaporation process for CCR evaporation mode, one can find

$$\frac{dV}{dt} = \frac{\pi}{2}(a^2 + h^2)\,\frac{dh}{dt} \qquad \text{S - 8}$$

Also, the height of droplet can be obtained from Eq. (S - 9)

$$\mathrm{h} = \mathrm{a}\,\frac{1 - cos\theta}{sin\theta} \qquad \text{S - 9}$$

Taking the derivative of Eq. (S - 9) with respect to time and simplifying

$$\frac{dh}{dt} = \frac{a}{1 + cos\theta}\,\frac{d\theta}{dt} \qquad \text{S - 10}$$

Substituting Eq. (S - 9), and Eq. (S - 10) into Eq. (S - 8), one has

$$\frac{dV}{dt} = \frac{\pi}{2}\left[a^2 + \left(\mathrm{a}\ \frac{1-cos\theta}{sin\theta}\right)^2\right]\left[\frac{a}{1+cos\theta}\ \frac{d\theta}{dt}\right] \qquad \text{S - 11}$$

which simplifies to:

$$\frac{dV}{dt} = \frac{\pi\ a^3}{(1+cos\theta)^2}\ \frac{d\theta}{dt} \qquad \text{S - 12}$$

By equating Eq. (S - 1) and Eq. (S - 12) multiplied by ρ_L

$$\frac{1-\frac{a}{L}}{1-\frac{a^2}{L^2}} \times \left[-2\pi\ a\ D\ \frac{sin\theta}{1+cos\theta}\ (C_s - C_\infty) \times 56.561\theta^{-0.892}\right] = \rho_L\ \frac{\pi.a^3}{(1+cos\theta)^2}\ \frac{d\theta}{dt} \qquad \text{S - 13}$$

Rearranging of Eq. (S - 13) and by integration with respect to θ and t

$$\int_{\theta_0}^{\theta_f} \frac{\theta^{0.892}}{56.561\ sin\theta\ (1+cos\theta)}\ d\theta = \frac{-2LD(C_S - C_\infty)}{(a+L)\ a^2\ \rho_L}\ t_e \qquad \text{S - 14}$$

Appendix C

Finite Difference Method

For a purely diffusive isothermal quasi-steady-state evaporation process the diffusion equation simplifies to the Laplace equation

$$\nabla^2 C = 0 \qquad \text{S - 15}$$

Eq. (S - 15) is usually solved using the following boundary conditions:

Saturated vapour concentration at the droplets surface ($C=C_{sat}$ at $r = R$).

The vapour concentration reaching a uniform ambient value far from the droplets ($C \rightarrow C_\infty$ as $r \rightarrow \infty$).

No mass flux normal perpendicular to the substrate $\left(\left.{}^{\partial C}/_{\partial Z}\right|_{Z=0} = 0\right)$

When the droplet is considered as a point mass source, the governing Laplace equation Eq. (S - 15), becomes the Poisson equation (S - 16)

$$\nabla^2 C = f(r) \qquad \text{S - 16}$$

where $f(r)$ is the source term (the mass per unit volume that is exchanged between the source and system). The source term, $f(r)$, is a function representing the density of the vapour concentration field sources, and for a single isolated point source located at r_j, is given by Eq. (S - 17), where q is the strength of the source and the Dirac delta function (δ) models the density of an idealised point mass.

$$f(r) = \text{ q } \delta(r - r_j) \qquad \text{S - 17}$$

Therefore, the governing equation for the model is obtained by substituting Eq. (S - 17) into Eq. (S - 16)

$$\nabla^2 C = \text{ q } \delta(r - r_j) \qquad \text{S - 18}$$

Castillo et al. [1], provided an expression to determine from Eq. (S - 19) for any contact angle.

$$\text{q} = \frac{\dot{m}_{iso}}{\pi\, D\, f(\theta)} \qquad \text{S - 19}$$

Eq. (S - 17) is solved using the Finite Difference Method (FDM) in a two main steps.

Step 1: Discretising the domain and defining the mesh grid:

The system is solved in a two-dimensional rectangular grid (b x d). The grid is created using cartesian coordinates (x, z) using the following formulas.

$$x_i = ih_x, \qquad for\ i = 0,1,2,\dots,M \qquad \text{S - 20}$$

$$z_k = kh_x, \qquad for\ k = 0,1,2,\dots,N \qquad \text{S - 21}$$

Also, the distance between grids can be determined by using the following formulas:

$$h_x = \frac{b}{M} \qquad \text{S - 22}$$

$$h_z = \frac{d}{N} \qquad \text{S - 23}$$

For our study we assume we have uniform gids with equal spacing in both direction at which $h_x = h_z$

Step 2: Discretising the equations:

The governing Poisson Eq. (S - 16) can be written as

$$\frac{\partial^2 C(i,k)}{\partial x^2} + \frac{\partial^2 C(i,k)}{\partial z^2} = f \qquad \text{S - 24}$$

The Taylor series expansion of the second order derivatives are:

$$\frac{\partial^2 C(i,k)}{\partial x^2} = \frac{C(i-1,k) - 2C(i,k) + C(i+1,k)}{h^2} \qquad \text{S - 25}$$

$$\frac{\partial^2 C(i,k)}{\partial z^2} = \frac{C(i,k-1) - 2C(i,k) + C(i,k+1)}{h^2} \qquad \text{S - 26}$$

Using Eq. (S - 25) and Eq. (S - 26) in Equation (S - 24):

$$\frac{C(i-1,k) - 2C(i,k) + C(i+1,k)}{h^2} + \frac{C(i,k-1) - 2C(i,k) + C(i,k+1)}{h^2} = f_{i,k} \qquad \text{S - 27}$$

Rearranging Eq. (S - 27), one can get

$$C(i,k) = \frac{C(i-1,k) + C(i,k-1) + C(i,k-1) + C(i,k+1) - h^2.f_{i,k}}{4} \qquad \text{S - 28}$$

Eq. (S - 28) is solved by using MATLAB R2021a to obtain the vapour concentration distribution around the droplets. the Dirac delta function δ, is approximated as $\frac{1}{h^2}$.

References

1. Castillo JE, Weibel JA (2018) A point sink superposition method for predicting droplet interaction effects during vapor-diffusion-driven dropwise condensation in humid air. Int J Heat Mass Transf 118:708–719. https://doi.org/10.1016/j.ijheatmasstransfer.2017.11.045
2. Annamalai K, Ryan W, Chandra S (1993) Evaporation of multicomponent drop arrays. J Heat Transfer 115:707–716. https://doi.org/10.1115/1.2910742
3. Chini SF, Amirfazli A (2017) Resolving an ostensible inconsistency in calculating the evaporation rate of sessile drops. Adv Colloid Interface Sci 243:121–128. https://doi.org/10.1016/j.cis.2016.05.015